U.PORTO

PROGRAMA DOUTORAL EM ENGENHARIA BIOMÉDICA

A novel approach based on bacteriophages to prevent orthopedic implant-related infections

Joana Alberta Ribeiro Barros

D

2019

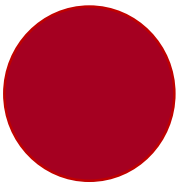

Joana Alberta Ribeiro Barros

A novel approach based on bacteriophages to prevent orthopedic implant-related infections

Dissertação submetida à Faculdade de Engenharia da Universidade do Porto para obtenção do grau de Doutor em Engenharia Biomédica

2019

Supervision:

Professor Doctor Fernando Jorge Monteiro – Faculdade de Engenharia da Universidade do Porto (FEUP); Instituto de Investigação e Inovação em Saúde, Universidade do Porto (i3S); Instituto de Engenharia Biomédica (INEB), Universidade do Porto (UP).

Co-supervision:

Doctor Joana Azeredo – Laboratório de Investigação em Biofilmes Rosário Oliveira, Center of Biological Engineering (CEB), University of Minho (UM).

Doctor Maria Pia Ferraz – University Fernando Pessoa Energy, Environment and Health Research Unit/Biomedical Research Center (FP-ENAS/CEBIMED).

Advisor:

Professor Doctor Maria Helena Fernandes – Laboratory for Bone Metabolism and Regeneration, Faculdade de Medicina Dentaria da Universidade do Porto (FMDUP).

Doctor Pedro Gomes - Laboratory for Bone Metabolism and Regeneration, Faculdade de Medicina Dentaria da Universidade do Porto (FMDUP).

The work described in this thesis was performed at:

FEUP - Faculdade de Engenharia da Universidade do Porto, Portugal;

INEB - Instituto de Engenharia Biomédica, Universidade do Porto, Portugal;

i3S - Instituto de Investigação e Inovação em Saúde, Universidade do Porto, Portugal;

CEB – Center of Biological Engineering (CEB), University of Minho, Braga, Portugal;

FMDUP – Laboratory for Bone Metabolism and Regeneration, Faculdade de Medicina Dentaria da Universidade do Porto, Portugal;

UTAD – Universidade Trás-os-Montes e Alto Douro, Portugal.

Financial Support:

This work was supported by FEDER – Fundo Europeu de Desenvolvimento Regional funds through the COMPETE 2020 – Operacional Programme for Competitiveness and Internationalisation (POCI), Portugal 2020, by Portuguese funds through FCT/MCTES in the framework of the project "Institute for Research and Innovation in Health Sciences (POCI-01-0145-FEDER-007274), by Project Biotherapies (NORTE-01-0145-FEDER-000012) and by Joana Barros' PhD grant (SFRH/BD/102148/2014).

ACKNOWLEDGMENTS

By the end of this journey, I would like to express my whole gratitude to all who helped me, directly and indirectly, in the course of this personal and scientific project.

I would like to acknowledge my supervisor, Professor Doctor Fernando Jorge Monteiro, for all the intellectual wisdom and guidance transmitted, entrepreneurial spirit, encouragement, and companionship, whose commitment was essential for the accomplishment of this work.

I would like to express my sincere gratitude to my co-supervisors Doctor Joana Azeredo (UMinho) and Doctor Maria Pia Ferraz, (UFP) for always giving me freedom of thought, for their availability, encouragement, and by sharing with me their scientific knowledge.

To Professor Doctor Maria Helena Fernandes and Doctor Pedro Gomes (FMDUP), I would like to express my deep gratefulness for all valuable and constructive guidance and the human values that they always demonstrated.

To the whole Biocomposites group team, I thank you for the companionship and support, that contributed to this journey being made in a relaxed environment but with efficiency.

To the whole Bacteriophage team, I would like to thank the support and knowledge shared throughout my presence at UMinho. Specially, to Doctor Luís Melo for all the help and companionship in and out of the lab.

I would like to thank Ricardo Vidal (BN), Maria Lazaro (b.IMAGE), Paula Magalhães and Tânia Meireles (CCGEN), Rui Fernandes and Rossana Correia (HEMS) and Rui Rocha (CEMUP), for their technical support and availability.

To FEUP, i3S, INEB, CEB, FMUP and UTAD, I thank for provision of all the conditions to carry out this work. Moreover, I thank whole colleagues and friends from these institutions, for being present at all the important moments.

I am equally grateful to Fundação para a Ciência e a Tecnologia (FCT) for my FCT grant (SFRH/BD/102148/2014) and Project Biotherapies (NORTE-01-0145-FEDER-000012) that financed all the work developed.

I would like to acknowledge Doctor Liliana Grenho, Doctor Andreia Azevedo, Doctor Ângela Carvalho, Catarina Coelho, Tatiana Padrão and Doctor Marta Ribeiro, that besides being my work-partners, are my friends. Thank you for always being there, in joy and in sadness.

I would like to thank at whole my friends "Os Berdadeiros", especially to Susana, Caniço, Sandra, Velhinho, Verónica and Mauro, for unconditional friendship and for always being here for me. To the nephews of my heart, Eva, Cristina, David, Lourenço, Martim and Rodrigo, I thank you for kisses, hugs, and love.

To whole members of my family "Fala Baixinho", "Mendes" and "Guedes", I thank you for the encouragement always shown.

To my parents, Maria Ribeiro e Joaquim Barros, and brother, Filipe Barros, I thank you for unconditional love, support, encouragement, and for everything that you always helped me to conquer throughout my life, without you I would not have succeeded.

To my partner of the good and bad moments, Mário Mendes, I would like to thank for the unconditional love, friendship, encouragement, and support. Without you, I would not have come this far.

Thank you to all who have made and make part of this journey. At the end, I won scientific and personal acquaintance and new experiences, but most importantly, I won FRIENDS. Thank you all!

PUBLICATIONS

The work performed in the frame of this thesis resulted in the following publications:

Barros J, Ferraz MP, Azeredo J, Fernandes MH, Gomes PS, Monteiro FJ. (2019). Alginate-nanohydroxyapatite hydrogel system: optimizing the formulation for enhanced bone regeneration. (**Material Science and Engineering C, Impact factor: 4.959, DOI: 10.1016/j.msec.2019.109985**)

Barros J, Melo LDR, Poeta P, Igrejas G, Ferraz MP, Azeredo J, Monteiro FJ. (2019). Lytic bacteriophages against multidrug-resistant *Staphylococcus aureus*, *Enterococcus faecalis* and *Escherichia coli* strains isolated from orthopaedic implant-associated infections**. (International Journal of Antimicrobial Agents, Impact factor: 4.615, DOI: 10.1016/j.ijantimicag.2019.06.007)**

Barros J, Melo L, Silva RA, Ferraz MP, Azeredo J, Pinheiro V, Colaço B, Fernandes MH, Gomes PS, Monteiro FJ. (2019). Encapsulated bacteriophages in alginate-nanohydroxyapatite hydrogel as a novel delivery system to prevent orthopedic implant-associated infections. (**Nanomedicine: Nanotechnology, Biology and Medicine. Impact factor: 5.570, Accepted for publication)**

ABSTRACT

In orthopedics, the use of implants allows a great improvement in the quality of life of many patients. However, the biomaterials' implantation entails a concomitant increase of surgical procedures, which are often associated to a high incidence of bacterial infections. Implant-related infections represent one of the most serious and devastating complications in the patient's quality life, socioeconomic and national healthcare systems underscoring the importance of prevention. Given the wide variety of pathogenic bacteria causing infections related to orthopedic implants, the emergence of bacteria resistant to antibiotics and cytotoxicity associated with them, new alternative approaches are required to prevent and control implant-related infections.

Bacteriophages, due to their lytic capacity to infect and kill specific bacteria, have been used as antimicrobial agents in the treatment of several infections such as diabetic foot ulcers, acute renal lesions and chronic otitis, instigated by clinical pathogens. Bacteriophages present countless advantages over commonly used antimicrobial agents, such as an increased efficiency at killing multidrug-resistant bacteria, self-reproducing ability in local infection and absence of cytotoxicity. Therefore, phage therapy would be a good approach for the prophylaxis and treatment of implant-related infections.

The work described in this thesis had, as main purpose, the development of a new strategy, based on the use of bacteriophages as antimicrobial agents, for the prevention of orthopedic implant-related infections. To this end, bacteriophages were encapsulated in a newly developed alginate hydrogel with nanohydroxyapatite particles, thereby forming a multifunctional composite, which was used as a biomaterial for local delivery of therapeutic agents within the bone tissue. The multi-functionality of the composite was addressed by the specific functions of each individual component. Bacteriophages were used as antimicrobial agents to prevent bacterial proliferation and colonization during bone integration. The alginate hydrogel, due to its biocompatibility and biodegradability properties, was used as the delivery vehicle and bone defect filling agent. While, nanohydroxyapatite, due to its chemical similarity with bone, and its inherent biocompatibility, bioactivity, osteoconductivity, and osseointegration, had the function to promote the regeneration of the bone tissue in the injured site. Thus, the work described herein was divided into three main tasks: 1) Preparation and characterization of alginate hydrogels with different concentrations of nanohydroxyapatite, in order to select the best amount of nanohydroxyapatite capable to efficiently promote the bone tissue

regeneration; 2) Isolation and characterization of bacteriophages capable to infect and kill bacteria associated with implant-related infections; 3) Preparation and characterization of the new composite system, based on encapsulated bacteriophages in alginate and nanohydroxyapatite hydrogel (Alg-nanoHA + bacteriophages), as an alternative approach to prevent and control implant-related infections.

Firstly, alginate hydrogels with different concentrations of nanohydroxyapatite (30, 50 and 70%) were developed and the influence of nanoHA concentration on physico-chemical properties of alginate-based hydrogels system was studied, as well as their influence on the biological activity of the system. The physico-chemical features of the composite decreased with increasing nanohydroxyapatite content, being this variation dose-dependent. The composite with the lowest nanohydroxyapatite concentration enhanced the osteoblastic cells' proliferation and osteogenic activation, while those with higher concentrations (50 and 70%) decreased the biocompatibility and gene expression of Runx2, Col1a1 and BGLAP. The results obtained showed that the nanohydroxyapatite content had a crucial role in the physico-chemical properties and the biological response of the composite, and a functional compromise between biomaterials must be guaranteed. Among the composites studied, the hydrogel alginate with 30% of nanohydroxyapatite showed a good synergy between materials culminating in the enhancement of bone regeneration.

Secondly, bacterial strains isolated from orthopedic implant-related infections (from a central hospital) were characterized in terms of antimicrobial resistance profiles, virulence factors, and epidemiology. The studied strains, *Staphylococcus aureus*, *Enterococcus faecalis*, and *Escherichia coli*, presented multidrug resistance, high virulence, and pathogenicity, emphasizing the urgent need to develop novel therapeutic approaches to fight this type of infection. In this context, virulent bacteriophages, LM12, LM99, and JB75, able to infect and kill the referred bacteria, were isolated and characterized. All phages presented high broad bactericidal spectrum and specificity against the target pathogenic bacteria, short latent periods, large burst sizes and high stability to several environmental conditions. Bacteriophages were able to efficiently infect and control the mentioned bacteria, including strains resistant to methacycline and vancomycin, emphasizing the potential of phage therapy in orthopedic implant-related infections.

At the end, the potentiality of a new therapeutic approach based on hydrogel Alg-nanoHA + bacteriophages in preventing and controlling implant-related infections were

evaluated. Two main functions addressed in this composite were the regeneration of bone tissue through nanohydroxyapatite and the prevention of bacterial proliferation and colonization through bacteriophages. Bacteriophages were efficiently entrapped into the alginate polymeric network, and the swelling-disintegration-degradation process of alginate hydrogel modulated the kinetic release of bacteriophages, without jeopardizing its viability. *In vitro* assays showed that the composite was able to reduce the planktonic and sessile bacterial populations. A good cytocompatibility, biocompatibility and safety profile were observed within an *in vivo* model of subcutaneous implantation, with a low inflammatory response, absence of implant rejection, a good cell invasion and extracellular matrix deposition. Finally, a proof of concept within an *ex vivo* femur model was performed, evaluating the bone tissue regeneration and, simultaneously the antimicrobial activity of composite. The osteogenic and mineralization response was positively influenced by hydrogel Alg-nanoHA + bacteriophages implantation, noticing that the increase of collagenous deposition and trabecular bone formation was promoted by nanohydroxyapatite. *Ex vivo* antimicrobial assay showed that the composite was able to reduce effectively proliferation and colonization of the multidrug-resistant VRE *E. faecalis*, surrounding the implant and within femurs. These findings revealed that the use of encapsulated bacteriophages in the alginate-nanohydroxyapatite hydrogel, as a biomaterial for implantation, may be a promising approach in the improvement of bone regeneration and, simultaneously, in the prevention of bacterial proliferation and colonization at the site of the bone defect.

Accordingly, a new approach based on a multifunctional biomaterial for the local release of therapeutic agents was developed in order to prevent implant-associated infections during bone integration and regeneration.

RESUMO

A utilização de implantes em ortopedia e traumatologia permite uma melhoria substancial da qualidade de vida de inúmeros pacientes. Contudo, a implantação de biomateriais acarreta um elevado número de procedimentos cirúrgicos, que se encontram muitas vezes aliados a uma elevada incidência de infeções, tais como osteomielite e infeções de próteses articulares. Estas infeções têm um grande impacto na qualidade de vida do paciente, nos sistemas socioeconómicos e sistemas nacionais de saúde, ressaltando a importância da sua prevenção. Dada a grande variedade de bactérias patogénicas causadoras de infeções, à emergência de bactérias resistentes a antibióticos, e à citotoxicidade associada aos agentes antimicrobianos, são necessárias novas abordagens para a profilaxia e tratamento de infeções associadas a implantes.

Os bacteriófagos, devido à sua capacidade de infetar e matar bactérias específicas, têm sido usados como agentes antimicrobianos no tratamento de diversas infeções, como úlceras de pé diabético, lesões renais agudas e otites crónicas, causadas por patogénicos clínicos. Os bacteriófagos apresentam inúmeras vantagens comparativamente aos agentes antimicrobianos habitualmente usados, tais como capacidade lítica contra bactérias multirresistentes, capacidade de se reproduzirem no local da infeção e inexistência de citotoxicidade associada. Assim, a terapia fágica poderá constituir um uma abordagem alternativa no tratamento e profilaxia de infeções associadas as implantes médicos.

O trabalho descrito nesta dissertação teve como objetivo principal o desenvolvimento de uma nova estratégia, baseada no uso de bacteriófagos, como agentes antimicrobianos, para prevenção de infeções associadas a implantes ortopédicos. Para tal, os bacteriófagos foram encapsulados num hidrogel de alginato com partículas de nanohidroxiapatite, formando assim um compósito multifuncional, que foi usado como biomaterial para libertação local dos agentes terapêuticos. A multifuncionalidade deste compósito deve-se às funções específicas de cada um dos seus componentes. Os bacteriófagos foram usados como agentes antimicrobianos capazes de impedir a proliferação e colonização bacteriana durante a integração óssea. O hidrogel de alginato, devido às suas propriedades de biocompatibilidade e biodegradabilidade, foi usado com veículo de transporte e agente preenchimento de defeito ósseo. A nanohidroxiapatite, devido à sua similaridade química com o osso, e à sua inerente biocompatibilidade, bioatividade, osteocondutividade e osteointegração, teve como função promover a regeneração do tecido ósseo no local lesado. Assim, este projeto foi divido em três partes fundamentais: 1) preparação e

caracterização de hidrogéis de alginato com diferentes concentrações de nanohidroxiapatite, de forma a selecionar a melhor concentração de nanohidroxiapatite capaz de promover eficientemente a regeneração óssea; 2) isolamento e caracterização de bacteriófagos capazes de infetar e matar as bactérias predominantes em infeções associadas a implantes, e por fim 3) preparação e caracterização de um novo sistema baseado num hidrogel de alginato com nanohidroxiapatite e bacteriófagos encapsulados (alginate-nanohidroxiapatite + bacteriófagos), como uma estratégia alternativa para prevenção e mitigação de infeções associadas a implantes.

Inicialmente, hidrogéis de alginato com diferentes concentrações de nanohidroxiapatite (30, 50 e 70%) foram desenvolvidos, de forma a avaliar a influência do conteúdo de nanohidroxiapatite nas propriedades físico-químicas do compósito, bem como a sua influência da atividade biológica do sistema. As características físico-químicas do compósito diminuíram com o aumento da concentração de nanohidroxiapatite, sendo um processo dose-dependente. O compósito com a concentração mais baixa de nanohidroxiapatite influenciou positivamente a proliferação celular e ativação osteogénica, enquanto os que possuíam as concentrações mais altas (50 e 70%) diminuíram a biocompatibilidade e expressão génica. Os resultados obtidos demonstraram que o conteúdo de nanohidroxiapatite teve um papel elementar nas propriedades físico-químicas e na resposta biológica do compósito, devendo ser assegurado um compromisso funcional entre os biomateriais. Entre os compósitos estudados, o hidrogel alginato com 30% de nanohidroxiapatite mostrou elevada sinergia que culminou na melhoria da regeneração óssea.

Na segunda parte deste projeto, estirpes bacterianas isoladas de infeções associadas a implantes ortopédicos (fornecidas por um hospital central) foram caracterizadas. Os perfis de resistências antimicrobiana, os fatores de virulência e a referente epidemiologia foram estudados. As estirpes *Staphylococcus aureus*, *Enterococcus faecalis* e *Escherichia coli* apresentaram padrões de multirresistência, virulência e patogenicidade, enfatizando a necessidade de uma nova abordagem terapêutica para o combate deste tipo de infeções. Neste contexto foram isolados e caracterizados bacteriófagos virulentos, LM12, LM99 e JB75, capazes de infetar e matar as bactérias referidas. Os bacteriófagos mostraram um elevado espectro bactericida e elevada especificidade contra as bactérias patogénicas-alvo, curtos períodos de latência, grandes "burst-size", e elevada estabilidade a diversas condições ambientais. Os bacteriófagos foram capazes de infetar e controlar com grande

eficiência as bactérias mencionadas, incluindo estirpes resistentes à meticilina e vancomicina, destacando a potencialidade da terapia fágica na patologia mencionada.

A última parte deste projeto visou na avaliação do potencial terapêutico do hidrogel de alginato-nanohidroxiapatite e bacteriófagos encapsulados na prevenção e controlar de infeções associadas a implantes. O estudo contemplou essencialmente à avaliação de duas funções principais – regeneração do tecido ósseo, promovida pela nanohidroxiapatite, e a prevenção da proliferação e colonização bacteriana, por meio dos bacteriófagos. Neste estudo, foi verificado que os bacteriófagos foram eficientemente aprisionados na rede polimérica do alginato, e que o processo de inchamento-desintegração-degradação do hidrogel de alginato modelou a cinética de libertação dos bacteriófagos. A viabilidade e reprodutibilidade dos bacteriófagos após encapsulamento e libertação não foi comprometida. Os ensaios *in vitro* efetuados mostraram que o compósito reduziu eficientemente as populações bacterianas planctónicas e sésseis. O perfil de citocompatibilidade, biocompatibilidade e biossegurança do compósito foi avaliado num modelo *in vivo* de implantação subcutânea, sendo observado uma baixa resposta inflamatória, ausência de rejeição do implante, com uma boa invasão celular e deposição de matriz extracelular. Por fim, foi efetuado a prova de conceito num modelo *ex vivo* de fémures, avaliando-se assim a regeneração óssea e simultaneamente a atividade antimicrobiana do compósito. A resposta osteogénica e de mineralização foi influenciada positivamente pela implantação do hidrogel alginato-nanohidroxiapatite + bacteriófagos, denotando-se que o aumento da deposição da matriz de colagénio e a formação óssea trabecular foi promovido pela presença de nanohidroxiapatite. A resposta antimicrobiana efetuada no modelo *ex vivo* mostrou a capacidade antimicrobiana deste compósito, reduzindo a proliferação e colonização da estirpe multirresistente VRE *E. faecalis* em redor do implante e no interior do fémur. Assim, os resultados obtidos revelaram que o uso do hidrogel de alginato-nanohidroxiapatite e bacteriófagos encapsulados, como biomaterial para implantação, pode ser uma abordagem promissora no melhoramento da regeneração óssea e, simultaneamente, na prevenção da proliferação e colonização bacteriana no local do defeito ósseo.

Em suma, neste trabalho foi desenvolvida uma nova estratégia baseada num biomaterial multifuncional para libertação local dos agentes terapêuticos, com o intuito de prevenir infeções associadas a implantes durante integração e regeneração óssea.

TABLE OF CONTENTS

CHAPTER 1

INTRODUCTION

1.1 Bone composition

Bone is a heterogeneous composite material and represents the main constituent of the vertebral skeleton. This dynamic tissue contributes to the regulation of electrolytes concentration, provides a framework for the support and attachment of softer tissues such as muscles, protects vital organs and the bone marrow, and provides all the necessary body support for locomotion and muscular contraction [1].

Bone tissue consists of mineralized extracellular matrix embedded with bone cells, blood vessels, and nerves (Fig. 1). The extracellular matrix is composed of mineral (65%) and organic (35%) components. The mineral components, such as calcium (Ca) and phosphorus (P), in the form of hydroxyapatite (HA crystals – the main inorganic component of the bone), sodium (Na), potassium (K), magnesium (Mg), fluoride (F), chlorine (Cl), carbonate (CO_3^{2-}), and trace elements such as silicon (Si), strontium (Sr), iron (Fe), zinc (Zn), and copper (Cu), are responsible for providing bone strength, due to the presence of apatite, carbonate ions and acid phosphate. Organic components, like collagen type I, non-collagenous proteins, proteoglycans, and phospholipids, are responsible to stabilizing through intra- and intermolecular crosslinks that enhance the tensile strength of the fibrils and regulate the bone structure and calcification process (Fig.1) [1, 2]. Bone cells, that are found within the mineralized extracellular matrix, are originated from two cell lines: mesenchymal stem cells (MSC) and hematopoietic stem cells (HSCs) (Fig. 1). MSCs are multipotent stromal cells that can differentiate into diverse cell types such as myocytes, adipocytes, pre-osteoblasts, osteoblasts, bone-lining cells, chondrocytes, and osteocytes. HSCs are stem cells that give rise to blood cells such as a monocyte, macrophages or platelets, but also pre-osteoclasts and osteoclasts [1].

Due to the cells' self-renewal capacity, bone tissue possesses intrinsic capacity to regenerate, as in the case of the repair process in response to injury, or during skeletal development or continuous remodeling throughout adult life [2, 3].

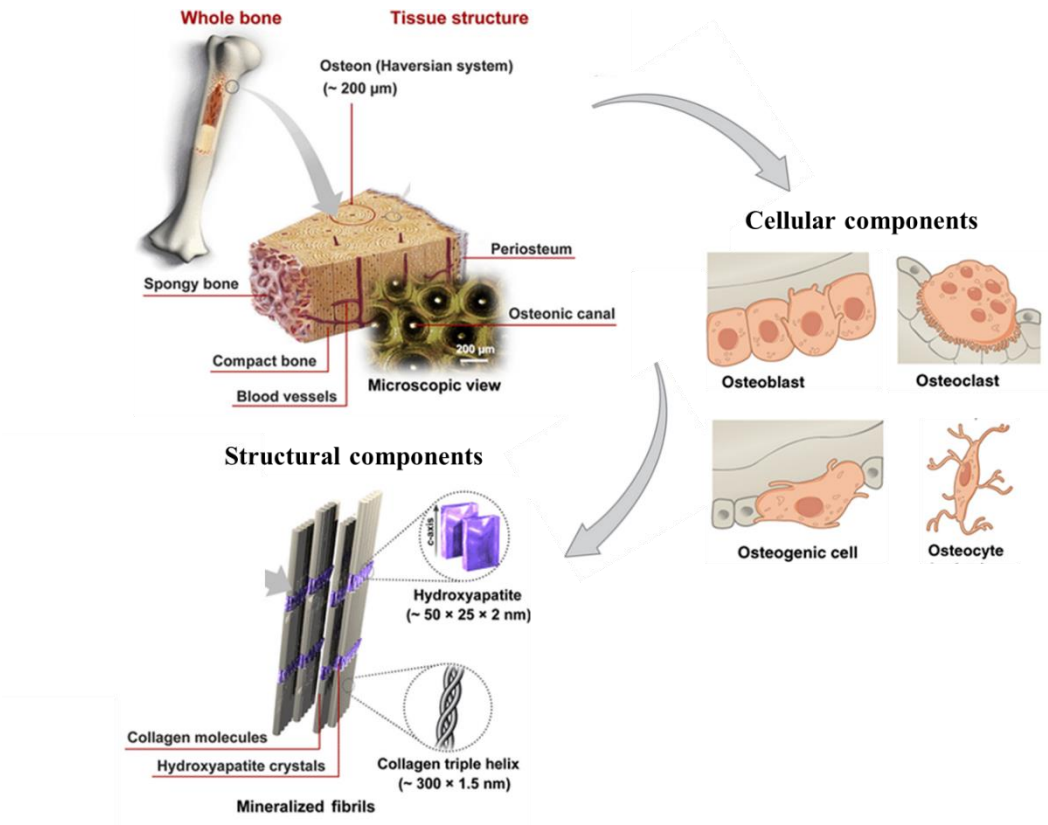

Figure 1 – Bone structure based on structural components, such as collagen fibrils with hydroxyapatite crystals, and cellular components, such as osteoblasts, osteoclasts, osteogenic cells and osteocytes (adapted from [4]).

1.1.1 Cells and molecular mechanisms involved in bone remodeling

Bone remodeling is comprised of a well-orchestrated series of biological events of bone induction and conduction, involving several cell types, i.e., osteoblast, osteoclast, osteocytes and bone lining cells, and intracellular and extracellular molecular signaling pathways, essential to maintain, repair and restore the skeletal function [3].

Osteoblasts are responsible for the production of the organic bone matrix and aid its mineralization [1, 5, 6]. Four maturational stages are identified in the osteoblastic differentiation: pre-osteoblasts, osteoblasts, bone-lining cells and osteocytes (Fig. 2). Osteoblasts derive from mesenchymal lineage (Fig. 2), through the expression of specific transcription factors, Runt-related transcription factor 2 (Runx2) and Osterix (Sp7), that are known to regulate osteoblasts differentiation. Their expression is activated and regulated by distinct effectors such as bone morphogenetic proteins (BMPs) and Wingless (Wnt)/β-catenin signaling pathways, respectively [5, 7, 8]. Runx2 is a master gene of osteoblast differentiation, controlling the osteogenic differentiation of mesenchymal stem

cells and inhibiting their differentiation into adipocytes and chondrocytes [7, 9]. Moreover, Runx2 up-regulates osteoblast-related genes such as Type-I collagen (COL-I), osteocalcin (OC), osteopontin (OPN), bone sialoprotein (BSP) and alkaline phosphatase (ALP), that are essential markers to osteoblast differentiation/maturation, organic matrix deposition and mineralization [7, 8]. Whereas, Sp7, a downstream gene of RUNX2, induces osteoblastic terminal differentiation and inhibits chondrogenesis. Sp7 is also believed to act in the regulation of certain osteogenesis-related markers such as osteonectin (ON), OC, OPN, COL-I and BSP [7, 8]. Osteoblasts synthesize predominantly COL-I, the main component of the osteoid, but also glycoproteins, like ON, OPN and BSP, enzymes, such as ALP and collagenases, γ-carboxyglutamic acid, other proteins, like OC, proteoglycans, proteolipids, and several growth factors, such as transforming growth factor-β (TGF-β) and bone morphogenic proteins (BMPs) [7, 8]. Osteoblasts also regulate mineralization by releasing small vesicles, with concentrate calcium and phosphate components, being also involved in the regulation of osteoclastogenesis via modulating receptor activator of nuclear factor Kappa-B ligand (RANKL)/osteoprotegerin (OPG) ratio [1, 6, 8]. Mature osteoblasts can follow one of three paths: terminally differentiate into osteocytes, become inactive bone lining cells or undergo apoptosis [7].

Bone-lining cells are quiescent flat-shaped osteoblasts that cover the bone surfaces (Fig. 2), with a specific role in the regulation of bone fluid composition, circulation and ion homeostasis, and bone resorption/formation by communicating with osteoblasts and pre-osteoclasts in the marrow [1, 7]. Moreover, they also act in the enzymatical removal of osteoids layer that covers the mineralized matrix, allowing osteoclasts to attach and begin resorption [1, 7]. These cells induce the expression of osteoclastogenic factors, such as RANKL, and OPG markers, needed for osteoclast differentiation and apoptosis [1, 7].

Osteocytes are osteoblast-derived post-mitotic cells within the bone matrix (Fig. 2), that act as mechanosensors, detecting mechanical deformation and bone micro-damage (microscopic cracks or fractures within the mineralized bone), and as a modulator of bone remodeling, through regulation of osteoblast (bone formation) and osteoclast (bone resorption) activities [5-7]. The osteocytes express several molecular markers, such as dentin matrix protein-1 (DMP-1) and sclerostin, involved in the regulation of mineralization and mineral metabolism [5-7].

Osteoclasts are cells with a hematopoietic origin, that dissolve bone mineral and enzymatically degrade extracellular matrix (ECM) proteins, contributing to the balance

between formation, maintenance, and destruction of bone tissue [1, 5, 6]. This equilibrium is maintained by mechanical factors and by the action of cytokines and hormones, such as calcitonin and parathyroid hormone (PTH), that can control the levels of calcium and phosphate in the blood [1]. Osteoclasts are originated from hematopoietic lineage (Fig. 2), and their proliferation, differentiation, survival and expansion are mediated by two osteoclastogenic factors, RANKL and OPG. RANKL binds to RANK, a type I transmembrane receptor expressed on osteoclast precursors, and induces pre-osteoclast differentiation into osteoclast [8]. While, OPG prevents osteoclast development and bone resorption, by blocking the RANKL/RANK interaction [6].

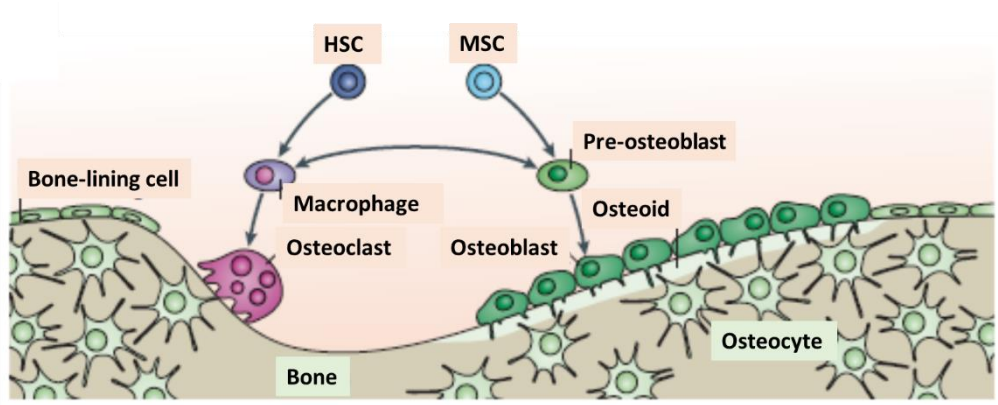

Figure 2 – Cell involved in bone remodeling (adapted from [6]).

1.1.2 Bone Remodeling: The Process

Bone remodeling is a highly coordinated process responsible for bone resorption and formation that contributes to repairing damaged bone and to maintain mineral homeostasis [5, 6]. Bone remodeling is performed by bone-forming osteoblasts, clusters of bone-resorbing osteoclasts, osteocytes, and bone-lining cells, arranged within Basic Multi-Cellular Units (BMUs). Bone remodeling cycle consists of 4 distinct phases: activation, resorption, reversal, and formation (Fig. 3) [10].

Remodeling process can be triggered either in response to micro-damage or to signaling molecules (e.g., insulin growth Factor-I (IGFI), PTH and interleukin-6 (IL-6)), or even in response to fluctuations in the calcium and phosphate homeostasis. This disequilibrium is sensed through osteocytes that activate the bone-lining cells and recruit pre-osteoclasts (activation phase). Therefore, RANKL/RANK complex is formed, inducing osteoclast differentiation and activation [5, 10, 11]. Once differentiated, osteoclasts adhere to the bone surface through integrin receptors in the cellular membrane,

that bind to RGD containing peptides in the bone matrix, creating an isolated sealed zone beneath the cell. This step marks the beginning of bone resorption phase [5, 10, 11]. In this phase, osteoclasts secrete protons, that acidify the medium, and endorse bone matrix demineralization. They also synthesize lysosomal enzymes (e.g. cathepsin K), which degrade the collagen matrix [5-7, 11]. Following the completion of resorption, osteoclasts undergo apoptosis, and the deposition of proteoglycans forming the cement line is initiated. This is the reversal phase. In this phase, matrix debris is removed by macrophage-like cells (reverse cells) and the resorption lacuna is leveled [5, 10, 11]. Although not yet fully understood, it is believed that during this phase mononuclear cells may release factors that could guide osteoblasts during the bone formation phase [10, 11]. The bone remodeling cycle is finished with the synthesis and deposition of bone matrix by osteoblasts, the bone formation phase. Growth factors, as BMPs, fibroblast growth factors (FGFs), TGF-β, and transcription factors, as Runx2 and Sp7, induce and mediate the osteoblast differentiation. Once differentiated, mature osteoblasts synthesize collagenous matrix (osteoid) and regulate its mineralization, by releasing small membrane-bound vesicles that concentrate calcium and phosphate [5, 8, 11]. The mineralization is achieved by deposition of calcium and phosphate, and subsequent nucleation and growth of crystals of HA [5, 11]. During this phase, mature osteoblasts are entrapped in the organic matrix and become osteocytes, while others can terminally differentiate into bone lining cells, building a canopy covering the surface and keeping the bone in a quiescent state until the next cycle [5, 10, 11].

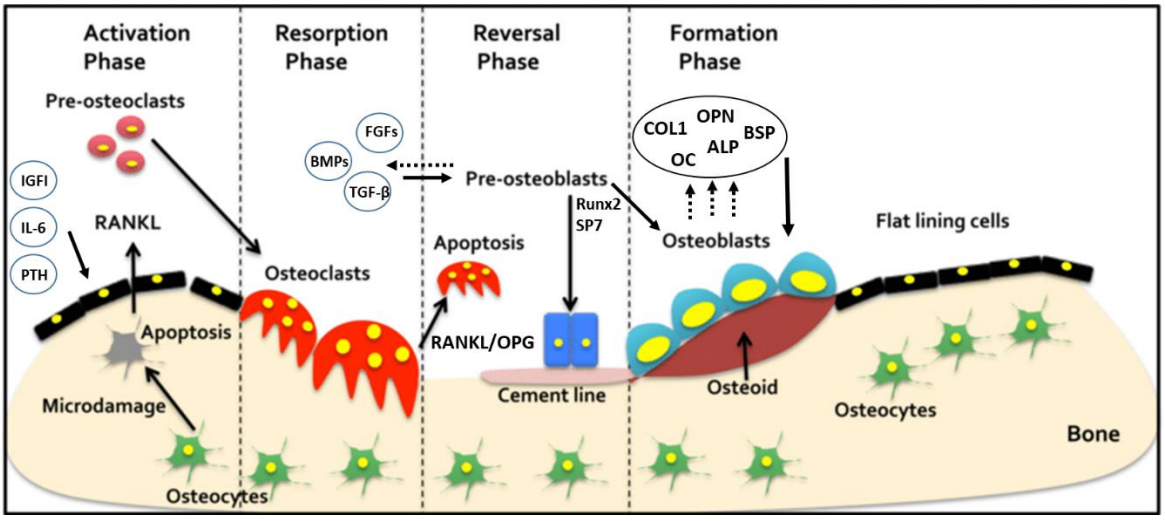

Figure 3 – Bone remodeling process (adapted from [5]).

1.2 Biomaterials for bone tissue regeneration

Bone tissue has the capacity to heal fractures or defects spontaneously, without inducing scar tissue formation [12]. However, complex or compromised bone fractures (i.e. fractures above critical size, or within severely damaged surrounding environment), co-morbidities (diabetes and, genetic factors), poor lifestyle (e.g. smoking or alcohol abuse) and inappropriate initial fracture treatment can lead to poor vascularization and an insufficient number of progenitor cells able to form new bone, resulting in failure and/or delay of the natural healing processes [12]. Moreover, bone defects resulting from the resection of bone tumors, infections, degenerative diseases or prosthetic revisions may result in complications leading to non-remodeling [12]. These conditions are a serious social problem, having a huge impact on diminishing patients' quality of life, and on healthcare systems, enforcing the need of developing bone graft substitutes able to enhance the tissue repair and regeneration [2].

Bone graft substitutes must provide structural guidance and similar composition to that of natural bone to promote cell adhesion, survival, migration, and proliferation [2, 13, 14]. Therefore, the biomaterial should be biocompatible, osteogenic (inherent ability to produce bone), osteoconductive (ability to allow the bone growth on surface of an implanted material), osteoinductive (ability to induce the osteogenesis by differentiation and maturation of the progenitor cells) and osteointegrative (ability to promote the structural and functional connection between bone tissue and implanted material) [14]. To ensure these properties, the synthetic material should present adequate porosity that provide space and environment for the growth of different cells and tissues and facilitate extracellular matrix (ECM) formation, nutrient transport, and nerve and blood vessel ingrowth [2, 14]. Furthermore, it should not elicit severe inflammatory or immune responses [14]. For a successful implantation, the biomaterial biodegradation rate should be coordinated to the new bone growth rate and it should be bioactive, i.e., able to form chemical bonding with biological tissues [14, 15].

Biomaterials currently used for bone tissue substitutes fabrication are metal, ceramics and polymers (natural or synthetic) [16]. The main advantages and disadvantages of these biomaterials are summarized in Table 1. Metals (e.g. titanium and its alloys), ceramics (e.g. bioactive glasses, tricalcium phosphate, HA) or their combinations, are widely used in bone tissue regeneration and/or osteointegration in bone defects due to their mechanical properties (mainly metals) and similarity to the bone mineral phase (mainly ceramics)

[16]. Natural polymers, e.g., polysaccharides, alginate, chitin/chitosan, hyaluronic acid derivates) or proteins (soy, collagen, fibrin gels, silk) and synthetic polymers, e.g., polymethylmethacrylate, poly(-hydroxy acids), or their copolymers are mainly used as matrix for bone tissue regeneration and as drug delivery vehicles of growth factors, therapeutic agents and cells [16].

Composites, composed of polymers and ceramics, have gained increasing attention as bone graft substitutes. With this approach, it is possible to obtain a functional synergism trough the combination of ceramics' strength, stiffness, bioactivity, and osteoconductivity with polymers' flexibility, toughness, biodegradability, and resorbability [2, 12, 14, 16]. Such composites can induce physiological regeneration of functional tissues by mimicking physico-chemical properties and to enhance the biological activity [1]. They are generally used as fillers and bone graft substitutes, occupying the available space in the damaged organ/tissue and providing the framework for growth of new tissue (partially or completely) [1].

Table 1 – Main advantages and disadvantages of metals, ceramics and polymers commonly used as biomaterial in bone tissue regeneration (Adapted from [16]).

Biomaterials	Advantages	Disavantages
Metals (Ti and its alloy, Ag, Au, Stainless steel, etc.)	• Mostly Biocompatible • Low degree of toxicity • High tensile and compressive strength • High toughness • Mostly ductile and malleable • Excelent structural stability	• Non degradable (except Mg alloys) • Non bioactive (except Ti alloys) • Non bioresorble • *In vivo* corrosion increasing inflammatory response • Non osteointegrating (except Ti alloys) • Can lead to the formation of fibrous tissue • High young´s modulus leading to stress shielding and bone resorption
Ceramics (Bioinert - Alumina, Zirconia; Bioactive - Hydroxyapatite, Bioglass, Tricalcium phosphate, etc.)	• Biocompatible • Some are bioactive • Some are osteogenic and osteocondutive (bioactive) • Non-inflamatory • Non-toxicity • Support *in vivo* differentiation (bioactive) • Load-bearing characteristics (bioinert)	• Brittleness • Slow degradation • Anisotropic mechanical properties under different loading conditions
Polymers (Natural: Chitosan, Collagen and Alginate; Synthetic: Polymethylmethacrylate, Poly(-hydroxy acids), Polyurethanes etc.)	• Biocompatible • Mostly biodegradable • Non-allergenic • Reabsorbable by the body • Easily chemically modified • Tunable properties • Low elastic modulus	• Poor bioactivity • Immune-response problems • Poor degradation rate control (mainly natural polymers) • Acidic or toxic degradation (mainly synthetic polymers) • Low mechanical stability • Low strength

1.2.1 Alginate-based biomaterials

Alginate-based biomaterials have been extensively studied to be used in medical applications due to their intrinsic characteristics such as biocompatibility, biodegradability, injectability, low toxicity, chelating ability, and relatively low cost [17]. Given those properties, this biomaterial has been widely used as wound-dressing material, drug-delivery system, and as material for bone tissue regeneration [17, 18].

Alginate (Alg) is an anionic and hydrophilic polysaccharide obtained from the brown algae (*Phaeophyceae*) [17, 18]. Alg comprises a linear polymeric chain of β-D-Mannuronate (M-monomers) and α-LGuluronate (G-monomers) residues linked by 1-4 glycosidic bonds (Fig. 4a) [16].

The ratio of M- and G-monomers varies depending on the natural source and influences the properties of Alg [17]. In chemical terms, Alg is characterized as a uronic acid where a primary hydroxyl group (-OH) on carbon six (C6) is oxidized, forming a carboxyl-group (-COO-). The protonation and deprotonation of the COO- group is directly dependent on the acid dissociation constant (pKa), which is 3.38 and 3.65 for M- and G-monomers, respectively [19]. The solubility is pH dependent, being Alg insoluble in low pH solutions below pKa due to protonation of the COO- group [19]. Alg with more heterogeneous structure (MG-blocks) is soluble at low pH compared to Alg with poly-M or poly-G blocks, which precipitate under these conditions [19]. The polymer composition, molecular weight, purity, concentration and distribution pattern of M-block and G-block of Alg play an important role in Alg-based biomaterial physico-chemical properties such as viscosity, sol/gel transition, biodegradability, water-uptake ability, mechanical strength and biological behavior [20]. For instance, the use of low molecular weight (37 kDa) Alg is attractive for *in vivo* tissue scaffolds' application, for bone regeneration, where degradation and clearance from the body are desirable. High molecular weight (196 kDa) Alg, on the other hand, is amenable for topical use as wound coverage because of its improved mechanical properties [20].

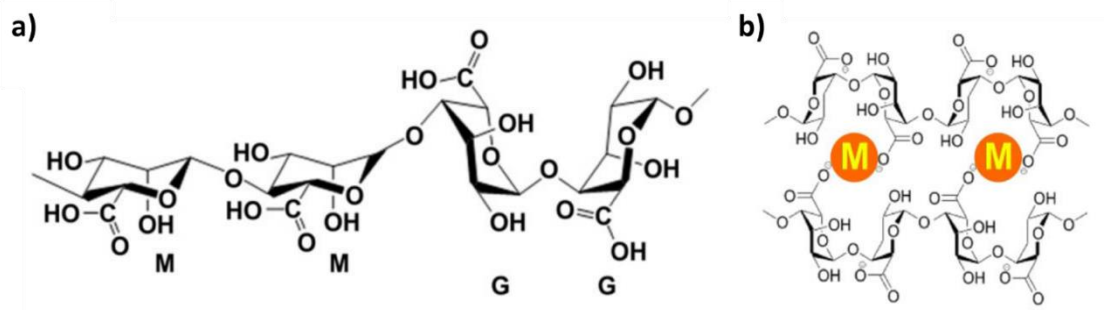

Figure 4 – (**a**) Chemical structure of Alg; (**b**) Mechanism of ionically interaction between Alg and divalent cations (Adapted from [21]).

Alg-based biomaterial can be used in any form such as microspheres, microcapsules, sponges, foams, fibers, and hydrogels [18] and they can be prepared by several methods involving lyophilization, electrospinning and crosslinking [17, 18]. Overall, Alg scaffolds (e.g., microspheres, microcapsules, sponges, foams, and fibers) are produced by freeze drying-lyophilization method, while the electrospinning method is one of the best ways to create nano-fibrous structure. Typically, Alg-based biomaterial is used in the form of a hydrogel, which is a three-dimensionally crosslinked network composed of hydrophilic polymers with high water content [17]. These hydrogels are structurally similar to the macromolecular-based components in the body, being often biocompatible, non-toxic and non-immunogenic [17]. Several studies have shown that Alg hydrogels can improve bone ingrowth, bone healing, and the treatment of tissue defects [21-23]. In addition, Alg hydrogels can be introduced into the body through a minimally invasive administration, due to their injectability which allows to fill irregularly shaped defects. Moreover, they can be chemically modified with adhesion ligands (e.g., RGD) and allow a controlled release of biomodulators (e.g., BMP, TGF-β) or therapeutic agents (e.g., antibiotics, bioactive agents or cells) [17, 18]. Chemical and/or physical crosslinking of hydrophilic polymers are typical approaches to generate hydrogels, and their physico-chemical properties are highly dependent on the crosslinking type and amount of crosslinking agent [17, 18]. The most common method to prepare Alg hydrogels from an aqueous solution involves crosslinking with divalent cations, such as calcium chloride, calcium carbonate, calcium sulfate and sodium hexametaphosphate. Calcium chloride ($CaCl_2$) is one of the most frequently used agents to ionically crosslink Alg for drug delivery systems, due to its high solubility in aqueous solutions, that allows immediate gelation without diffusion of the therapeutic agent [18]. In the presence of divalent cations, the crosslinking of the

polymer chains occurs through the “egg-box” model (Fig. 4b), with G-blocks of the Alg chains providing cavities that facilitate high affinity to divalent cations. So, the divalent cations bind to G-blocks conformation causing dimerization of Alg chains, which enables the formation of a gel network with dimeric junction zones (Fig. 1b) [17, 19]. The gelation rate is a critical parameter in controlling the gelation process, once slow gelation provides uniform gel structures with mechanical integrity [19]. This can be achieved, for instance, by using phosphate buffers (e.g., sodium hexametaphosphate), since phosphate groups present in the buffer compete with calcium ions and slow down the gelation process [17, 19]. Additionally, calcium sulfate and calcium carbonate with lower solubility also prolong the gel formation. The gelation rate is also dependent on temperature; at lower temperatures, the reactivity of ionic cross-linkers is reduced, and the crosslinking becomes slower [17, 19]. The resulting crosslinked network structure has increased order, leading to enhanced mechanical properties [17]. In addition, the shrinkage and flexibility of ionically crosslinked Alg gels can vary significantly depending on their structure, proportions of M-, G- and MG-blocks. For example, gels prepared from Alg with a high content of G residues exhibit high stiffness and brittleness [17, 19]; while, Alg with a predominant M-block content, as a result of high water absorption, forms soft and more elastic gels than those with a higher amount of G-block residues [17, 19].

A critical drawback of ionically crosslinked Alg is the limited long-term stability because of the swelling-disintegration-erosion of these hydrogels in physiological conditions [17, 19]. However, their chemical modifications, like the oxidation or introduction of chemical moieties in the backbone of this polymer, may enhance the solubility, mechanical stability and viscoelastic behavior of the hydrogels [19]. Moreover, the addition of other polymers and/or ceramics components may also influence the solubility, mechanical stability, viscoelastic behavior, as well as, improve their bioactivity and biological activity [23]. In this regard, Balakrishnan et al. produced a promising self-crosslinked oxidized Alg-gelatin hydrogel for neo-cartilage formation for the management and treatment of osteoarthritis [24]. Park et al. showed that hyaluronate-Alg hydrogel, obtained by ionic crosslinking could be useful in regenerating cartilage in a mouse model following subcutaneous injection into the dorsal region with primary chondrocytes [25]. Zhao et al. showed that the mechanical and biological properties (e.g. bioactivity, viability, and osteodifferentiation) were improved by combining calcium phosphate and Alg [26].

1.2.2 Hydroxyapatite for bone regeneration

Synthetic HA ($Ca_{10}(PO_4)_6(OH)_2$) has been extensively used as a bone substitute or as a coating for orthopedic implants due to its crystallographic and chemical similarities with the bony apatite structure (Fig. 5) [16, 27]. In bone biological apatite is typically consisted in Ca-deficient carbonated apatite, and is characterized by the presence of various ions, incorporated within the apatite lattice, by partially substitution of Ca^{2+}, PO_4^{3-} or OH^- ions by bivalent or monovalent cations or anions (e.g. Mg^{2+}, Na^+, CO_3^{2-} or F^-) [16, 27]. Synthetic HA is theoretically composed of 39.68 wt% Ca, 18.45 wt% P; Ca/P wt ratio of 2.151 and Ca/P molar ratio of 1.667. Generally, HA is more stable and less soluble in aqueous media (pH range of 4.2-8.0), than other CaP ceramics. The mechanical properties of HA depend on porosity, density, sintering conditions, crystal size, phase composition [16, 27]. HA is hard but brittle, with a very slow degradation rate *in vivo*, and that is why it should be joined with natural or synthetic polymers, in order to improve its performance as a bone graft substitute [16, 27].

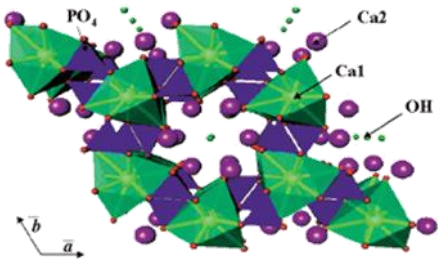

Figure 5 – Schematic representation of hydroxyapatite structure (Adapted from [27]).

On the other hand, HA can be very beneficial for bone applications, because it stimulates the biological response through induction of distinct mediators (e.g., BMPs and ALP) in mesenchymal stem cells (MSCs) [16]. Furthermore, as a major natural inorganic component of bone, HA shows excellent biocompatibility, osteoconductivity and non-inflammatory characteristics [16, 28, 29]. As a bioactive ceramic, the coating of implants with HA stimulates bone growth, where newly formed bone binds directly to HA through a carbonated calcium deficient apatite, at the bone-implant interface [28, 29]. HA surface supports osteoblastic cell adhesion, growth, and differentiation, and new bone is deposited. Moreover, HA contains only calcium and phosphate ions and therefore no adverse local or systemic toxicity has been reported in any study [28]. In addition, HA scaffolds can also serve as delivery vehicles for cytokines, growth factors, biomodulators, with a capacity to bind and concentrate different molecules, *in vivo* [28].

Nowadays, it is well established that nanosized HA particles, nanohydroxyapatite (nanoHA) can mimic the dimensions of constituent components of calcified tissues such as bone and teeth, due to their small particle size, large surface to volume ratio and chemical/electronic synergistic effect, thus improving HA biological response [28, 30]. Furthermore, nanoHA has enhanced bioactivity, bioresorbility and dissolution than coarser crystals, as well as outstanding biocompatibility, osteoinduction and osteointegration properties [28-30]. Some studies have shown that nanoHA is able to enhance bone ingrowth and accelerated bone formation within and around the implanted material [30, 31]. NanoHA powder exhibits improved sinterability and enhanced densification due to a greater surface area, which could improve fracture toughness as well as other mechanical properties [28, 30]. It is possible to enhance both the mechanical and biological performance of HA by controlling the characteristic features of powders such as surface area, crystallinity, morphology, particle size, particle distribution, sintering temperature and agglomeration [28, 30].

Therefore, nanoHA is commonly used as a bone graft substitute for bone tissue regeneration, as well as a coating of metallic implants or filler of small bone defects [28, 30-33]. As bone graft substitute, scaffolds of nanoHA closely simulating spongy bone morphology have been developed and used in clinical settings to increase bone regeneration, in a variety of orthopedic and maxillofacial procedures [30-33]. NanoHA particles have also been applied in controlled release systems due to their binding capability to a wide variety of molecules either pharmaceutical species (e.g., antibiotics, anti-inflammatory drugs, and anticancer and anti-metastatic drugs) or nucleic acids for gene therapy [30, 34]. However, nanoHA lack of flexibility and its brittleness make it difficult to shape on its own into specific shapes for bone tissue engineering. These limitations could be overcome by the incorporation of nanoHA into a suitable polymeric scaffold [28].

1.2.3 Alginate-hydroxyapatite composites

The combination of ceramic particles with polymeric matrices has been extensively investigated in tissue engineering and regenerative medicine [35]. Once, these composite systems can effectively combine the injectability, biocompatibility and biodegradation of polymers matrices and osteoconductive/osteoinductive characteristics, biocompatibility and bioactivity of ceramic particles, improving the physico-chemical properties and biological response of the obtained composites [35]. Furthermore, they can be designed

to adjust to bone defects' shape and geometry, occupying the available space in the damaged organ/tissue, precluding invagination of the neighboring tissues and priming tissue healing [35].

The inclusion of nanoHA particles within Alg hydrogels has been explored by several authors as an attractive approach for bone tissue engineering and drug-delivery application [18, 36-38]. Nabavinia et al. showed that the inclusion of nanoHA into Alg-based hydrogel increased the mechanical strength of the resulting composite and decreased the swelling and degradation rate [37]. These phenomena could occur due to the presence of nanoHA, as a filler agent, that would fill the hydrogel pores, or act as bivalent ion crosslinker, increasing the compressive strength of cell-laden 3D micro-environment [37]. Moreover, they observed that Alg-nanoHA composites showed a higher proliferation, mineralization and ALP activity of micro-encapsulated osteoblast-like cells than the control hydrogel, underscoring the importance of nanoHA bioactivity in the composite hydrogel [37]. In addition, it was observed that encapsulated osteoblast-like cells viability and proliferation was not affected by Alg hydrogel, suggesting that the hydrogel could be a promising injectable and cell-attracting adhesive scaffold for tissue engineering application [37]. In another study, it was observed that Alg-HA nanocomposites enhanced the dental pulp cells differentiation and biomineralization, promoting adhesion, colonization, and matrix deposition of osteoblast-like cells [39]. Cai et al. observed that, *in vivo*, nanoHA and alginate/gelatin composites were able to promote the implant-bone integration, by the formation of new bone and blood vessels, while reducing the inflammation [36]. Other study showed the potential of calcium Alg hydrogel system as a drug delivery vehicle for oral tissue regeneration [38]. The drug release from the hydrogel system was explained by the swelling and degradation ratio of Alg network structure. Moreover, those authors observed that the degradation of this hydrogel system involved Ca^{2+} release into the surrounding medium, which led to an enhance of osteogenesis and osteoinductivity of calcium Alg hydrogel [38].

1.3 Infections associated to orthopedic implants

Bone grafting is one of the most common surgical method used for bone loss repair and bone augmentation in orthopedic and traumatology [40, 41]. However, bone graft implantation needed in cases like osteomyelitis post-debridement, prosthetic joint and orthopedic implant devices (e.g., pins, screws, plates and external fixators), is highly susceptible to microorganisms' contamination, and subsequent development of infection.

These infections have raised serious concern in orthopedic and traumatology due to their strong impact in healthcare systems, the prolonged patient suffering, endorsed by delayed healing, implant removal, or/and amputation, high morbidity, and even mortality [41-43].

Infecting microorganisms can be introduced by continuous or hematogenous contamination [44]. Continuous contamination results from direct contact of resident microorganisms on the patient's skin or mucous membranes, ambient atmosphere of the operating room, surgical equipment and clothing worn by medical professionals or from infiltration into the bone often following injury, surgery or implantation [44-47]. On the other land, hematogenous spread takes place in any time after surgery through the bloodstream contamination of pathogens already resident in the body [44-47].

The implant-related infection rate varies according to the type of bone involved (e.g., hip, knee, ankle or tibia), grade/type of fracture (i.e., closed or open) or type of surgery (i.e., primary or revision) [44, 48, 49]. For instance, the occurrence of infection after prosthesis hip implantation is 0.3-2.4%, while for total knee replacement is of 1-3% [44]. In closed fractures, the incidence of infection after internal fixation is generally lower (0.5–2%) when compared to open fractures, wherein the infection rate may exceed 30% [8, 44, 48]. In revision surgeries, addressed in implant removal, amputation or tissue debridement, the risk of infection is higher as compared to primary ones. For instance, the incidence of infection for total hip arthroplasties revision is 14.8% whereas for total knee revision is 25.2% [50].

Overall, implant-related infections are the result of a complex interaction of various factors such as patient risk factors (e.g., rheumatoid arthritis, immunocompromised states, *diabetes mellitus*, poor nutritional status, obesity, psoriasis, long-term urinary catheterization, advanced age), inherent characteristics of the offending microorganism (e.g., inoculation load, virulence factors), environmental determinants of exposure (e.g., size, timing, and location of the surgical wound) and surgical techniques (e.g., procedures and type of implant) [44, 50].

1.3.1 Implant-infecting microorganisms

Implanted materials are highly susceptible to bacterial and fungal colonization and the consequent infection [40]. These microorganisms are often opportunists taking advantage of the weakening of the body defenses at the implant surface–tissue interface for attaching to tissues or implant surfaces and instigate a biofilm formation and subsequent development of infection [42, 44]. The establishment of biofilm leads to tissue

destruction, systemic dissemination of the pathogen and dysfunction of the implant/bone, resulting in failure of implanted material [18, 44, 51]. Moreover, the contaminated implant can be a reservoir for infection of the surrounding tissue where microorganism can reside intracellularly [18]. In addition, the biofilm increases the pathogenesis of infection since that structure offers protection against host defenses and antimicrobial therapies [18, 52].

In Europe and U.S, the most prevalent microorganisms on implant-related infections are Gram-positive bacteria, mainly *Staphylococcus aureus* (*S. aureus* – 33-43%) and *Staphylococcus epidermidis* (*S. epidermidis* – 17-21%) [53, 54]. Other Gram-positive bacteria, such as *Streptococcus viridans* (*S. viridans*) and *Enterococcus spp*. (mainly *Enterococcus faecalis* – *E. faecalis*) are encountered in 1%–10% and 3-7% of infections, respectively [49, 53, 54]. Gram-negative organisms, including *Pseudomonas aeruginosa* (*P. aeruginosa*), *Escherichia coli* (*E. coli*), *Klebsiella pneumonia* (*K. pneumonia*), *Proteus mirabilis* (*P. mirabilis*) and *Proteus vulgaris* (*P. vulgaris*) are less common than Gram-positive, causing around 6% of cases [45]. Anaerobic bacteria (including *Propionibacterium acnes* (*P. acnes*)) and fungi (mainly *Candida albicans*) are also involved on implant-related infections (2%–3%) [45, 54]. Polymicrobial infections are reported in about 10–11% of the cases, the majority are caused by two bacterial species such as methicillin-resistant *S. aureus* (MRSA) and *Klebsiella* spp. [45, 55]. It should be noticed that bacteria isolation and identification depends always on the quality of the diagnostic procedure and preceding antimicrobial therapy [45].

The infecting bacteria vary depending on the type and the site of the implant (Table 2), as well as the time since implantation [47, 54]. In general, the most dominant etiological agent involved in knee and hip arthroplasty infections are *S. epidermidis*, while *S. aureus* is frequently associated with external and internal fixation infections (Table 2). According to the time since implantation, the implant-related infection could be classified as early (less than 3 months), delayed (3−24 months), and late (more than 24 months) infections [47]. Early infections are commonly instigated by virulent microorganisms, such as *S. aureus*, and by continuous contamination [47, 54]. Delayed infections are often caused by microorganisms of low virulence, such as Coagulase-negative Staphylococci and *P. acnes*, and as the duration of infection extends, biofilms become more resistant to antibiotic therapy and host defenses. Whereas, late infections result from hematogenous spread originating from the skin, respiratory, dental, and urinary tract infections [46, 47, 54].

Table 2 – Prevalence of implant-infecting bacteria in Europe and the U.S according to the type and the site of the implant (adapted from [54]).

Species	Prevalence in Knee arthoplasty infections (%)	Prevalence in Hip arthoplasty infections (%)	Prevalence in infections involving external fixation (%)	Prevalence in infections involving internal fixation (%)
S. aureus	26.4	24.4	47.8	42.5
S. epidermidis	41.8	43.6	15.2	21.9
E. faecalis	2.6	3.5	8.7	5.3
P. aeruginosa	4.4	3.7	14.1	4.3
E. coli	5.3	ND	ND	ND

A common practice in orthopedics is the administration of antibiotics, such as first- or second-generation cephalosporins (e.g. cephalothin, cefuroxime), quinolones (e.g. ciprofloxacin), streptogramins (e.g. quinupristin-dalfopristin), ansamycins (e.g. rifampin), β-lactams (e.g. penicillin, ampicillin), glycopeptides (e.g. vancomycin), and aminoglycosides (e.g. streptomycin), either for prophylaxis and treatment of implant-related infections [51, 56]. However, the widespread use of antibiotics has contributed to increasing of emergency and spread of antibiotic resistance bacteria, which represents a huge threat for human health [53, 57, 58]. Overall, pathogenic bacteria can acquire resistance to antimicrobial agents through chromosomal mutations or through horizontal transfer of mobile genetic elements (e.g. plasmids, transposons and staphylococcal cassette chromosome), in addition to their inherent intrinsic resistance [43, 59].

An alarming increase of Methicillin-resistant *S. aureus* (MRSA), Vancomycin-resistant *S. aureus* (VRSA), Methicillin-resistant *S. epidermidis* (MRSE), Vancomycin-resistant *Enterococcus* (VRE) and extended spectrum β-lactamase producing Enterobacteriaceae (ESBLs), as well as multidrug-resistant bacteria has been found among the strains isolated from implant-related infections [43, 53, 58]. In addition, the pathogenicity of these bacteria is increased by the production of virulence factors (e.g. catalase, hyaluronidase, collagenase, toxins), that play an important role in the degree of severity of the infection, once they promote bacterial adherence to the bone and implant and severe tissue damage [54, 60]. These findings increase the concern about the choice of therapeutic option to treat and control these pathogens [61, 62].

1.3.2 Pathogenesis of implant-related infections

Upon implantation, the material triggers a local immune response, derived from inflammatory activity, granulation tissue formation, and fibrous encapsulation around or

on the surface of such a device, which is susceptible to microbial colonization and infection [53, 54]. Consequently, there is a competition between tissue integration and microbial adhesion and colonization of the implant surface (Fig. 6). Therefore, a prompt integration of biomaterial into host tissues is crucial for preventing microbial adhesion and colonization [54]. In ideal situations, the host cells (osteoblasts, in the bone tissue) adhere to the implant surface and start to proliferate and differentiate with collagenous matrix-production. The calcification of this matrix will eventually result in bone apposition on the implant surface (Fig. 4) [53].

However, if bacterial adhesion occurs before tissue integration, host defenses cannot avoid surface colonization and biofilm formation [54]. Bacterial adhesion is the first step and has a pivotal role in the pathogenesis of implant infections. Since the biofilms can also contribute to the recalcitrance of implant infection, which is a source of bacterial dissemination to other body sites [54].

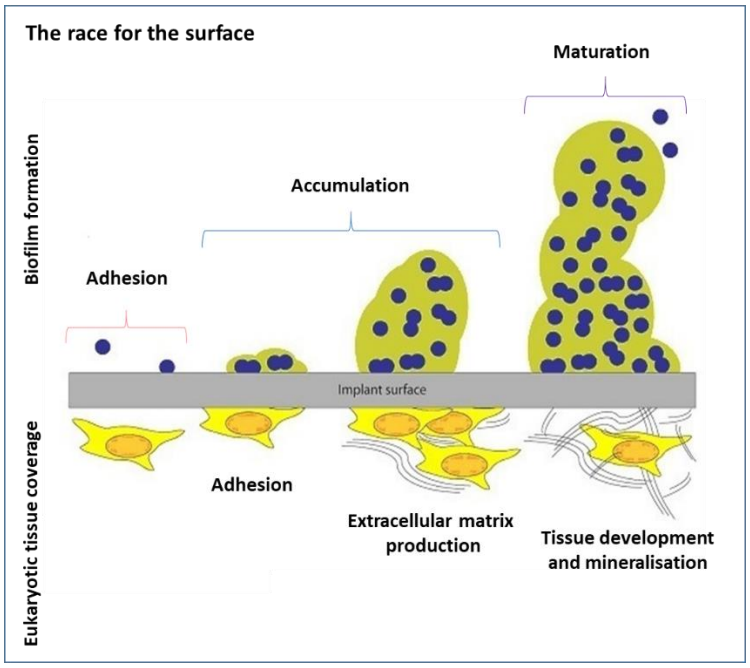

Figure 6 – Schematic representation of the biofilm formation and eukaryotic cell colonization with subsequent tissue development surrounding the implant surface (adapted from [53]).

So, after implantation, host extracellular matrix proteins (e.g. collagen, fibrinogen, fibronectin, and elastins) rapidly coat the surface of the implant and, simultaneously, the planktonic bacteria (bacteria living as free-floating cells) are passively adsorbed onto the

material surfaces (Fig. 6) [53, 54]. Then, adhesins, that act as agents of anchorage to surface and invasion agents in the process of bacterial internalization in the host cells, mediate the irreversible bacterial attachment to the surface (adhesion phase) [51, 53, 54]. During the accumulation phase the bacterial cluster occurs (formation of microcolonies), which proliferate and colonize the implant surface. During this period, bacterial cells produce extra polymeric substances (EPS), which act as retention of nutrients and as a protective barrier against to antimicrobial agents and immune host response [53, 54]. After this period, the biofilm becomes mature, and it secretes virulent factors (e.g. toxins) which disrupt the biofilm matrix, leading to dispersal and dissemination of bacterial clusters to elsewhere in the body (maturation phase) [53, 54].

Although pathogens such as *S. aureus*, *S. epidermidis* or *E. faecalis* strains are generally extracellular, they can internalize into osteoblasts cells and escape immune response, increasing the pathogenesis of implant-related infections (Fig. 7). When internalized, these bacterial species can provoke osteoblast apoptosis by inducing the expression of TNF-related apoptosis-inducing ligand (TRAIL) and activation of caspase 8. The osteoblast apoptosis induces the release of internalized bacteria, which can grow and colonize bone and implant surfaces, contributing to the recalcitrance of implant-related infections [54].

In addition, bacteria such as *S. aureus* and *E. coli* are able to produce exotoxins, like hemolysins and leucocidins, which protect the bacteria from host immune response (Fig. 7). Those exotoxins can inhibit leukocytes activation, opsonization, and chemotaxis; protect the bacterium from leukocyte-derived products (e.g., reactive oxygen species, enzymes and antimicrobial peptides (AMPs)), and disassemble neutrophil extracellular traps (NETs), thus potentiating the bacterial colonization in bone and implant surfaces [54].

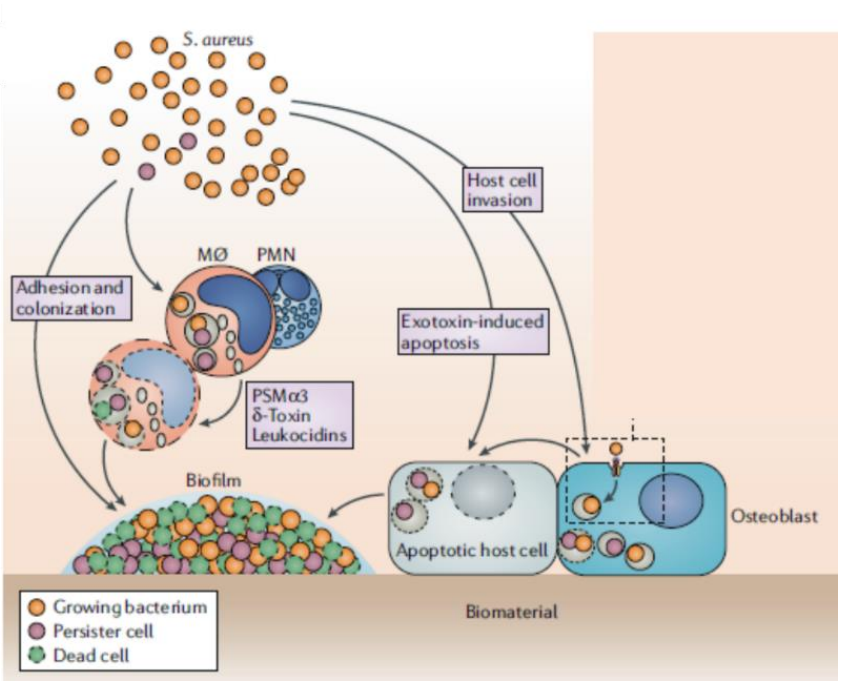

Figure 7 – Strategies of bacteria to invade host immunity and promote biofilm recalcitrance and formation (Adapted from [54]).

1.4 Anti-infective biomaterials as a preventive strategy

Currently, prophylactic systemic antibiotic therapy is administrated as a preventive and therapeutic measure to patients to whom an implant is applied [63]. However, this therapy entails many disadvantages including the need of defining time and frequency of administration, the low drug concentration reaching the target site, and the corresponding limited antimicrobial activity at the target site [63]. Alternatively, the use of local strategies as vehicles for the delivery of antimicrobial agents has emerged as a regular adjunct in the prevention and treatment of bone graft-related infections [54, 63, 64].

A broad variety of concepts and approaches have been developed to obtain biocompatible and osteointegrative biomaterials endowed with anti-infective properties, i.e., capable to prevent bacterial adhesion and colonization of bone tissue and implant surfaces, as well as to create a bacteria-free environment around the implant (Fig. 8) [42, 64]. According to their strategy of action, anti-infective biomaterials can be classified in three groups: passive surfaces, active surfaces and multifunctional surfaces [64], that are described in detail below.

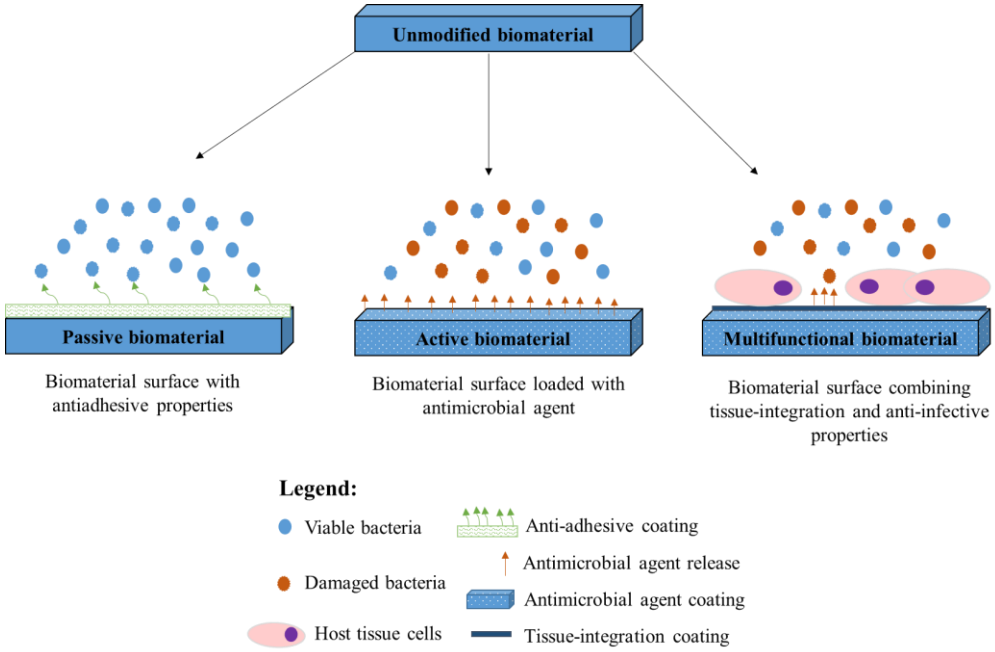

Figure 8 – Different strategies to achieve anti-infective biomaterials surfaces (Adapted from [51]).

1.4.1 Passive surface approach

Microbial adhesion depends strongly on the physico-chemical properties of the materials integrating the implant surface. Thus, modifications of material surface chemistry, functional groups, roughness or topography may result in a substantial change to their susceptibility to bacterial adhesion and colonization [41, 64]. Thus, the passive surface approach consists in the chemistry and/or surface topography modification, aimed at preventing or reducing bacterial adhesion, without releasing bactericidal agents to the surrounding tissues [64].

The biomaterial surface wettability may influence protein adsorption, platelet adhesion/activation, blood coagulation, cells and bacterial adhesion to the implant [65]. In general, hydrophobic material surfaces are more prone to bacterial adhesion and proliferation than hydrophilic ones, due to hydrophobic interactions occurring at implant-bacteria surfaces. In contrast, hydrophilic material surfaces present, generally, anti-infective properties due to the repulsive forces arising from strongly bound water at the surface, which limits the contact between the bacterium and potential surface adhesion sites [63, 65, 66].

Some studies showed that ultraviolet (UV) irradiation increased the hydrophilic properties of titanium alloy surfaces, promoting inhibition of bacterial adhesion without

compromising the cytocompatibility on the implant [66, 67]. Moreover, the adsorption of hydrophilic polymers, based on poly(ethylene glycol) or poly(ethylene oxide), to the implant surface could also prevent bacterial attachment [68].

Recently, several studies have focused on obtaining material surfaces with extreme wettability, super-hydrophobic or super-hydrophilic, as potential anti-infective surfaces [63, 69]. Super-hydrophobic surfaces can present bacterial repellency properties, through their high surface roughness and low surface energy, that creates a stable or metastable air layer at the material surface (called "lotus effect"), where debris and pathogens are removed as water contacts and subsequently rolls off the surface [69-71]. Alternatively, extremely water-attractive surfaces can also exhibit anti-infective performance via their super-hydrophilicity, that is able to form a dense layer of water molecules, which weakens the interaction between bacteria and substratum [69, 71].

Besides chemistry, the biomaterial structure and morphology can be modified to produce anti-adhesive surfaces. Theoretically, implant surfaces with higher values of roughness could, via increased surface area, potentiate the bacterial colonization and provide shelter to bacteria, protecting them from shear stress [9, 72, 73]. Some studies have shown that surfaces roughness below 0.2 μm induced low susceptibility to bacterial attachment [26, 69, 72]. This phenomenon could be explained by: i) the size of bacterium, that generally is over 0.2 μm; ii) the micrometric and nanometric peaks and valleys of the implant surface can affect the organization of bacterial cells and, hence, their intracellular transduction signaling pathways, and iii) changing of surface properties such as wettability [9, 72-75]. Therefore, engineered materials have been explored to create surfaces with controlled roughness and well-defined topographic patterns for the reduction of biofouling and subsequent biofilm formation [66, 67]. Micro- and nano-fabrication techniques such as electrochemical oxidation, electron beam evaporation, photolithography, soft lithography, micro-contact printing, hot embossing and microfluids have been used to produce antifouling surfaces with microorganism-repellent and tissue-friendly properties [66, 69, 76]. For instance, Pucket et al. showed that on nano-rough titanium surfaces produced by electron beam evaporation, the amount of adhered *S. aureus*, *S. epidermidis* and *P. aeruginosa* was lower as compared to conventional titanium surfaces [74]. Moreover, they observed that the hydrophilicity of nano-tubular and nano-textured titanium surfaces, produced through anodizing processes, also contributed to increasing the antifouling surfaces [74]. Other authors have clearly shown that nanostructured titanium increased osteoblast proliferation and enhanced

osseointegration while decreasing bacterial attachment onto the implant when compared to conventional titanium [77, 78].

Another strategy to achieve lower bacterial adhesion to biomaterials consists in the treatment of surfaces with serum, plasma or proteins solutions that induce modifications in the physico-chemical characteristics of the biomaterials surfaces or compete with host adhesins adsorption. Upon implantation, biomaterials are covered with serum or tissue proteins from blood and interstitial fluids, such as albumin, fibrinogen, fibronectin, laminin, denatured collagens, serum and plasma, that can promote or inhibit the bacterial adhesion to a specific biomaterial [63, 64, 79, 80]. An et al. using a rabbit model, showed that albumin-coated implants presented a lower infection rate than non-coated implants [81]. This inhibition can be explained through binding to the bacterial receptors or by changing the substratum surface to a more hydrophilic behavior [82]. Serum and plasma coated materials also affected negatively the attachment of bacteria due to the same reasons [82].

More recently, novel strategies include the production of self-assembled mono- or multilayers, either surface grafting or hydrogels, with excellent anti-adhesive properties [65, 83]. For example, Zhang et al. produced 2-methacryloyloxyethyl phosphorylcholine-containing composite, by the protein-repellent method, with strong protein- and bacteria-repellent activity [84]. Polymer brush-coatings are another method to improve anti-infective properties to implant surfaces, as shown by Nejadnik and co-workers [85].

1.4.2 Active surface approach

The active surface strategy consists in the development of biomaterial surfaces with antimicrobial properties, through the incorporation of antimicrobial agents (such as metals, antibiotics, antiseptics or antibacterial peptides) that may act by the delivery of high local concentrations, or may have a direct or synergistic antibacterial activity, at the biomaterial-tissues interface, without compromising the characteristics of the bulk material [63, 64, 86]. These surfaces can be classified according to their functional principle as: (i) contact-active surfaces, due to covalent immobilization of active agent on the surface of the implant in order to prevent the bacterial attachment; or (ii) active-releasing surfaces, where the antimicrobial agents are entrapped in the bulk or in the coating of a biomaterial, to be released upon interaction with its surrounding environment and/or stimuli, killing the planktonic and sessile bacteria [64, 87].

Biocidal substances can be mixed with ingredients during the phase of production, *a posteriori* absorbed in permeable or porous biomaterials, covalently bound to functionalized coatings, incorporated in self-assembling mono/multilayer organic coatings, among others [88]. The drug-release can consequently occur by different modalities: diffusion to the aqueous phase, erosion/degradation of resorbable loaded matrices or hydrolysis of covalent bonds. Systems with different delivery kinetics of the active principle have been obtained, depending on the stability of the molecular bonds or on the rate of biodegradation/bioerosion of the matrices entrapping the antimicrobial agent [88].

The antimicrobial metal ions (e.g. Ag^{+}, Cu^{2+} and Zn^{2+}) can be used as dopant in solids, in the formulation of alloys or glasses or hydrogel materials, and in the form of micro- and nanoparticles by sputtering-based deposition [63, 75, 89]. The metals antimicrobial activity is closely linked to the ionic or nano form, rather than to the bulk material. The antimicrobial activity of these metals is dose-dependent, and after their dissolution as ions, they can interfere with critical enzymes of the respiratory chain, cell membrane permeability, hydroxyl radical formation, and subsequent DNA damage [64]. Though metals show attractive characteristics as antimicrobial agents, further information is needed regarding both their stability in physiological fluids and their biological safety. Some studies have shown that such metals can adversely affect surrounding cells and lead to potentially harmful accumulation in distant locations, especially in the form of nanoparticles, being their cytotoxicity also dependent on the dose [90, 91].

Another efficient approach for prevention of implant-related infections is the loading of organic components (e.g. antibiotics, antiseptics or peptides) onto implant coatings. These compounds can be adsorbed to the surface by immersion in organic solutions, dip/spray coating, or can be covalently linked on the implant's surface [64, 92]. Adsorption of antiseptics or antibiotics onto implant surface has been shown, by several authors, to be an effective antimicrobial strategy [93-95]. However, adsorbed molecules are often weakly bound to the implant surface and can be rapidly desorbed under physiological conditions [92]. The leaching of the antimicrobial agent from the surface into the surrounding area following implantation may provide relatively short-term potency in the local tissue area [92]. Covalent coatings present advantages over non-covalent ones, such as reduction of local toxicity and a long-lasting antibacterial activity [96, 97]. Gerits et al. showed that titanium surfaces functionalized with a new bioactive compound, SPI031, were able to reduce significantly *S. aureus* and *P. aeruginosa*

viability both *in vitro* and *in vivo* without affecting adhesion or proliferation of cells involved in osseointegration and bone repair [96]. Antibiotics and antimicrobial peptides have also been covalently linked to implant surfaces to allow cell attachment while inhibiting bacterial colonization [92, 97]. Townsend et al. showed the potential of antimicrobial peptides-coated HA as an anti-infective surface against *S. aureus*, *S. epidermidis* and *P. aeruginosa*, with a long-term sustained antimicrobial activity of the surface [92]. However, covalent bindings only prevent bacterial adhesion and colonization over the surface of the implant. These surfaces are not able to create a bacteria-free environment around the implant, which could limit their clinical application [63]. To overcome this issue, combinations of antibiotics or antiseptics with polymers have been proposed either alone or in association with a particular mechanism of controlled release [63]. Drug-loaded biodegradable polymers-coated biomaterials have been developed to improve the prophylaxis against implant-related infections, and prolong the drug release kinetics and biodegradability, minimizing their effect on bone tissue regeneration [98-100]. However, the long-term impact of permanently coated implants with bioactive agents often entails some problems regarding the induction of bacterial resistance, local cytotoxicity, immunoreactivity, and genotoxicity. These can potentially affect host cell viability in peri-prosthetic tissues and, in the presence of specific tissue tropisms of the released chemical species, even in cells residing at distant anatomic sites [62, 88].

1.4.3 Multifunctional anti-infective approach

Osseointegration is very important to the success of orthopedic devices implanted within bone. The concept of multifunctional surface coating has been explored in order to develop an anti-infective, self-responsive, self-repairing and tissue friendly biomaterial implant [41]. The multifunctional biomaterial should present: i) antimicrobial attachment activity, preventing the initial microorganism's adhesion; ii) antimicrobial delivery system, preventing the bacterial colonization and proliferation on the surrounding of the implant; and iii) selective biointeraction pattern, allowing the proliferation and growth of adequate cell populations [41, 63]. Therefore, these biomaterials should possess synergistic passive and active anti-infective functionalities while simultaneously enhancing the healing and restoration of tissue homeostasis. Moreover, these materials should be easily applied and effective, have optimal temporal and dosing release profiles,

facilitate (or even promote) adjacent tissue integration, no local or systemic toxicity, and be cost-effective [41, 63, 75].

Several technologies for multifunctional surfaces have been proposed and tested [38, 75, 101, 102]. The first step in the development of multifunctional surfaces is to make a bioactive surface. This property can be obtained – for bone tissue applications – by different ways, including the use of HA obtained by cold spraying and dip coating, calcium phosphates cements introduced into reservoirs obtained on metallic implants, composite coatings with chitosan obtained by electrochemical methods, bioactive glasses co-deposited with chitosan electrophoretic deposition and bioactive layers obtained by sputtering or chemical oxidation [75]. The second step consists of conferring antimicrobial activity to the implant surface, through the loading of antimicrobial agents. These agents can be loaded by solvent evaporation, spreading or dipping on the prepared bioactive coatings, co-deposition in the electrophoretic process, loading in additional carriers or inclusion in the bioactive precursor of the coating [75]. Chen et al. designed a multifunctional biomaterial, composed by PCL/chitosan nanofibers with antibiotic-eluting micropatterns, which was able to effectively kill *S. epidermidis* and prevent biofilm formation without putting at risk the osteogenic properties [103].

All these functionalities are required for an excellent physiologic osseointegration of the implanted biomaterial, avoiding the risks of chronic inflammation or bacterial contamination [75].

1.5 Bacteriophages as antibacterial agents for clinical therapy

As previously referred, antibiotics are widely employed for the prevention and treatment of peri-prosthetic infections [75]. In fact, despite wide research on several antibacterial surfaces, the antibiotic-loaded implant materials are the only approach that has reached the market up to now [75]. One of their main advantages is their widely recognized and accepted effective antibacterial activity [75]. However, their main drawbacks are the increasing risk of bacterial resistance, particularly when associated to an initial burst release, followed by a prolonged releasing values below the minimum inhibitory concentration (MIC), which increases the risk of resistance development, and a potential adverse effect on osseointegration [75].

The emergence of bacteria resistant to antibiotics and their ability to produce virulence factors have contributed to enhancing the pathogenicity and severity of orthopedic

implant-associated infections [43]. According to World Health Organization (WHO) and Centers for Disease Control and Prevention (CDC) these pathogens are classified as a serious threat to public health due to confining the therapeutic options, being crucial the development and design of new alternatives to prevent and manage implant-related infections [61, 62, 104].

Bacteriophages (phages) are viruses that exclusively infect bacteria, without modifying the established commensal microbiome, and can act as bactericidal agents. Phages have recently emerged as an alternative approach to current antimicrobial chemotherapy in implant-related infections, mainly because of their high-specificity, their ability to replicate at the site of infection, and unique properties to fight multidrug-resistant bacterial strains [105-112].

1.5.1 Phages particles

Phages are viruses capable of infecting and killing bacteria, through a dynamic phage-bacteria interaction [113, 114]. They are the most abundant biological entity in ecosystems on Earth (from 10^{30} to 10^{32} virions), being widely distributed throughout nature, urbanized locations and in the human/animal body (Table 3) [115, 116].

Table 3 – Phages distribution throughout nature, urbanized places and animal body (Adapted from [116]).

Phage in nature	Soil Fresh water Ocean Plants
Urbanized places	Hospital Wastewater treatment plants
Animal Body	Digestive tract Vagina Respiratory and oral tract Skin Mucosal epithelium

Phages infect the bacterial cells by recognizing specific receptors at the bacterial surface and inserting their genetic material [116]. It is estimated that there are ten different bacteriophages for every bacterial cell, some of which are highly specific for their bacterial host, either monophages (recognizing only one type of receptor) or polyphages (displaying a broader host range and recognizing more than one type of receptor) [116].

As phages are entities totally devoid of any metabolic machinery, they use the host biochemical machinery to replicate new phages' particles and enzymes, which can promote the bacterial lyse, depending on the life cycle [113, 116].

Phage particles can be tailed, polyhedral, filamentous or pleomorphic, depending on their morphology [114, 116]. The majority exhibits a well-defined three-dimensional structure, with an icosahedral protein capsid that encloses the genetic material in its core, and a tail with fibers containing receptor binding proteins, responsible for recognizing specific molecules at the surface of the bacterial membrane [114, 116].

In relation to genetic material, phages can be divided into four major groups: single-stranded DNA phages (ssDNA), double-stranded DNA phages (dsDNA), single-stranded RNA phages (ssRNA), and double-stranded RNA phages (dsRNA) [117].

According to the International Committee for Taxonomy of Viruses (ICTV), more than 90% of identified and well-studied phages belong to *Caudovirales* order, possessing, generally, deoxyribonucleic acid (DNA) genomes and a complex morphology with a capsid of regular symmetry (the head) and a helicoidal symmetry (the tail) (Fig. 9) [118, 119, 120, 121]. The members of this order are grouped into five families: *Myoviridae* (with a long and contractile tail), *Siphoviridae* (with a long and non-contractile tail), *Podoviridae* (with a short and non-contractile tail), *Herelleviridae* (with a long and contractile tail) and *Ackermannviridae* (with a long and contractile tail), according to the ICTV (Fig. 9) [117, 118, 119, 120].

1.5.2 Mechanisms of action and life cycles

Depending on phage nature, lytic, filamentous and temperate, phages can have different mechanisms of action. Virulent phages have bactericidal activity and have the ability to replicate exponentially and release new viral particles *in situ*, thus making them potentially good candidates for antibacterial therapy [121, 122]. Temperate phages reside as stable elements – called prophages – inside the host cells, as a free plasmid molecule, or integrated into the host chromosome [121, 122]. Filamentous phages induce the release of the progeny viruses by extrusion or budding without lysis of the host cell over several generations, having a strong impact on many aspects of biology, pathogenesis and physiology of their host bacteria [123]. Many questions related to filamentous phages, such as the structure of the virion capsid, mechanisms of infection, assembly and replication, remain unanswered [123], and will not be considered in this text.

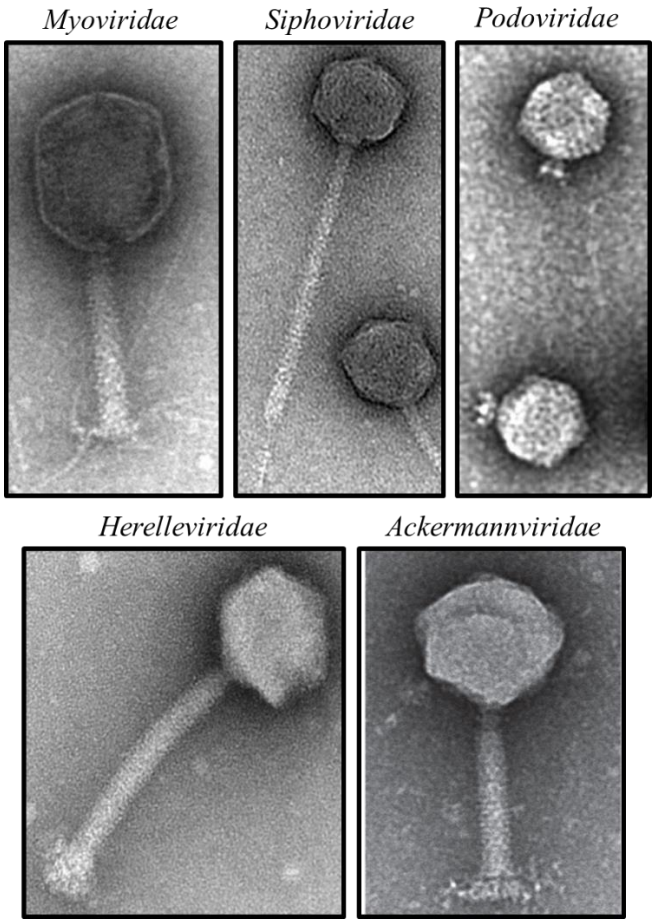

Figure 9 – Example of phage particles of the order *Caudovirales* divided into families: *Myoviridae, Siphoviridae, Podoviridae, Herelleviridae* and *Ackermannviridae*, according to the ICTV [117, 118, 119, 120].

Overall, the phage life cycle can be classified as lytic or lysogenic (temperate) (Fig. 10a). Virulent phages have lytic cell cycle and temperate phages can develop both lytic or lysogenic cycles [114, 115, 121, 122]. The lytic cycle results in the lysis of the bacterium accompanied by the release of multiple phage particles (Fig. 10a). The new progeny phages produced by the host bacterium can spread to infect other bacterial cells. The lytic cycle consists of the following sequential steps: adsorption, penetration, latent period, maturation, and lysis (Fig. 10a). Initially, the infection starts with the binding of phage receptor-binding proteins to receptors at the bacterial surface (e.g. lipopolysaccharides, flagella, pili, capsules or the plasma membrane) [114, 115, 121, 122]. The phage adsorption consists of phage-bacterium chemical and physical interaction, mediated through the environment and some co-factors, such as Ca^{2+} and Mg^{2+} ions. During the penetration phase, enzymes like lysozymes or transglycosylases, located in the tip of the phage tail, degrade a small portion of the peptidoglycan layer and

disrupt the membrane of bacterial cell, in order to inject the phage nucleic acids inside of bacterial host [114, 115, 121, 122]. Mechanisms of this process are specific for each phage, or phage group. Electrochemical membrane potential, ATP molecules, enzymatic splitting of peptidoglycan layer or all three factors may be vital for penetration of genetic material inside the bacterial cell [114, 115, 121, 122]. The expression of phage proteins begins immediately after the entry of the viral genome. They are needed to replicate the phage genome and to modify the cellular machinery so that the synthetic capacity of the cell is diverted to phage replication [114, 122]. During this latent period the synthesis of several copies of their genetic material takes place. Each of these copies can then be used for transcription and translation of the second set of proteins, that make up the capsomeres and the various components of the tail assembly [114, 121, 122]. At the end of the replication process, the components are assembled into virions, where, capsid and tails are assembled and are joined together after genetic material encapsulation (maturation process) [115, 121, 122]. The lytic cycle ends up with the release of infectious phages, , by hydrolysis of the bacteria cell wall (lysis phase) [115, 121, 122]. In this phase, holin (that assembles pores in the inner membrane to let the endolysin reach the peptidoglycan layer) and endolysin (degrades the cell wall peptidoglycan) disrupt the cell membrane and cell wall, respectively, causing the bacterial cell to burst and phages are released into the surrounding medium, which are capable of starting the cycle over again and infecting new susceptible host cells [121, 122]. Furthermore, phages propagation and persistence depend always on its host bacterial pathogen presence, which contributes to regulate phages number in direct relation with pathogen level and facilitates diffusion into the surrounding areas in a gradient dependent on pathogen availability [114, 115, 121].

In the lysogenic cycle (Fig. 10a), the phage genome is integrated into the host bacteria genome, leading to a permanent association as a prophage with the cell and all its progeny [114]. During lysogeny, temperate phages neither produce virions nor lyse bacteria, but they are replicated into host bacteria. The host bacterium may carry prophage in the quiescent state for many generations, due to the synthesis of a repressor protein that blocks the transcription of its own genes and also those of closely related phages. However, when a prophage escapes regulation by the repressor, its genomic material is cut free, allowing it to embark upon a lytic cycle, producing new copies of phages that leading to lysis and release of progeny phages [114, 122]. This reactivation process is usually triggered when the host cell is placed under adverse environmental conditions, e.g., DNA-damaging agents, such as ultraviolet light or mitomycin C [121].

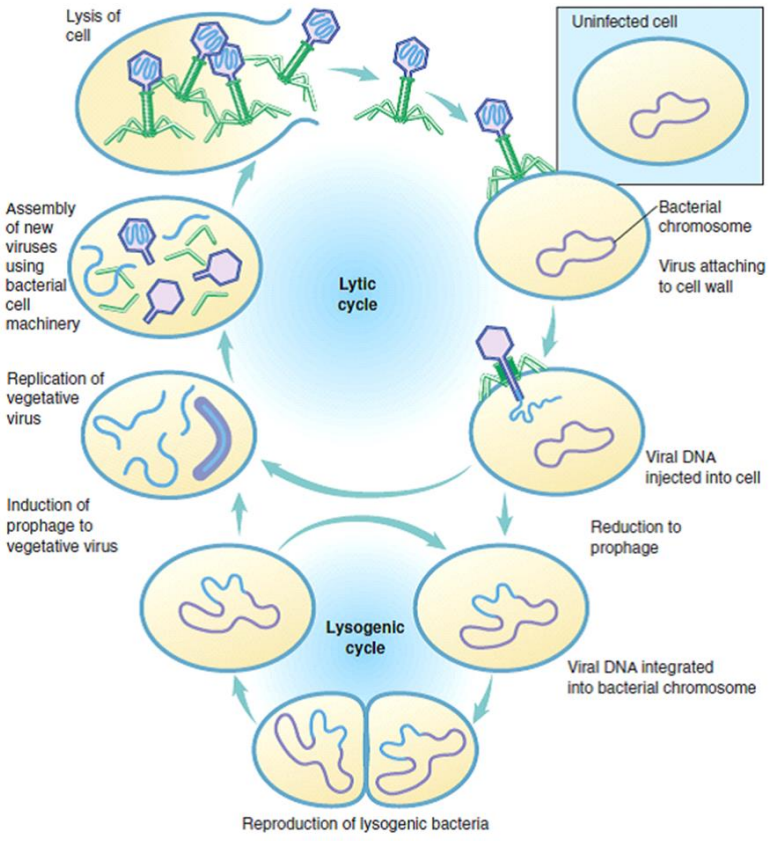

Figure 8 – Phages life cycles depicting the lytic and lysogenic pathways of a typical phage when infects a bacterial cell (Adapted from [114]).

However, with the excision of prophage genomic material, the excision of bacterial genes adjacent to prophage occur naturally. These may be incorporated into the infectious phages and then transferred to subsequent host cells [114, 122]. Therefore, temperate phages may potentiate the increasing of the pathogenicity or virulence of lysogenic bacteria, through acquisition and transference of virulence and resistance genes [115, 122]. For instance, Shiga toxins found in *E. coli* and cholera toxin in *Vibrio cholerae* are two toxin genes acquired by transduction process [122].

1.5.3 Phage therapy

Phage therapy is based on the therapeutic use of phages to prevent and treat pathogenic bacterial infections both in humans and animals. The high specificity and bactericidal effect of phages for target bacteria, make them good candidates for antibacterial therapy, since they only replicate inside their specific host and promote host bacterial lysis without interfering with commensal microbiome [115, 121]. Furthermore, phages are capable of

replicating exponentially and increase the viral progeny where hosts are located, meaning that they are able to spread and infect other target bacteria nearby [115, 121, 124, 125]. In addition, phages are not pathogenic for eukaryotic cells, despite being able to interact with phagocytic cells and be adsorbed through mammalian cells' surface receptors, they are not threatening [115, 121]. Another great characteristic of phage therapy is the capacity of phages to lyse bacteria present in a biofilm, mucous membrane and medical wounds, once they can produce enzymes that are able to degrade the extracellular polymeric substance of biofilms allowing the phages to reach and kill bacterial cells. Finally, phages are ecologically safe, and present low-cost isolation and production [115, 121].

Although phage therapy has many advantages, there are also a number of drawbacks to this approach. The great specificity of phages is both an advantage and a limitation, once prior to their application, it is necessary to determine which bacteria are causing the disease. A way to solve this setback is the use of phage cocktails, as this widens the range of action [115, 121]. The pharmacokinetics of phages is depending on phage dose, burst size (large progenies in a short time) and virulence, which in turn depends on the bacterial density. So, for clinical phage administration is always required to have a knowledge of phages genomes and pharmacodynamics (interactions between phage and bacteria), in order to select the virulent phage with greater burst size and broader spectrum of action [115, 121]. Additionally, there are some questions regarding the possibility that phages themselves or their products and enzymes might be recognized by the immune system and induce immune responses. However, Roach et al. defined the concept of "immune-phage synergy" [126], which means that the local innate immune response is stimulated by phage- and bacterial-derived pathogen-associated molecular patterns released after bacterial lysis, although this response could promote bacterial clearance and help the phages in treating bacterial infections [126, 127]. Additionally, phages can dissipate very quickly throughout the body reaching almost every organ, but the immune system would swiftly clear systemic phages and thus the use of phages for an extended period would not be possible. One strategy to improve the lifespan of phages in an organism would be the use of biomaterials that do not interfere in phage activity, as liposomes or alginate capsules but ensure their persistence/release at the desired location [126, 127]. Another drawback regarding phage therapy is the possible emergence of phage-resistant bacterial strains, which could hamper the outcomes. Some of these mechanisms of resistance are associated with phages' receptors, e.g., bacteria can hide, change, or even lose phage

receptors. If the loss of the receptor occurs, the phage cannot recognize the bacteria, and, subsequently, no new phages will be generated [115, 128]. However, an interesting way to increase phage fitness against bacteria and to reduce the emergence of resistance could include the combination of phages with antibiotics, since phages can kill antibiotic-resistant variants and vice versa [115, 128]. Besides, these combinations can promote a phage-antibiotic synergistic effect, increasing the phage infectivity as a result of the administration of sub-lethal concentrations of antibiotics. Therefore, the success of combinations depends on the target cell, phage and antibiotic type. It is further important to ensure that phages and antibiotics detect different regions of the union of pathogenic bacteria to ensure the effectiveness of the treatment [115, 128]. In addition, the use of phage cocktails can also to solve issues relating to resistance and a low range of action [115]. However, their application can be challenging in terms of regulatory approval due to phage structures, life cycles, and genomes organization [129]. Genetically engineered phages may be possible to overcome many of these limitations. The engineering of specific phages and components has been facilitated by the ever-growing abundance of fully sequenced phage genomes in public databases and by researching to elucidate the structures of phage components and the interactions between phages and their host bacteria [129].

Above all, the most urgent point that should be solved is the scarcity of basic information related to doses, administration routes, protocols, and the correct mode of application of this therapy [115]. Besides, regulatory schemes and guidelines specific should be established for the safe and sustained use of phage therapy in the prophylaxis and treatment of infectious diseases [115].

1.5.4 Clinical application of phage therapy

Phage therapy has been used not only to prevent and treat human bacterial infections, but also to control plant diseases, detect pathogens, and assess food safety [129]. Phage therapy has been used since 1915-1917, mainly in eastern European countries following different guidelines for clinical trials [129]. Currently, in some European countries and in North America, there has been some efforts to build guidelines for clinical trials for the use of phages in clinical practice. Currently, there is an European project under clinical trial, called Phagoburn, founded in 2013 by the European Commission, which has used a phage cocktail for the treatment of burn injuries infected with *E. coli* or *P. aeruginosa* [130]. An increasing number of works have been published showing the therapeutic

application of phages, in the cure and control of bacterial infections such as diabetic foot ulcers, acute kidney injuries, ulcers and chronic otitis [131-134].

The efficacy and accuracy of phage therapy through parenteral (e.g. intramuscular, subcutaneous or intraperitoneal) or topical administration of a phage-containing solution has been sustained in several animal experimental studies [106, 111, 112, 135-139]. For instance, Capparelli et al. showed that the intravenous and subcutaneous administrations of phages active against *S. aureus*, including MRSA, were able to reduce the bacterial load and prevent abscess formation, protecting mice from a systemic *S. aureus* infection [135]. In another study, using a mouse model of *P. aeruginosa* keratitis, Furusawa et al. observed a great reduction of bacterial proliferation with a low-dosage of phages applied to the corneal surface [137]. Drilling et al. showed that the phage therapy could be a promising approach to treat sinonasal *S. aureus* biofilms, by the topical application on frontal sinus region of sheep [138]. The potential of systemic administration of phage solutions in treating *in vivo* orthopedic infections has also been proven [106, 112, 139]. Kishor et al. reported the eradication of both acute and chronic osteomyelitis caused by MRSA, in a rabbit model, by the systemic administration of *S. aureus*-specific phages [139]. Fish et al. injected *S. aureus*-specific phages into a distal toe phalanx and surrounding tissue, and observed an efficient antibacterial activity, leading to the complete resolution of the infected ulcer and associated osteomyelitis, in humans [112].

The local administration based on phages loaded to medical devices has emerged as an alternative approach in the control and treatment of medical device-related infections, with interesting studies being reported in the literature [107, 108, 110, 140-142]. Fu et al. showed that a *P. aeruginosa*-specific phage cocktail could be included into hydrogel-coated silicone catheters, reducing the attachment and biofilm formation by *P. aeruginosa*, in a laboratory model system [140]. In another study, it was investigated the covalent immobilization of *P. aeruginosa*-specific phages on polycaprolactone nanofibers, as a potentially effective antimicrobial construct, which was laundry resistant and non-toxic dressing for application focused on skin infections [141]. At the surface, this dressing revealed the immobilization of phages' capsids on polycaprolactone nanofibers, with oriented phage tails to interact with bacteria, showing an excellent bacterial reduction (6 log) [141]. Liposome-encapsulated phages were used as orally administered phage therapy to treat *Salmonella* infections in commensal broilers. This system allowed a prolonged intestinal residence time of the encapsulated phages and their efficient release from liposomes in the intestinal tract, resulting in potent and long-lasting

therapeutic effects [142]. Other authors investigated the treatment efficacy of liposome-encapsulated phages against established *K. pneumoniae* infections in a murine pneumonia model. Liposome-entrapped phages were effective in treating infection, even when therapy was delayed by 3 days after induction of pneumonia [143]. Some experimental studies using phages-loaded biomaterials for local delivery to treat orthopedic implant-related infections have been also performed with promising results [107, 108, 110]. Meurice et al. tested the *in vitro* feasibility to impregnate ceramics, hydroxyapatite and beta-tricalcium phosphate, with *E. coli*-specific phages to induce local antibacterial effects against *E. coli* strains [110]. The loading into and releasing from ceramics was dependent on ceramic porosity and composition, and loaded phages were able to promote *E. coli* lysis, indicating that this system could be used for prophylactic treatment, in bone surgery [110]. Kaur et al. assessed *in vitro* and *in vivo* the efficiency of biopolymer impregnated with linezolid and phages to prevent and treat MRSA colonization [107, 108]. This dually coated implant was able to prevent and treat implant-associated infections both through *in vitro* and *in vivo* experiments. This local delivery system was able to attack the adhered as well as surrounding MRSA present near the implant site [107, 108]. Nonetheless, all these experimental studies focused only on the phages release and antimicrobial activity, without exploring simultaneously the potential combination with a regeneration inductive biomaterial.

REFERENCES

[1] Tozzi G, De Mori A, Oliveira A, Roldo M. Composite Hydrogels for Bone Regeneration. Materials 2016;9.

[2] Gao CD, Peng SP, Feng P, Shuai CJ. Bone biomaterials and interactions with stem cells. Bone Res 2017;5.

[3] Dimitriou R, Jones E, McGonagle D, Giannoudis PV. Bone regeneration: current concepts and future directions. Bmc Med 2011;9.

[4] Sadat-Shojai M, Khorasani MT, Dinpanah-Khoshdargi E, Jamshidi A. Synthesis methods for nanosized hydroxyapatite with diverse structures. Acta Biomater 2013;9:7591-621.

[5] Crockett JC, Rogers MJ, Coxon FP, Hocking LJ, Helfrich MH. Bone remodelling at a glance. J Cell Sci 2011;124:991-8.

[6] Long FX. Building strong bones: molecular regulation of the osteoblast lineage. Nat Rev Mol Cell Bio 2012;13:27-38.
[7] Florencio-Silva R, Sasso GRD, Sasso-Cerri E, Simoes MJ, Cerri PS. Biology of Bone Tissue: Structure, Function, and Factors That Influence Bone Cells. Biomed Res Int 2015.
[8] Maruotti N, Corrado A, Cantatore FP. Osteoblast role in osteoarthritis pathogenesis. J Cell Physiol 2017;232:2957-63.
[9] Deschaseaux F, Sensebe L, Heymann D. Mechanisms of bone repair and regeneration. Trends Mol Med 2009;15:417-29.
[10] Raggatt LJ, Partridge NC. Cellular and Molecular Mechanisms of Bone Remodeling. J Biol Chem 2010;285:25103-8.
[11] Gallagher JC, Sai AJ. Molecular biology of bone remodeling: Implications for new therapeutic targets for osteoporosis. Maturitas 2010;65:301-7.
[12] Ho-Shui-Ling A, Bolander J, Rustom LE, Johnson AW, Luyten FP, Picart C. Bone regeneration strategies: Engineered scaffolds, bioactive molecules and stem cells current stage and future perspectives. Biomaterials 2018;180:143-62.
[13] Winkler T, Sass FA, Duda GN, Schmidt-Bleek K. A review of biomaterials in bone defect healing, remaining shortcomings and future opportunities for bone tissue engineering the unsolved challenge. Bone Joint Res 2018;7:232-43.
[14] De Witte TM, Fratila-Apachitei LE, Zadpoor AA, Peppas NA. Bone tissue engineering via growth factor delivery: from scaffolds to complex matrices. Regen Biomater 2018;5:197-211.
[15] Wang WH, Yeung KWK. Bone grafts and biomaterials substitutes for bone defect repair: A review. Bioact Mater 2017;2:224-47.
[16] Chocholata P, Kulda V, Babuska V. Fabrication of Scaffolds for Bone-Tissue Regeneration. Materials 2019;12.
[17] Lee KY, Mooney DJ. Alginate: Properties and biomedical applications. Prog Polym Sci 2012;37:106-26.
[18] Venkatesan J, Bhatnagar I, Manivasagan P, Kang KH, Kim SK. Alginate composites for bone tissue engineering: A review. Int J Biol Macromol 2015;72:269-81.
[19] Szekalska M, Pucilowska A, Szymanska E, Ciosek P, Winnicka K. Alginate: Current Use and Future Perspectives in Pharmaceutical and Biomedical Applications. Int J Polym Sci 2016.

[20] Bonino CA, Krebs MD, Saquing CD, Jeong SI, Shearer KL, Alsberg E, et al. Electrospinning alginate-based nanofibers: From blends to crosslinked low molecular weight alginate-only systems. Carbohyd Polym 2011;85:111-9.
[21] Sun JC, Tan HP. Alginate-Based Biomaterials for Regenerative Medicine Applications. Materials 2013;6:1285-309.
[22] Parhi P, Ramanan A, Ray AR. Preparation and characterization of alginate and hydroxyapatite-based biocomposite. J Appl Polym Sci 2006;102:5162-5.
[23] Liu M, Zeng X, Ma C, Yi H, Ali Z, Mou XB, Li S, Deng Y, He N. Injectable hydrogels for cartilage and bone tissue engineering. Bone Res 2017;5.
[24] Balakrishnan B, Joshi N, Jayakrishnan A, Banerjee R. Self-crosslinked oxidized alginate/gelatin hydrogel as injectable, adhesive biomimetic scaffolds for cartilage regeneration. Acta Biomater 2014;10:3650-63.
[25] Park H, Woo EK, Lee KY. Ionically cross-linkable hyaluronate-based hydrogels for injectable cell delivery. J Control Release 2014;196:146-53.
[26] Zhao LA, Weir MD, Xu HHK. An injectable calcium phosphate-alginate hydrogel-umbilical cord mesenchymal stem cell paste for bone tissue engineering. Biomaterials 2010;31:6502-10.
[27] Vallet-Regi M. Ceramics for medical applications. J Chem Soc Dalton 2001:97-108.
[28] Kattimani VS, Kondaka S, Lingamaneni KP. Hydroxyapatite–Past, Present, and Future in Bone Regeneration. Bone and Tissue Regeneration Insights 2016;7:BTRI.S36138.
[29] Fox K, Tran PA, Tran N. Recent Advances in Research Applications of Nanophase Hydroxyapatite. Chemphyschem 2012;13:2495-506.
[30] Roveri N, Iafisco M. Evolving application of biomimetic nanostructured hydroxyapatite. Nanotechnology, science and applications 2010;3:107-25.
[31] Hao YQ, Yan HQ, Wang XP, Zhu BS, Ning CQ, Ge SF. Evaluation of Osteoinduction and Proliferation on Nano-Sr-HAP: A Novel Orthopedic Biomaterial for Bone Tissue Regeneration. J Nanosci Nanotechno 2012;12:207-12.
[32] Komakula SSB, Raut S, Verma NP, Raj TA, Kumar MJ, Sinha A, Singh S. Assessment of injectable and cohesive nanohydroxyapatite composites for biological functions. Prog Biomater 2015;4:31-8.
[33] Appleford MR, Oh S, Oh N, Ong JL. In vivo study on hydroxyapatite scaffolds with trabecular architecture for bone repair. J Biomed Mater Res A 2009;89a:1019-27.

[34] Xue B, Zhang C, Wang YH, Wang JC, Zhang J, Lu M, Li G, Cao Z, Huang Q. A Novel Controlled-Release System for Antibacterial Enzyme Lysostaphin Delivery Using Hydroxyapatite/Chitosan Composite Bone Cement. Plos One 2014;9.
[35] Biondi M, Borzacchiello A, Mayol L, Ambrosio L. Nanoparticle-Integrated Hydrogels as Multifunctional Composite Materials for Biomedical Applications. Gels-Basel 2015;1:162-78.
[36] Cai YR, Yu JH, Kundu SC, Yao JM. Multifunctional nano-hydroxyapatite and alginate/gelatin based sticky gel composites for potential bone regeneration. Mater Chem Phys 2016;181:227-33.
[37] Nabavinia M, Khoshfetrat AB, Naderi-Meshkin H. Nano-hydroxyapatite-alginate-gelatin microcapsule as a potential osteogenic building block for modular bone tissue engineering. Mat Sci Eng C-Mater 2019;97:67-77.
[38] Chen LY, Shen RZ, Komasa S, Xue YX, Jin BY, Hou YP, Okazaki J, Gao J. Drug-Loadable Calcium Alginate Hydrogel System for Use in Oral Bone Tissue Repair. Int J Mol Sci 2017;18.
[39] Sancilio S, Gallorini M, Di Nisio C, Marsich E, Di Pietro R, Schweikl H, Cataldi A. Alginate/Hydroxyapatite-Based Nanocomposite Scaffolds for Bone Tissue Engineering Improve Dental Pulp Biomineralization and Differentiation. Stem Cells Int 2018.
[40] Zimmerli W. Clinical presentation and treatment of orthopaedic implant-associated infection. J Intern Med 2014;276:111-9.
[41] Goodman SB, Yao ZY, Keeney M, Yang F. The future of biologic coatings for orthopaedic implants. Biomaterials 2013;34:3174-83.
[42] Campoccia D, Montanaro L, Arciola CR. The significance of infection related to orthopedic devices and issues of antibiotic resistance. Biomaterials 2006;27:2331-9.
[43] Li B, Webster TJ. Bacteria antibiotic resistance: New challenges and opportunities for implant-associated orthopedic infections. J Orthop Res 2018;36:22-32.
[44] Birt MC, Anderson DW, Toby EB, Wang JX. Osteomyelitis: Recent advances in pathophysiology and therapeutic strategies. J Orthop 2017;14:45-52.
[45] Zimmerli W, Moser C. Pathogenesis and treatment concepts of orthopaedic biofilm infections. Fems Immunol Med Mic 2012;65:158-68.
[46] Trampuz A, Widmer AF. Infections associated with orthopedic implants. Curr Opin Infect Dis 2006;19:349-56.

[47] Metsemakers WJ, Kuehl R, Moriarty TF, Richards RG, Verhofstad MHJ, Borens O, et al. Infection after fracture fixation: Current surgical and microbiological concepts. Injury 2018;49:511-22.
[48] Geurts J, Arts JJC, Walenkamp GHIM. Bone graft substitutes in active or suspected infection. Contra-indicated or not?. Injury 2011;42:S82-S6.
[49] Moriarty TF, Kuehl R, Coenye T, Metsemakers WJ, Morgenstern M, Schwarz EM, et al. Orthopaedic device-related infection: current and future interventions for improved prevention and treatment. EFORT open reviews 2016;1:89-99.
[50] Kaufman MG, Meaike JD, Izaddoost SA. Orthopedic Prosthetic Infections: Diagnosis and Orthopedic Salvage. Seminars in plastic surgery 2016;30:66-72.
[51] Arciola CR, Campoccia D, Ehrlich GD, Montanaro L. Biofilm-based implant infections in orthopaedics. Adv Exp Med Biol 2015;830:29-46.
[52] Montanaro L, Speziale P, Campoccia D, Ravaioli S, Cangini I, Pietrocola G, Giannini S, Arciola CR. Scenery of *Staphylococcus* implant infections in orthopedics. Future Microbiol 2011;6:1329-49.
[53] Odekerken JCE, Welting TJ, Walenkamp GHIM, Arts JJ. 5 - Experimental models in orthopedic infection research. Book chapter. In: Arts JJC, Geurts J, editors. Management of Periprosthetic Joint Infections (PJIs): Woodhead Publishing; 2017. p. 81-116.
[54] Arciola CR, Campoccia D, Montanaro L. Implant infections: adhesion, biofilm formation and immune evasion. Nat Rev Microbiol 2018;16:397-409.
[55] Fernandes A, Dia M. The microbiological profiles of infected prosthetic implants with an emphasis on the organisms which from biofilms. J Clin Diagn Res. 2013; 7:219-223.
[56] Ribera A, Benavent E, Lora-Tamayo J, Tubau F, Pedrero S, Cabo X, Ariza J. Murrilo O. Osteoarticular infection caused by MDR *Pseudomonas aeruginosa*: the benefits of combination therapy with colistin plus beta-lactams. J Antimicrob Chemother 2015;70:3357-65.
[57] Uckay I, Harbarth S, Ferry T, Lubbeke A, Emonet S, Hoffmeyer P, Pittet D. Meticillin resistance in orthopaedic coagulase-negative staphylococcal infections. J Hosp Infect 2011;79:248-53.
[58] Vasso M, Schiavone Panni A, De Martino I, Gasparini G. Prosthetic knee infection by resistant bacteria: the worst-case scenario. Knee Surg Sports Traumatol Arthrosc 2016;24:3140-6.

[59] Foster TJ. Antibiotic resistance in *Staphylococcus aureus*. Current status and future prospects. FEMS microbiology reviews 2017;41:430-49.
[60] Printzen G. Relevance, pathogenicity and virulence of microorganisms in implant related infections. Injury 1996;27:9-15.
[61] Phumisantiphong U, Siripanichgon K, Reamtong O, Diraphat P. A novel bacteriocin from *Enterococcus faecalis* 478 exhibits a potent activity against vancomycin-resistant enterococci. Plos One 2017;12:e0186415.
[62] Guzman Prieto AM, van Schaik W, Rogers MR, Coque TM, Baquero F, Corander J, Willems RJ. Global Emergence and Dissemination of Enterococci as Nosocomial Pathogens: Attack of the Clones? Front Microbiol 2016;7:788.
[63] Gallo J, Holinka M, Moucha CS. Antibacterial Surface Treatment for Orthopaedic Implants. Int J Mol Sci 2014;15:13849-80.
[64] Romano CL, Scarponi S, Gallazzi E, Romano D, Drago L. Antibacterial coating of implants in orthopaedics and trauma: a classification proposal in an evolving panorama. J Orthop Surg Res 2015;10.
[65] Knetsch MLW, Koole LH. New Strategies in the Development of Antimicrobial Coatings: The Example of Increasing Usage of Silver and Silver Nanoparticles. Polymers-Basel 2011;3:340-66.
[66] Lorenzetti M, Dogsa I, Stosicki T, Stopar D, Kalin M, Kobe S, Novak S. The Influence of Surface Modification on Bacterial Adhesion to Titanium-Based Substrates. Acs Appl Mater Inter 2015;7:1644-51.
[67] Gallardo-Moreno AM, Pacha-Olivenza MA, Saldana L, Perez-Giraldo C, Bruque JM, Vilaboa N, González-Martín L. *In vitro* biocompatibility and bacterial adhesion of physico-chemically modified Ti6Al4V surface by means of UV irradiation. Acta Biomater 2009;5:181-92.
[68] Martin ML, Pfaffen V, Valenti LE, Giacomelli CE. Albumin biofunctionalization to minimize the *Staphylococcus aureus* adhesion on solid substrates. Colloids Surf B 2018;167:156-64.
[69] Song F, Koo H, Ren D. Effects of Material Properties on Bacterial Adhesion and Biofilm Formation. J Dent Res 2015;94:1027-34.
[70] Falde EJ, Yohe ST, Colson YL, Grinstaff MW. Superhydrophobic materials for biomedical applications. Biomaterials 2016;104:87-103.

[71] Yoon SH, Rungraeng N, Song W, Jun S. Superhydrophobic and superhydrophilic nanocomposite coatings for preventing *Escherichia coli* K-12 adhesion on food contact surface. J Food Eng 2014;131:135-41.
[72] Damiati L, Eales MG, Nobbs AH, Su B, Tsimbouri PM, Salmeron-Sanchez M, Dalby MJ. Impact of surface topography and coating on osteogenesis and bacterial attachment on titanium implants. J Tissue Eng 2018;9:2041731418790694.
[73] Zhao YY, Zhao B, Su X, Zhang S, Wang S, Keatch R, Zhao Q. Reduction of bacterial adhesion on titanium-doped diamond-like carbon coatings. Biofouling 2018;34:26-33.
[74] Puckett SD, Taylor E, Raimondo T, Webster TJ. The relationship between the nanostructure of titanium surfaces and bacterial attachment. Biomaterials 2010;31:706-13.
[75] Spriano S, Yamaguchi S, Baino F, Ferraris S. A critical review of multifunctional titanium surfaces: New frontiers for improving osseointegration and host response, avoiding bacteria contamination. Acta Biomater 2018;79:1-22.
[76] Ermis M, Antmen E, Hasirci V. Micro and Nanofabrication methods to control cell-substrate interactions and cell behavior: A review from the tissue engineering perspective. Bioact Mater 2018;3:355-69.
[77] Durmus NG, Webster TJ. Nanostructured titanium: the ideal material for improving orthopedic implant efficacy? Nanomedicine 2012;7:791-3.
[78] Desrousseaux C, Sautou V, Descamps S, Traore O. Modification of the surfaces of medical devices to prevent microbial adhesion and biofilm formation. J Hosp Infect 2013;85:87-93.
[79] Wagner C, Aytac S, Hansch GM. Biofilm growth on implants: bacteria prefer plasma coats. Int J Artif Organs 2011;34:811-7.
[80] Vadillo-Rodriguez V, Pacha-Olivenza MA, Gonzalez-Martin ML, Bruque JM, Gallardo-Moreno AM. Adsorption behavior of human plasma fibronectin on hydrophobic and hydrophilic Ti6Al4V substrata and its influence on bacterial adhesion and detachment. J Biomed Mater Res A 2013;101:1397-404.
[81] An YH, Bradley J, Powers DL, Friedman RJ. The prevention of prosthetic infection using a cross-linked albumin coating in a rabbit model. J Bone Joint Surg Br 1997;79b:816-9.
[82] Katsikogianni M, Missirlis YF. Concise review of mechanisms of bacterial adhesion to biomaterials and of techniques used in estimating bacteria-material interactions. Eur Cell Mater 2004;8:37-57.

[83] Francolini I, Vuotto C, Piozzi A, Donelli G. Antifouling and antimicrobial biomaterials: an overview. Apmis 2017;125:392-417.
[84] Zhang N, Chen C, Melo MAS, Bai YX, Cheng L, Xu HHK. A novel protein-repellent dental composite containing 2-methacryloyloxyethyl phosphorylcholine. Int J Oral Sci 2015;7:103-9.
[85] Nejadnik MR, Engelsman AF, Fernandez ICS, Busscher HJ, Norde W, van der Mei HC. Bacterial colonization of polymer brush-coated and pristine silicone rubber implanted in infected pockets in mice. J Antimicrob Chemoth 2008;62:1323-5.
[86] Campoccia D, Montanaro L, Arciola CR. A review of the biomaterials technologies for infection-resistant surfaces. Biomaterials 2013;34:8533-54.
[87] Bazaka K, Jacob MV, Chrzanowski W, Ostrikov K. Anti-bacterial surfaces: natural agents, mechanisms of action, and plasma surface modification. Rsc Adv 2015;5:48739-59.
[88] Arciola CR, Campoccia D, Ehrlich GD, Montanaro L. Biofilm-Based Implant Infections in Orthopaedics. Biofilm-Based Healthcare-Associated Infections, Vol I 2015;830:29-46.
[89] Wahid F, Zhong C, Wang HS, Hu XH, Chu LQ. Recent Advances in Antimicrobial Hydrogels Containing Metal Ions and Metals/Metal Oxide Nanoparticles. Polymers-Basel 2017;9.
[90] Albers CE, Hofstetter W, Siebenrock KA, Landmann R, Klenke FM. *In vitro* cytotoxicity of silver nanoparticles on osteoblasts and osteoclasts at antibacterial concentrations. Nanotoxicology 2013;7:30-6.
[91] Zhou ZH, Liu XP, Liu QQ, Liu LH. Evaluation of the Potential Cytotoxicity of Metals Associated with Implanted Biomaterials (I). Prep Biochem Biotech 2009;39:81-91.
[92] Townsend L, Williams RL, Anuforom O, Berwick MR, Halstead F, Hughes E, Stamboulis A, Oppenheim B, Grover L, Scott RA, Webber M, Peacock AF, Belli A, Logan A, de Cogan F. Antimicrobial peptide coatings for hydroxyapatite: electrostatic and covalent attachment of antimicrobial peptides to surfaces. J R Soc Interface 2017;14.
[93] Coelho CC, Sousa SR, Monteiro FJ. Heparinized nanohydroxyapatite/collagen granules for controlled release of vancomycin. J Biomed Mater Res A 2015;103:3128-38.

[94] Barros J, Grenho L, Fernandes MH, Manuel CM, Melo LF, Nunes OC, Monteiro FJ, Ferraz MP. Anti-sessile bacterial and cytocompatibility properties of CHX-loaded nanohydroxyapatite. Colloid Surface B 2015;130:305-14.

[95] Stigter M, Bezemer J, de Groot K, Layrolle P. Incorporation of different antibiotics into carbonated hydroxyapatite coatings on titanium implants, release and antibiotic efficacy. J Control Release 2004;99:127-37.

[96] Gerits E, Kucharikova S, Van Dijck P, Erdtmann M, Krona A, Lovenklev M, Fröhlich M, Dovgan B, Impellizzeri F, Braem A, Vleugels J, Robijns SC, Steenackers HP, Vanderleyden J, De Brucker K, Thevissen K, Cammue BP, Fauvart M, Verstraeten N, Michiels J. Antibacterial activity of a new broad-spectrum antibiotic covalently bound to titanium surfaces. J Orthop Res 2016;34:2191-8.

[97] Nie BE, Long T, Ao HY, Zhou JL, Tang TT, Yue B. Covalent Immobilization of Enoxacin onto Titanium Implant Surfaces for Inhibiting Multiple Bacterial Species Infection and *In Vivo* Methicillin-Resistant *Staphylococcus aureus* Infection Prophylaxis. Antimicrob Agents Ch 2017;61.

[98] Fuchs T, Stange R, Schmidmaier G, Raschke MJ. The use of gentamicin-coated nails in the tibia: preliminary results of a prospective study. Arch Orthop Traum Su 2011;131:1419-25.

[99] Tang YW, Zhao Y, Wang HX, Gao Y, Liu X, Wang XG, Lin T. Layer-by-layer assembly of antibacterial coating on interbonded 3D fibrous scaffolds and its cytocompatibility assessment. J Biomed Mater Res A 2012;100a:2071-8.

[100] Guillaume O, Garric X, Lavigne JP, Van Den Berghe H, Coudane J. Multilayer, degradable coating as a carrier for the sustained release of antibiotics: Preparation and antimicrobial efficacy *in vitro*. J Control Release 2012;162:492-501.

[101] Tran PA, Sarin L, Hurt RH, Webster TJ. Titanium surfaces with adherent selenium nanoclusters as a novel anticancer orthopedic material. J Biomed Mater Res A 2010;93a:1417-28.

[102] Pishbin F, Mourino V, Flor S, Kreppel S, Salih V, Ryan MP, Boccaccini AR. Electrophoretic Deposition of Gentamicin-Loaded Bioactive Glass/Chitosan Composite Coatings for Orthopaedic Implants. Acs Appl Mater Inter 2014;6:8796-806.

[103] Chen XN, Gu YX, Lee JH, Lee WY, Wang HJ. Multifunctional surfaces with biomimetic nanofibres and drug-eluting micro-patterns for infection control and bone tissue formation. Eur Cell Mater 2012;24:237-48.

[104] WHO. World Health Organization (WHO). 2018.

[105] Chan CW, Carson L, Smith GC, Morelli A, Lee S. Enhancing the antibacterial performance of orthopaedic implant materials by fibre laser surface engineering. Appl Surf Sci 2017;404:67-81.
[106] Dublanchet A, Patey P. Phage therapy for bone and joint infections: report of french cases. Orthopaedic Proceedings 2017;99-B:35.
[107] Kaur S, Harjai K, Chhibber S. Bacteriophage Mediated Killing of *Staphylococcus aureus In Vitro* on Orthopaedic K Wires in Presence of Linezolid Prevents Implant Colonization. Plos One 2014;9.
[108] Kaur S, Harjai K, Chhibber S. *In Vivo* Assessment of Phage and Linezolid Based Implant Coatings for Treatment of Methicillin Resistant *S. aureus* (MRSA) Mediated Orthopaedic Device Related Infections. Plos One 2016;11.
[109] Morris J, Kelly N, Elliott L, Grant A, Wilkinson M, Hazratwala K, McEven P. Evaluation of Bacteriophage Anti-Biofilm Activity for Potential Control of Orthopedic Implant-Related Infections Caused by *Staphylococcus Aureus*. Surg Infect 2019;20:16-24.
[110] Meurice E, Rguiti E, Brutel A, Hornez JC, Leriche A, Descamps M, Bouchart F. New antibacterial microporous CaP materials loaded with phages for prophylactic treatment in bone surgery. J Mater Sci-Mater M 2012;23:2445-52.
[111] Yilmaz C, Colak M, Yilmaz BC, Ersoz G, Kutateladze M, Gozlugol M. Bacteriophage Therapy in Implant-Related Infections An Experimental Study. J Bone Joint Surg Am 2013;95a:117-25.
[112] Fish R, Kutter E, Bryan D, Wheat G, Kuhl S. Resolving Digital Staphylococcal Osteomyelitis Using Bacteriophage-A Case Report. Antibiotics-Basel 2018;7.
[113] Torres-Barcelo C. The disparate effects of bacteriophages on antibiotic-resistant bacteria. Emerg Microbes Infec 2018;7.
[114] Brovko LY, Anany H, Griffiths MW. Bacteriophages for detection and control of bacterial pathogens in food and food-processing environment. Adv Food Nutr Res 2012;67:241-88.
[115] Domingo-Calap P, Delgado-Martinez J. Bacteriophages: Protagonists of a Post-Antibiotic Era. Antibiotics-Basel 2018;7.
[116] Harada LK, Silva EC, Campos WF, Del Fiol FS, Vila M, Dabrowska K, Krylov VN, Balcão VM. Biotechnological applications of bacteriophages: State of the art. Microbiol Res 2018;212:38-58.

[117] Krupovic M, Prangishvili D, Hendrix RW, Bamford DH. Genomics of Bacterial and Archaeal Viruses: Dynamics within the Prokaryotic Virosphere. Microbiol Mol Biol R 2011;75:610.
[118] https://talk.ictvonline.org/. 2019.
[119] Day A, Ahn J, Salmond GPC. Jumbo Bacteriophages are represented within an increasing diversity of environmental viruses infecting the emerging Phytopathogen, *Dickeya solani*. Front Microbiol. 2018;9:2169.
[120] Peng C, Hanawa T, Azam AH, LeBlanc C, Ung P, Matsuda T, Onishi H, Miyanaga K, Tanji Y. Silviavirus phage ϕMR003 displays a broad host range against methicillin-resistant Staphylococcus aureus of human origin. Appl Microbiol Biotechnol. 2019;18:7751-7765.
[121] Ryan EM, Gorman SP, Donnelly RF, Gilmore BF. Recent advances in bacteriophage therapy: how delivery routes, formulation, concentration and timing influence the success of phage therapy. J Pharm Pharmacol 2011;63:1253-64.
[122] Hanlon GW. Bacteriophages: An appraisal of their role in the treatment of bacterial infections. Int J Antimicrob Ag 2007;30:118-28.
[123] Rakonjac J, Bennett NJ, Spagnuolo J, Gagic D, Russel M. Filamentous Bacteriophage: Biology, Phage Display and Nanotechnology Applications. Curr Issues Mol Biol 2011;13:51-75.
[124] Oliveira H, Sillankorva S, Merabishvili M, Kluskens LD, Azeredo J. Unexploited opportunities for phage therapy. Front Pharmacol 2015;6.
[125] Loc-Carrillo C, Abedon ST. Pros and cons of phage therapy. Bacteriophage 2011;1:111-4.
[126] Roach DR, Leung CY, Henry M, Morello E, Singh D, Di Santo JP, Weitz JS, Debarbieux L. Synergy between the Host Immune System and Bacteriophage Is Essential for Successful Phage Therapy against an Acute Respiratory Pathogen. Cell Host Microbe 2017;22:38.
[127] Krut O, Bekeredjian-Ding I. Contribution of the Immune Response to Phage Therapy. J Immunol 2018;200:3037-44.
[128] Oechslin F. Resistance Development to Bacteriophages Occurring during Bacteriophage Therapy. Viruses-Basel 2018;10.
[129] Pires DP, Cleto S, Sillankorva S, Azeredo J, Lu TK. Genetically Engineered Phages: a Review of Advances over the Last Decade. Microbiol Mol Biol R 2016;80:523-43.

[130] Phagoburn project. http://www.phagoburn.eu/2013-2019.
[131] Watanabe R, Matsumoto T, Sano G, Ishii Y, Tateda K, Sumiyama Y, Uchiyam J, Sakurai S, Matsuzaki S, Imai S, Yamaguchi K. Efficacy of bacteriophage therapy against gut-derived sepsis caused by *Pseudomonas aeruginosa* in mice. Antimicrob Agents Chemother 2007;51:446-52.
[132] Biswas B, Adhya S, Washart P, Paul B, Trostel AN, Powell B, Carlton R, Merril CR. Bacteriophage therapy rescues mice bacteremic from a clinical isolate of vancomycin-resistant *Enterococcus faecium*. Infect Immun 2002;70:204-10.
[133] Wang J, Hu B, Xu M, Yan Q, Liu S, Zhu X, Sun Z, Tao D, Ding L, Gong J, Li QQ, Hu J. Therapeutic effectiveness of bacteriophages in the rescue of mice with extended spectrum beta-lactamase-producing *Escherichia coli* bacteremia. Int J Mol Med 2006;17:347-55.
[134] Wright A, Hawkins CH, Anggard EE, Harper DR. A controlled clinical trial of a therapeutic bacteriophage preparation in chronic otitis due to antibiotic-resistant *Pseudomonas aeruginosa*; a preliminary report of efficacy. Clin Otolaryngol 2009;34:349-57.
[135] Capparelli R, Parlato M, Borriello G, Salvatore P, Iannelli D. Experimental phage therapy against *Staphylococcus aureus* in mice. Antimicrob Agents Ch 2007;51:2765-73.
[136] Oduor JMO, Onkoba N, Maloba F, Nyachieo A. Experimental phage therapy against haematogenous multi-drug resistant *Staphylococcus aureus* pneumonia in mice. Afr J Lab Med 2016;5.
[137] Furusawa T, Iwano H, Hiyashimizu Y, Matsubara K, Higuchi H, Nagahata H, et al. Phage Therapy Is Effective in a Mouse Model of Bacterial Equine Keratitis. Appl Environ Microb 2016;82:5332-9.
[138] Drilling AJ, Ooi ML, Miljkovic D, James C, Speck P, Vreugde S, Clark J, Wormald PJ. Long-Term Safety of Topical Bacteriophage Application to the Frontal Sinus Region. Front Cell Infect Mi 2017;7.
[139] Kishor C, Mishra RR, Saraf SK, Kumar M, Srivastav AK, Nath G. Phage therapy of staphylococcal chronic osteomyelitis in experimental animal model. Indian J Med Res 2016;143:87-94.
[140] Fu WL, Forster T, Mayer O, Curtin JJ, Lehman SM, Donlan RM. Bacteriophage Cocktail for the Prevention of Biofilm Formation by *Pseudomonas aeruginosa* on Catheters in an *In Vitro* Model System. Antimicrob Agents Ch 2010;54:397-404.

[141] Nogueira F, Karumidze N, Kusradze I, Goderdzishvili M, Teixeira P, Gouveia IC. Immobilization of bacteriophage in wound-dressing nanostructure. Nanomed-Nanotechnol 2017;13:2475-84.
[142] Colom J, Cano-Sarabia M, Otero J, Cortes P, Maspoch D, Llagostera M. Liposome-Encapsulated Bacteriophages for Enhanced Oral Phage Therapy against *Salmonella spp*. Appl Environ Microb 2015;81:4841-9.
[143] Singla S, Harjai K, Katare OP, Chhibber S. Bacteriophage-Loaded Nanostructured Lipid Carrier: Improved Pharmacokinetics Mediates Effective Resolution of *Klebsiella pneumoniae*-Induced Lobar Pneumonia. J Infect Dis 2015;212:325-34.

NOTE: In the following Chapters whenever the text reproduces a manuscript from the author of this thesis, published in a scientific journal or under submission, the respective numbers of figures, tables and references are attributed specifically in accordance with that article, exactly as they appear in the original text.

CHAPTER 2

Alginate-nanohydroxyapatite hydrogel system: optimizing the formulation for enhanced bone regeneration

J. Barros[a,b,c,*], M.P. Ferraz[d], J. Azeredo[e], M.H. Fernandes[f,g], P.S. Gomes[f,g], F.J. Monteiro[a,b,c]

[a]i3S–Instituto de Investigação e Inovação em Saúde, Universidade do Porto, Porto, Portugal;

[b]INEB–Instituto de Engenharia Biomédica, Universidade Porto, Porto, Portugal;

[c]FEUP–Faculdade de Engenharia, DEMM, Universidade do Porto, Porto, Portugal;

[d]FP-ENAS/CEBIMED–University Fernando Pessoa Energy, Environment and Health Research Unit/Biomedical Research Center, Porto, Portugal;

[e]Laboratório de Investigação em Biofilmes Rosário Oliveira, Center of Biological Engineering, University of Minho, Braga, Portugal;

[f]Laboratory for Bone Metabolism and Regeneration—Faculty of Dental Medicine, U. Porto, Porto, Portugal,

[g]LAQV/REQUIMTE, U. Port, Porto, Portugal.

Material Science and Engineering C, DOI: 10.1016/j.msec.2019.109985

ABSTRACT

Ceramic/polymer-based biocomposites have emerged as potential biomaterials to fill, replace, repair or re-generate injured or diseased bone, due to their outstanding features in terms of biocompatibility, bioactivity, injectability, and biodegradability. However, these properties can be dependent on the amount of ceramic component present in the polymer-based composite. Therefore, in the present study, the influence of nanohydroxyapatite content (30 to 70 wt%) on alginate-based hydrogels was studied in order to evaluate the best formulation for maximizing bone tissue regeneration. The composite system was characterized in terms of physic-chemical properties and biological response, with *in vitro* cytocompatibility assessment with human osteoblastic cells and *ex vivo* functional evaluation in embryonic chick segmental bone defects. The main morphological characteristics of the alginate network were not affected by the addition of nanohydroxyapatite. However, physic-chemical features, like water-swelling rate, stability at extreme pH values, apatite formation, and Ca^{2+} release were nanoHA dose-dependent. Within *in vitro* cytocompatibility assays it was observed that hydrogels with nanoHA 30% content enhanced osteoblastic cells proliferation and expression of osteogenic transcription factors, while those with higher concentrations (50 and 70%) decreased the osteogenic cell response. *Ex vivo* data underlined the *in vitro* findings, revealing an enhanced collagenous deposition, trabecular bone formation and matrix mineralization with Alg-nanoHA30 composition, while compositions with higher nanoHA content induced a diminished bone tissue response. The outcomes of this study indicate that nanohydroxyapatite concentration plays a major role in physic-chemical properties and biological response of the composite system and the optimization of the components ratio must be met to maximize bone tissue regeneration.

Keywords – Biomaterials, Nanohydroxyapatite, Alginate, Hydrogel, Composite, Solubility, Biocompatibility, Osteogenic activity.

GRAPHICAL ABSTRACT

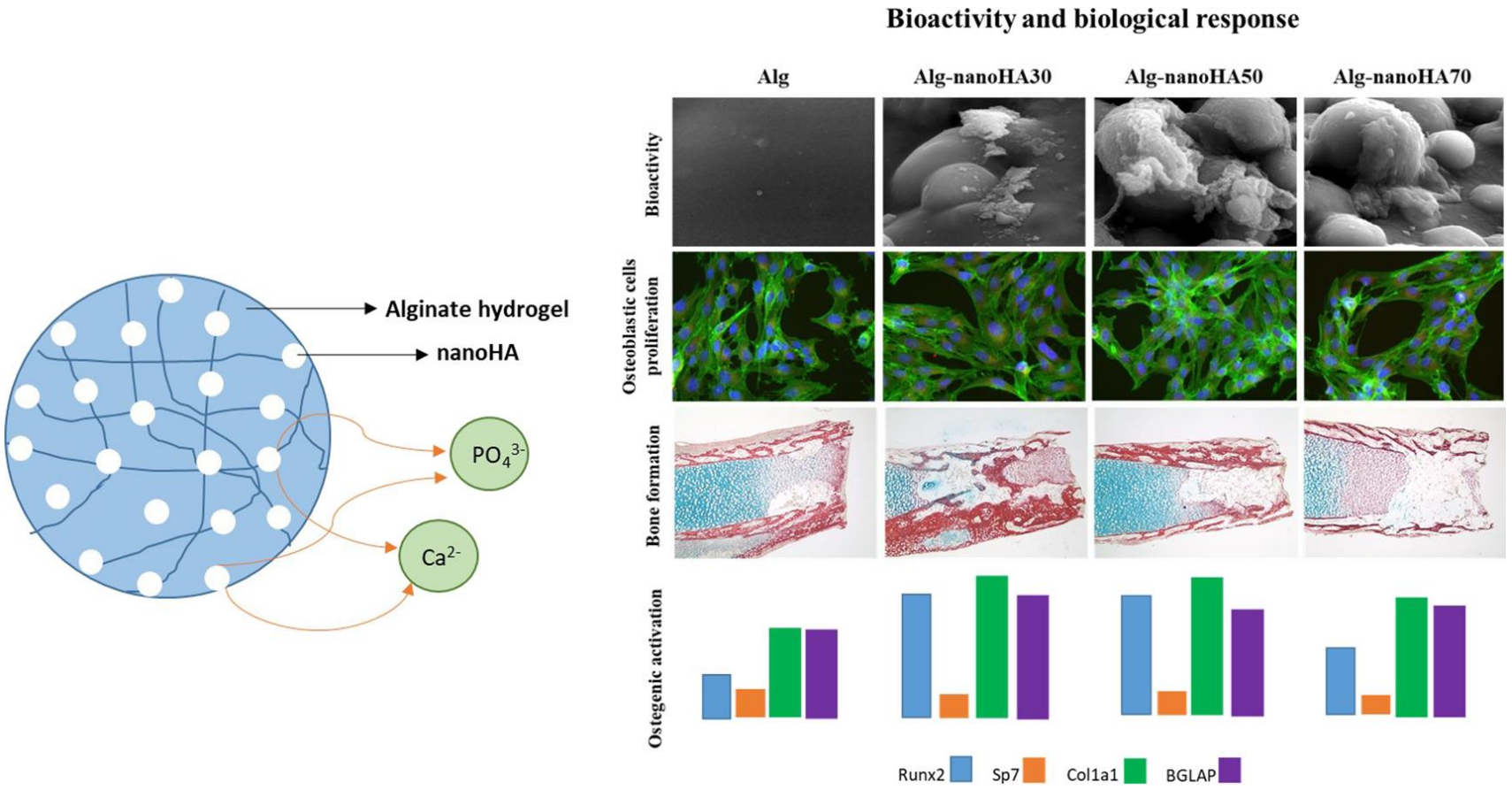

1. INTRODUCTION

Bone is a complex and dynamic tissue, which has the capability of remodeling and regenerating, up to a certain extent [1]. However, these physiological processes that contribute to tissue homeostasis can be impaired due to osteoporosis, rheumatoid arthritis, vitamin D deficiency and other metabolic conditions or traumatic fractures. These conditions have a huge impact on diminishing patients' quality of life and strongly affect healthcare costs, owing to requirements for surgeries, long-term hospitalization and difficult recoveries [1-4]. Materials like auto-/allografts, inert metallic and ceramic implants have been used to fill, replace, repair or regenerate injured or diseased bone with clinical success [1-3]. However, these applications have shown some associated limitations such as the risk of long-term foreign body reaction, pathogen transmission, immunogenic rejection, impaired bone formation, poor vascularization and integration, and inaccurate fitting to the defect size and shape [2-5].

Composites, based on the combination of different materials, such as polymers and ceramics, have emerged, aiming to solve these limitations in bone tissue engineering applications [6]. They can be designed to adjust to bone defects' shape and geometry, occupying the available space in the damaged organ/tissue, precluding invagination of the neighboring tissues and priming tissue healing [2, 6]. Furthermore, they can easily be modified or co-formulated with other components which impart additional properties such as osteoconduction, osteoinduction and osteogenicity [2].

Among polymers, polysaccharides are very versatile, enabling signaling molecules loading (e.g. growth factors, biomodulators, drugs) and an intrinsic interaction with inorganic components [7]. In this regard, alginate is a pH-sensitive, natural, hydrophilic, biocompatible, injectable and biodegradable polysaccharide extracted from seaweed. It is composed of two monomers, β-D-mannuronate and α-L-guluronate, known to form gels in the presence of bivalent cations such as calcium (Ca^{2+}) [6, 8, 9]. Given these characteristics, this polymer has been widely used for drug and growth factor delivery, cell encapsulation, and as a scaffold in tissue engineering applications [8, 9]. However, alginate exhibits some limitations in the regard of prospective bone tissue applications, such as the absence of sites for cell attachment or specific receptor interactions, which limits its long-term functionality, further impaired by the swelling-disintegration-erosion of these hydrogels' upon implantation, week biomechanical properties, poor bioresorbability and bioactivity [10-13]. Therefore, the use of nanohydroxyapatite

(nanoHA) as a reinforcing component with osteocondutive capabilities can contribute to overcome some of these potential limitations [4, 14]. NanoHA is commonly used in bone tissue regeneration due to its chemical similarity to the inorganic component of the bone matrix and its inherent characteristics such as biocompatibility, osteoinduction, osteocondutive and osteointegration [4, 15, 16]. Although in some studies nanoHA was already used to reinforce Alg matrixes [14, 17-20], no studies have yet addressed the systematic influence of nanoHA on alginate-based hydrogel systems, neither the effect of distinct nanoHA amounts on its physic-chemical properties and biological response. This is of the utmost relevance, since the amount of nanoHA within the composition of polymer-based hydrogels is crucial to design an efficient composite for bone tissue regeneration. Once nanoHA is gradually degraded, it releases calcium (Ca^{2+}) and phosphate (PO_4^{-3}) ions, which can modulate cellular behavior within the microenvironment, through different signaling pathways, influencing the bone mineralization process and bonding to the surrounding tissues [21]. Accordingly, some authors have reported that the level of solubility, bone-like apatite layer formation, cell attachment, proliferation and differentiation and, ultimately, bone growth rate, could be dependent on the concentration of nanoHA incorporated into polymer-based composites [21-23].

Therefore, an optimizing the ratio composite components must be guaranteed for enhancing its potential clinical application. In this context, the influence of nanoHA concentration on alginate-based hydrogel system was evaluated in terms of: (i) physic-chemical properties (i.e., morphology, chemical analysis, water content, swelling behavior, influence of pH on degradation and stability, surface charge, release of calcium and phosphate ions, bioactivity response in simulated body fluid), and (ii) biological response, with *in vitro* cytocompatibility evaluation with human osteoblastic cells and *ex vivo* functional assessment of bone formation studies, in order to define the best possible combination of Alg-nanoHA for enhancing bone tissue regeneration.

2. MATERIAL AND METHODS

2.1 Preparation of Alg-nanoHA hydrogels

Initially, a 2 % (w/v) alginate solution (Alg), was prepared by dissolving the sodium alginate (Sigma-Aldrich) powder in distilled water, at room temperature. Then, this solution was mixed with nanoHA powder (spherical microaggregates of nanoHA with

average particle size of 5μm, nanoXIM.HAp202, FLUIDINOVA, S.A), at 0, 30, 50 and 70 wt %, during 1 h at 60 rpm. After homogeneity, each mixture was dropped into a 250 mM calcium chloride ($CaCl_2$, Sigma-Aldrich) solution, and allowed to harden for 1 h. Spherical hydrogels were collected and washed three times with sterile distilled water. Four hydrogel compositions were produced: Alg (control), Alg-nanoHA30, Alg-nanoHA50, Alg-nanoHA70, containing respectively 0, 30, 50 and 70 wt % nanoHA.

2.2 Characterization of Alg-nanoHA hydrogels

2.2.1 Morphology

The composites matrix was characterized by transmission electron microscopy (TEM, JEOL JEM 1400 TEM). Samples were initially fixed in 2,5 % glutaraldehyde and 2 % paraformaldehyde in cacodylate buffer 0.1 M (pH 7.4) (both Sigma-Aldrich), dehydrated and embedded in Epon resin (TAAB). Ultrathin sections (40–60 nm thick) were stained with uranyl acetate and lead citrate and examined using a JEOL JEM 1400 microscope (TEM). Images were digitally recorded using a CCD digital camera Orious 1100W. Three samples were used for image acquisition.

External and internal structure and morphology of hydrogels were observed by scanning electron microscopy (SEM). Samples (n = 3) were coated with a gold layer (SPI-Module) in an argon atmosphere, and examined using a FEI Quanta 400FEG/ESEM microscope.

2.2.2 Chemical Analysis

Chemical characterization was performed using attenuated total reflectance – Fourier transformed infrared spectroscopy (ATR – FTIR), with a Perkin –Elmer 2000 FTIR spectrometer. The samples (n = 3) were analyzed at a spectral resolution of 2 cm^{-1} and 100 scans were accumulated per sample.

2.2.3 Water content and swelling behavior

Gravimetric method was employed to calculate the water content and swelling ratio, as previously described [24]. Briefly, for water content (W) evaluation, the samples were dried at 60 °C until a constant weight was reached. The water content was calculated using Eq. (1):

$$Water\ content\ (\%) = \frac{W_w - W_d}{W_w} \times 100 \text{ (Eq.1).}$$

Where W_w (g) and W_d (g) are the wet and dried weights of the samples, respectively. The results were taken as the mean values of eight measurements.

The swelling behavior was evaluated by measuring the changes in sample weight versus sample immersion time, in phosphate buffer saline (PBS, Sigma-Aldrich). Swelling behavior was evaluated for 28 days at 37 °C, and the media was replaced every 4 days to maintain the initial media volume. The equilibrium swelling ratio was calculated using Eq. (2):

$$Swelling\ ratio\ (\%) = \frac{W_f - W_i}{W_i} \times 100 \text{ (Eq. 2).}$$

Where, W_i and W_f are the initial and final weights of the samples, respectively. The results were taken as the mean values of eight measurements.

2.2.4 Influence of pH on stability

The stability of composites, at different pH values, were evaluated through changes in samples weight, as previously described [6]. The samples were immersed at different pH values, ranging between 1 and 13, at 4 °C for 24 h. Afterwards, they were weighted and the weight alteration ratio (%), at different pH was quantified using Eq. (2). The results were taken as the mean values of eight measurements.

2.2.5 Zeta potential – charge surface

Zeta potential was determined from streaming potential measurements with a commercial electrokinetic analyzer (EKA, Anton Paar) using a special powder cell adapter inside a cylindrical cell. The samples were mounted inside the power cell occupying a volume of about 48.75 mm^3, thus maintaining an overall constant height of sample for all measurements. Streaming potential was measured using Ag/AgCl electrodes installed at both ends of the streaming channel. The electrolyte used was 1 mM KCl at pH of 6.06 ± 0.10. Experiments were performed at 24 °C. The conductivity of the electrolyte solution was measured during the assay. The streaming potential was measured while applying an electrolyte flow in alternating directions and pressure ramps from 0 to 200 mbar. For each test, six pressure ramps were performed (three in each flow direction to cope with the asymmetric potential fluctuations). The results were taken as the mean values of eight measurements.

2.2.6 Release of Calcium ions

The concentration of calcium (Ca^{2+}) ions released from composites were determined according to ISO 10993-14 - "Biological evaluation of medical devices- Part 14: Identification and quantification of degradation products from ceramics". Briefly, the samples were placed in Tris[hydroxymethyl]aminomethane-HCl (Tris-HCl) solution (pH 7.4, Sigma-Aldrich) at 37 ºC and 120 rpm. At each time-point, supernatant was collected and filtered (0.2µm, Merck). Ca^{2+} concentration was determined by inductively coupled-plasma atomic emission spectroscopy (ICP-AES). The results were taken as the mean values of five measurements.

2.2.7 Bioactivity assay in simulated body fluid

The apatite deposition on composites was evaluated according to Kokubo's method [25]. Samples were immersed in Simulated Body Fluid (SBF) and incubated at 37 °C and 120 rpm, for 7 days. The apatite formation was evaluated by SEM, as described above. The surface elemental composition was carried out by Energy-dispersive X-ray spectroscopy (EDS), and the mass fractions of the elements were quasi-quantitatively calculated from at least three large field analysis measurements. Three samples were used for image acquisition and SEM-EDS analysis.

2.3 *In vitro* cytocompatibility assessment with human osteoblastic cells

Human mesenchymal stromal cells (hMSCs) isolated from femoral bone marrow, were obtained from an orthopedic surgical procedure, in accordance with established protocols [26]. hMSCs were maintained in minimum essential medium alpha modification (α-MEM), containing 10% fetal bovine serum (FBS), 100 unit's/mL penicillin, 100 µg/mL streptomycin and 2.5 µg/mL of amphotericin B (all reagents from Gibco). To evaluate the cell response to composites, third subculture cells were seeded at 10^4 cells/cm^2, at 37 ºC for 24 h in a humidified atmosphere of 5% CO_2. Afterwards, the medium was discarded and the composites were incubated with adherent cells. Cultures, grown in the presence of composites were further characterized throughout the culture time up to 21 days, regarding cell proliferation, metabolic activity, cytoskeletal and mitochondrial organization, cell morphology, alkaline phosphatase activity and gene expression analysis of relevant osteogenic markers. hMSCs grown directly on tissue culture plates, in the absence of composites, were used as controls. The results were taken as the mean values of five measurements.

Additionally, for the analysis of gene expression, an osteogenic-induced control, established in osteogenic-induced conditions - culture medium further supplemented with 10 mM β-glycerophosphate 10^{-8} M dexamethasone and 50 µg/mL ascorbic acid (all reagents from Sigma-Aldrich), was established.

2.3.1 Metabolic activity of the cultures and cell proliferation

Cultures metabolic activity was evaluated using the MTT assay. At each time-point, cultures were incubated with 10% MTT solution (3-(4,5-dimethyl-2-thiazolyl)-2,5-diphenyl-2H-tetrazolium bromide, 5 mg/mL, Sigma-Aldrich) for 3 h at 37 °C. After the incubation period, the culture medium was removed, and the formazan salts were dissolved with dimethylsulfoxide (DMSO, Panreac). Absorbance was determined at 550 nm on a microplate reader (BioTek).

DNA content was measured using the Quant-iT Picogreen DNA assay (Invitrogen) according to the manufacturer's instructions. Initially, cells were washed with PBS and solubilized with 0.1% (v/v) Triton X-100 solution. Cell lysate was then mixed with the Pico-Green solution and incubated in the dark at room temperature for 5 min. The fluorescence intensity was measured with a microplate reader at 485 and 528 nm for emission and excitation, respectively. The results are expressed in nanograms of DNA.

2.3.2 Immunofluorescence analysis

Cell cytoskeleton filamentous actin (F-actin) organization and mitochondrial distribution, as well as the morphology of the cells were assessed by immunofluorescence imaging. Briefly, live cells were incubated with MitoSpy™ Red CMXRos (250 nM, Biolegend) for 30 min, at 37 ºC. Cells were then washed with PBS and fixed with 3.7% paraformaldehyde for 15 min. Following cells' permeabilization, nonspecific binding sites were blocked with 1% bovine serum albumin (Sigma-Aldrich) for 30 min. F-actin was stained with Alexa-Fluor 488 phalloidin-conjugated antibody (1:50, 30 min, Molecular Probes), and nucleus counterstaining with DAPI (1 µg/mL, 10 min, Sigma-Aldrich). Images of fluorescent-labelled cells were obtained with a Selena S digital imaging system (Logos Biosystems). Three samples were used for image acquisition.

2.3.3 Gene expression analysis

At 21 days of culture, quantitative reverse-transcriptase polymerase chain reaction (qRT-PCR) analysis was performed to evaluate the expression of relevant osteogenesis-

related markers. Briefly, total RNA was extracted using TRIZOL® reagent (Invitrogen) and reverse transcribed into complementary DNA (cDNA) with iScript™ Adv cDNA Kit (BioRad), according to the manufacturer's instructions. The expression of genes: Runt-related transcription factor 2 (RUNX-2, BioRad ID: qHsaCED0044067), Sp7 transcription factor (SP7, BioRad ID: qHsaCED0003759), collagen type I (COL1A1, BioRad ID: qHsaCED0043248) and bone gamma-carboxyglutamate protein (BGLAP, BioRad ID: qHsaCED0038437), was quantitatively determined in a RT-PCR equipment (CFX96, BioRad) using iQ™SYBR®Green Supermix (BioRad). Beta-actin (ACTB**,** qHsaCED0036269) gene was used as the reference gene for normalization. The cycling conditions were as follows: an activation cycle at 95ºC for 3 min, followed by 40 cycles of 95º C degeneration for 10 secs, 60ºC annealing and extension for 30 sec. The melting curve analysis was carried out on each sample to ensure a single amplicon at 55-95ºC for 10 secs/cycle, with 0.5ºC increment each cycle. The cycle threshold (Ct) for each transcript expression was export from Bio-rad CFX maestro software. The relative intensity of each target gene was normalized to ACTB levels, and calculated via the $2^{-\Delta\Delta Ct}$ method.

2.4 *Ex vivo* functional assessment of bone formation

The biofunctionality of composites was assayed *ex vivo* in an embryonic chick femoral segmental defect model. Briefly, femurs were dissected from day 11 chick embryos (*Gallus domesticus*), where the soft tissues, such as adherent muscles and ligaments, were carefully removed while preserving the periosteum. The femurs were cut at mid diaphysis for the establishment of a segmental defect, with a number 11 scalpel blade. Femurs, with composites being implanted within the mid-diaphysis defect, were carefully settled onto Netwell™ Insert (440 µm mesh size polyester membrane, Corning) in 6 well plates. Implanted femurs were maintained for 11 days in minimum essential medium (α-MEM), containing ascorbic acid (50 µg/mL), penicillin (100 units/mL)/streptomycin (100 µg/mL) and 2.5 µg/mL amphotericin B, at liquid/gas interface, in a humidified atmosphere of 5% CO_2 and 37 °C. Culture media was changed daily for the duration of the experiment. At the end of the culture period, femurs were fixed in 4% paraformaldehyde (Sigma-Aldrich) and prepared for histological examination. Samples were dehydrated through a series of graded alcohols, cleared in Histoclear® and embedded in paraffin. Tissue sections 6 µm thick were cut from across the femur samples and stained with Alcian blue/Sirius red (AB/SR), Masson's trichrome or von Kossa

staining, as previously described [27]. Images were captured with an Olympus BX-51/22 dotSlide digital virtual microscope and created using OlyVIA 2.1 software (Olympus Soft Imaging Solutions, GmBH). Eight femurs (n=8) per experimental condition, with a total of six sections from each femur for each histological stain were evaluated.

2.5 Statistical analysis

All experiments were performed in triplicate as independent experiments. The results were reported as the arithmetic mean ± standard deviation. The experimental data were analyzed using IBM® SPSS® Statistics (vs. 22.0, Statistical Package for the Social Sciences Inc). The one-way analysis of variance (ANOVA) followed by the post hoc Turkey HSD multiple comparison tests were used to determine the significant difference ($p < 0.05$).

3. RESULTS

3.1 Alg-nanoHA hydrogel system characterization

3.1.1 Morphology characterization

Figure 1 presents digital images of composites that were obtained by mixing Alg and nanoHA, at different weight percentages (0, 30, 50 and 70 wt.%), into spherical hydrogels, via external gelation. Overall, the samples showed tightly knit and smooth surface, and a whitened coloration proportional to the amount of nanoHA added (Fig. 1A), which also led to a slight increase in terms of area and weight, although no significant differences were found between different conditions (Table 1).

The matrix, structure and morphology of composites is shown in Figure 1B and 1C. TEM analysis allowed to characterize the Alg matrix as network of fibril-like structures, and to observe that nanoHA content increased the crosslinking of the Alg network (Fig. 1B). Through SEM analysis, it was shown that all samples present a lamellar structure with irregular pores in the inner layer (Fig. 1C). Alg hydrogels showed a smooth surface, whereas Alg-nanoHA showed a rougher surface, as comparing to control, due to the presence of nanoHA (Fig. 1C). The nanoHA particles were well embedded and homogeneously dispersed throughout the Alg matrix, both externally and internally (Fig. 1C).

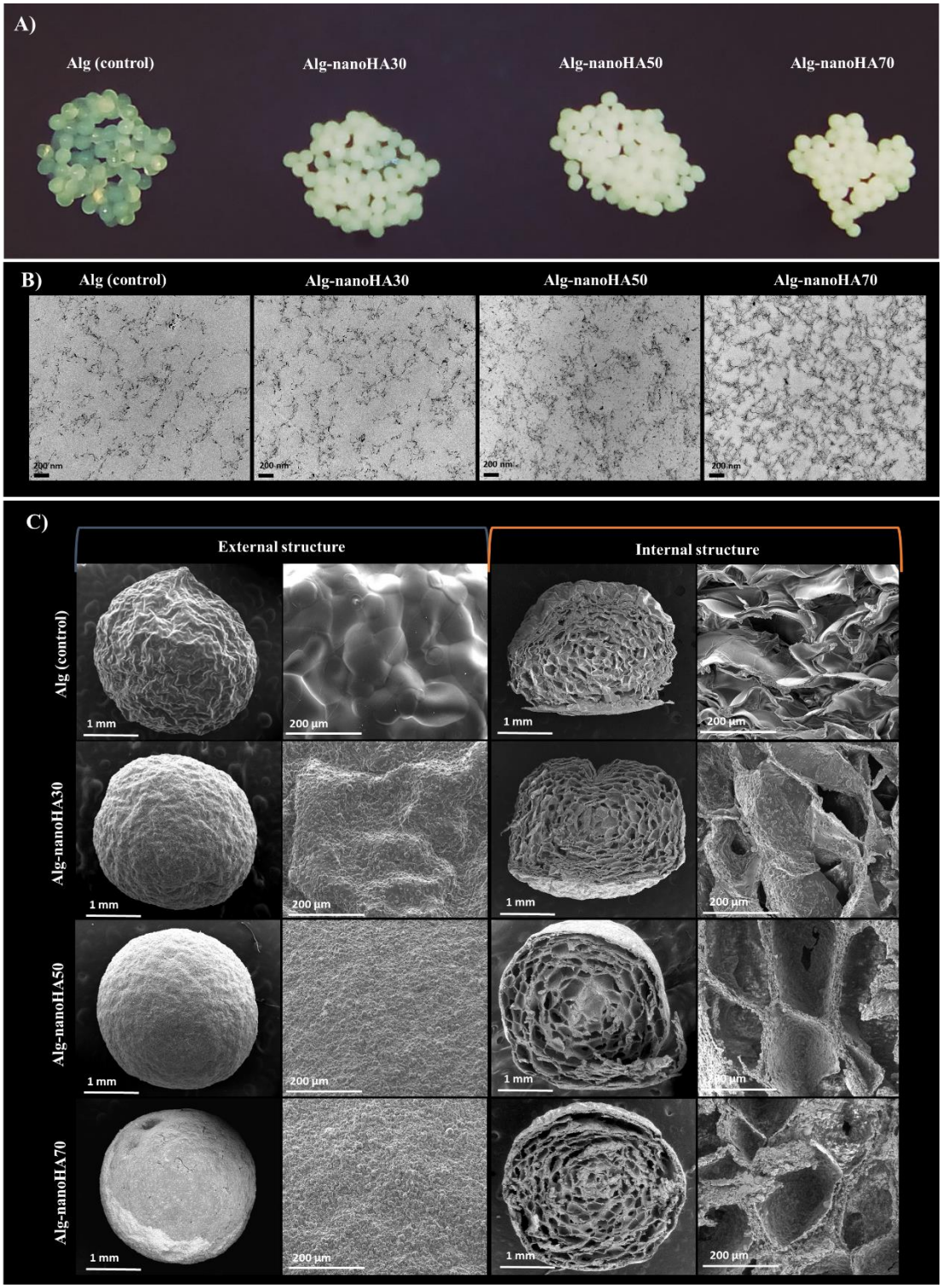

Figure 1 – (A) Digital images of composites with different nanoHA weight ratios (0, 30, 50 and 70%). (B) Matrix of hydrogels observed by TEM. Scale bar corresponds to 200 nm. (C) SEM micrographs of external and internal structure of composites. Scale bars correspond to 1 mm and 200 µm.

3.1.2 Chemical Analysis

The ATR – FTIR spectra (Fig. 2A) shows the chemical composition of the hydrogels. Alg displayed the characteristic alginate bands, as the asymmetric and symmetric stretching of carboxylic group (COO^-) on the polymeric backbone, found at 1592 and 1417 cm^{-1}, respectively. The broad peak spread over the range 3311 to 3307 cm^{-1} corresponds to hydroxyl group (OH^-). The bending of the OH^- group of the carboxyl is depicted at 819 cm^{-1}. ATR – FTIR spectra of the Alg-nanoHA showed a shift of the COO^- bands towards lower wavelengths, proportionally to the increase in nanoHA ratio. Bending and stretching of the phosphate group (PO_4^{3-}) were observed at 1020 cm^{-1} and 559 cm^{-1}, respectively, that are attributed to the overlap of COO^- stretching of Alg and PO_4^{3-} stretching of nanoHA. Moreover, their intensity increased with increasing of nanoHA content. The presence of bands at 3365 cm^{-1} and 629 cm^{-1} was assigned to OH^- group, corresponding to lattice water.

3.1.3 Water content and swelling behavior

Table 1 shows the water content and swelling ratio of the composites. The water content was inversely proportional to the amount of nanoHA (Table 1). No significant differences in the water content were observed between Alg (control) and, Alg-nanoHA30, and Alg-nanoHA50 hydrogels. However, the water content of Alg-nanoHA70 was significantly lower compared to Alg (control) and other Alg-nanoHA hydrogels (Table 1).

The swelling behavior of the hydrogels were evaluated by measuring the changes in sample weight over time. No weight differences were observed between samples over time (data not shown). For all samples, the swelling equilibrium was observed after 18 h. The swelling ratio was inversely proportional to the nanoHA amount (Table 1). All Alg-nanoHA hydrogels showed significantly lower swelling ratio compared to Alg (control). However, no significant differences on the swelling ratio were observed between Alg-nanoHA30 and Alg-nanoHA50. While, the swelling ratio of Alg-nanoHA70 was significantly lower than that of Alg-nanoHA30 and Alg-nanoHA50.

3.1.4 Zeta potential – charge surface

Zeta potential values of composites are presented in Table 1. All samples showed a negative zeta potential, which was affected by high nanoHA content. No differences of zeta potential values were found between Alg and Alg-nanoHA30. However, Alg-

nanoHA50 and Alg-nanoHA70 showed higher zeta potential values than that of Alg (control) and Alg-nanoHA30 hydrogels.

Table 1 – Physical characteristics of the composites.

Hydrogels	Weight (g)	Area (cm^2)	Water content (%)	Swelling ratio (%)	Zeta potential (mV)
Alg (control)	0.021 ± 0.003	0.270 ± 0.013	95.9 ± 1.6	172.7 ± 6.8	-14.358 ± 1.431
Alg-nanoHA30	0.021 ± 0.003	0.283 ± 0.013	94.8 ± 1.7	150.1 ± 5.5*	-13.144 ± 1.670
Alg-nanoHA50	0.022 ± 0.003	0.291 ± 0.012	93.1 ± 1.5	149.6 ± 4.1*	-9.111 ± 1.812*#
Alg-nanoHA70	0.025 ± 0.003	0.303 ± 0.013	88.2 ± 1.1*#	104.3 ± 6.0*#	-9.747 ± 0.741*#

*significant differences compared to Alg (control), with $p < 0.05$, obtained by Tukey's post-hoc test; #significant differences different between Alg-nanoHA hydrogels, with $p < 0.05$, obtained by Tukey's post-hoc test. Data are expressed as mean ± SD (n=8).

3.1.5 Influence of pH on stability

In Figure 2B the stability of the composites at different pH values are presented. The introduction of nanoHA did not affect the behavior of hydrogels, in which a shrinkage and breakdown of the matrixes were verified, at acid and alkaline pH values, respectively. However, composites stability was proportional to the nanoHA content. The Alg-nanoHA hydrogels were more stable at higher pH values compared with Alg (control).

3.1.6 Release of calcium ions

Figure 2C depicts the released Ca^{2+} concentration from hydrogels detected by ICP-AES. At day 1, the Ca^{2+} release from Alg (control) was 86 ppm, while from Alg-nanoHA hydrogels, the Ca^{2+} concentration was proportional to the amount of nanoHA. The released Ca^{2+} concentration maintained constant for all composites until day 3. Afterward, this period, an increase of released Ca^{2+} concentration released was observed for Alg-nanoHA hydrogels, where, from Alg-nanoHA30, the Ca^{2+} ions release was significantly lower than released from Alg-nanoHA50 and Alg-nanoHA70 throughout the 28 days of incubation.

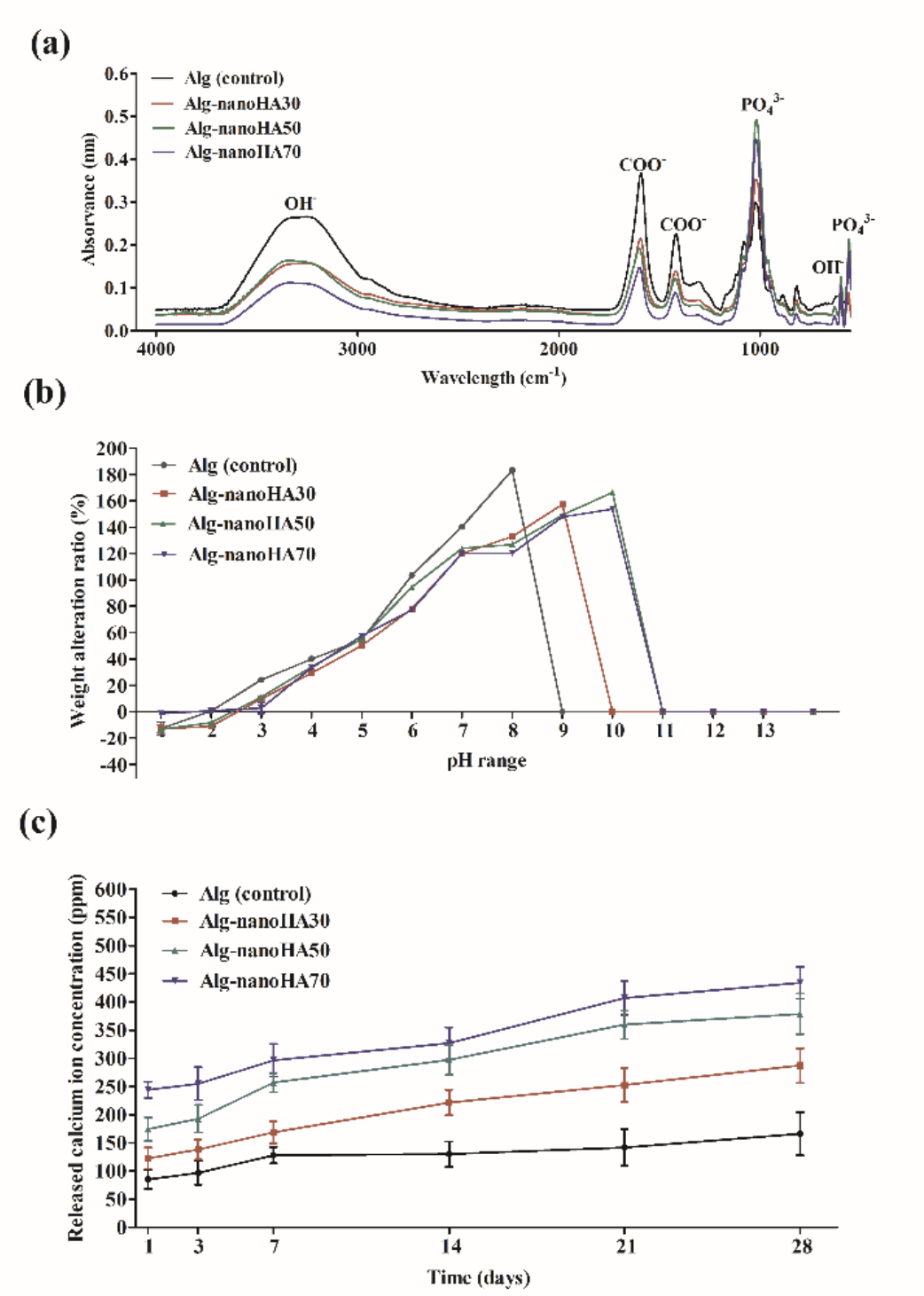

Figure 2 – (A) ATR–FTIR spectra of composites. (B) Stability of the hydrogels at different pH, after 24 h incubation. (C) Released Ca^{2+} ions concentration from composites over time. Data are expressed as mean ± SD (FTIR (n=3); pH stability (n=8) and released calcium (n=5)).

3.1.7 Bioactivity assay in simulated body fluid

The bioactivity of developed composites was addressed by SEM imaging and EDS spectra, after 7 days' immersion in SBF solution (Fig. 3). No apatite crystals deposition was observed on Alg hydrogel, while on Alg-nanoHA, an increase of apatite crystals deposition was observed, evidencing bumps and clusters of apatite's crystals on the composites' surface. Through EDS elemental analysis, the chemical composition of these crystals were identified, attesting to be CaP particles. On Alg surface, only Ca was detected, whereas, on Alg-nanoHA surfaces Ca and P were identified, confirming its surface apatite mineralization (Fig. 3). EDS semi-quantitative analysis revealed an increase of Ca/P ratio proportional to the content of nanoHA within the composite: Alg-nanoHA30 – Ca/P = 1.04, Alg-nanoHA50 – Ca/P = 1.44, and Alg-nanoHA70 – Ca/P = 1.60.

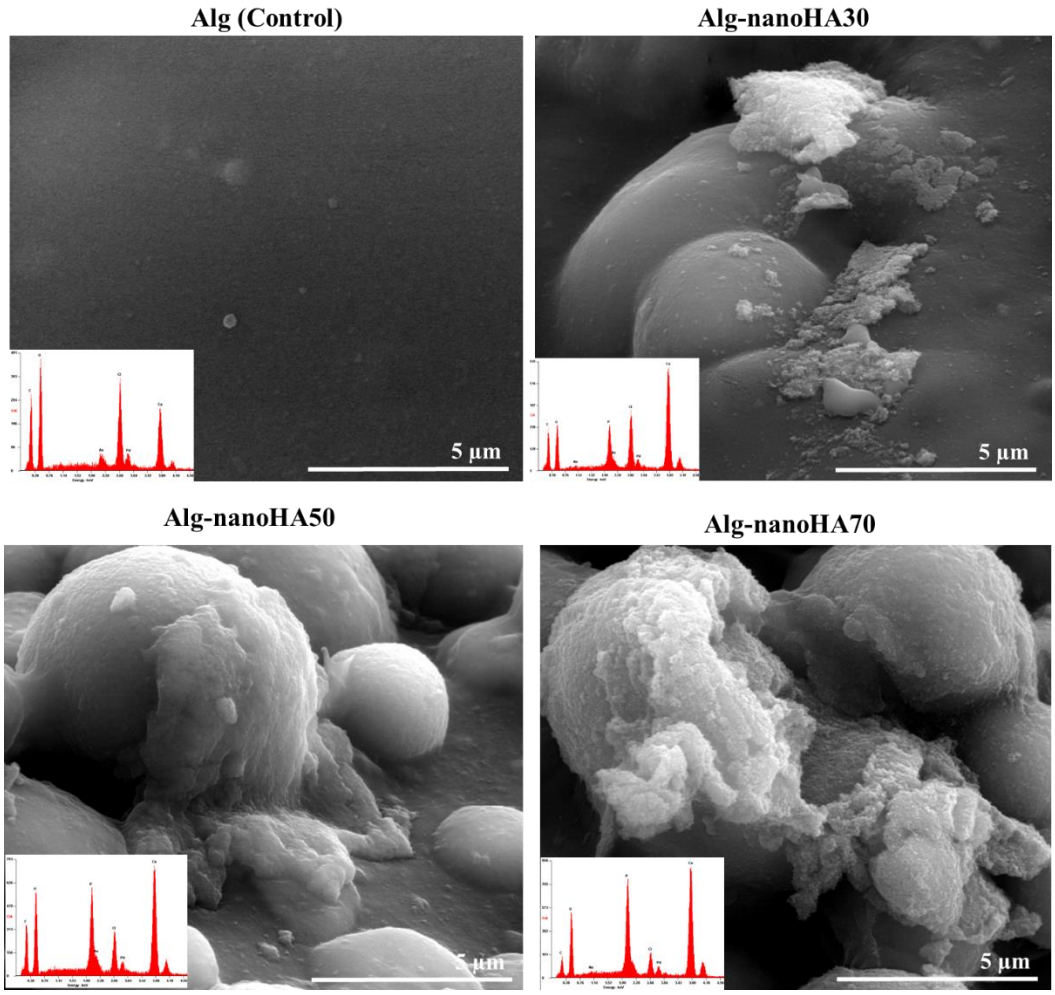

Figure 3 – SEM images and EDS spectra of composites surface after immersion in SBF for 7 days. Scale bar corresponds to 5 µm.

3.2 *In vitro* cytocompatibility assessment with human osteoblastic cells

3.2.1 Metabolic activity of the cultures and cell

The hMSCs cultures metabolic activity and cell proliferation were evaluated by MTT assay (Fig. 4A) and DNA quantification (Fig. 4B), respectively. Either in the control conditions or in the presence of hydrogels, hMSCs metabolic activity increased throughout the culture period with no significant differences between experimental conditions, at any time of incubation (Fig. 4A). Regarding total DNA content, in control conditions, an increase level was attained throughout the culture time suggesting an active cell proliferation throughout the entire culture period. Comparatively, Alg and Alg-nanoHA30 hydrogels induced a similar cell proliferation whereas Alg-nanoHA50 and Alg-nanoHA70 showed a significantly reduced cell proliferation, at day 14 and 21, as compared to the other experimental conditions (Fig. 4B).

3.2.2 Immunofluorescence analysis

The hMSCs cytoskeleton, mitochondrial organization and morphology of cells grown in the presence of developed hydrogels were assessed by immunofluorescence following F-actin and mitochondrial staining, and nucleus counterstaining. Representative micrographs of the cellular culture at day 3 and day 14 are presented on Figure 5. In control conditions, at day 3, cells presented a dense network of F-actin filaments arranged as stress fibers, with cells presenting a flattened and elongated morphology with evident cytoplasmic extensions and long filopodia. Mitochondrial probe revealed an organized tubular network of fused mitochondria, with a preferential perinuclear localization. In addition, cells were found to establish prominent cell-to-cell contacts. Cultures grown on the presence of Alg or Alg-nanoHA hydrogels presented a similar morphology and mitochondrial structure, inducing a similar cytoplasmic organization, F-actin polymerization and mitochondrial arrangement under the different experimental conditions. On day 14, established cultures presented a confluent cell layer within control and in cultures grown with Alg or Alg-nanoHA hydrogels. Cells presented an elongated morphology and a dense mitochondrial network with perinuclear organization.

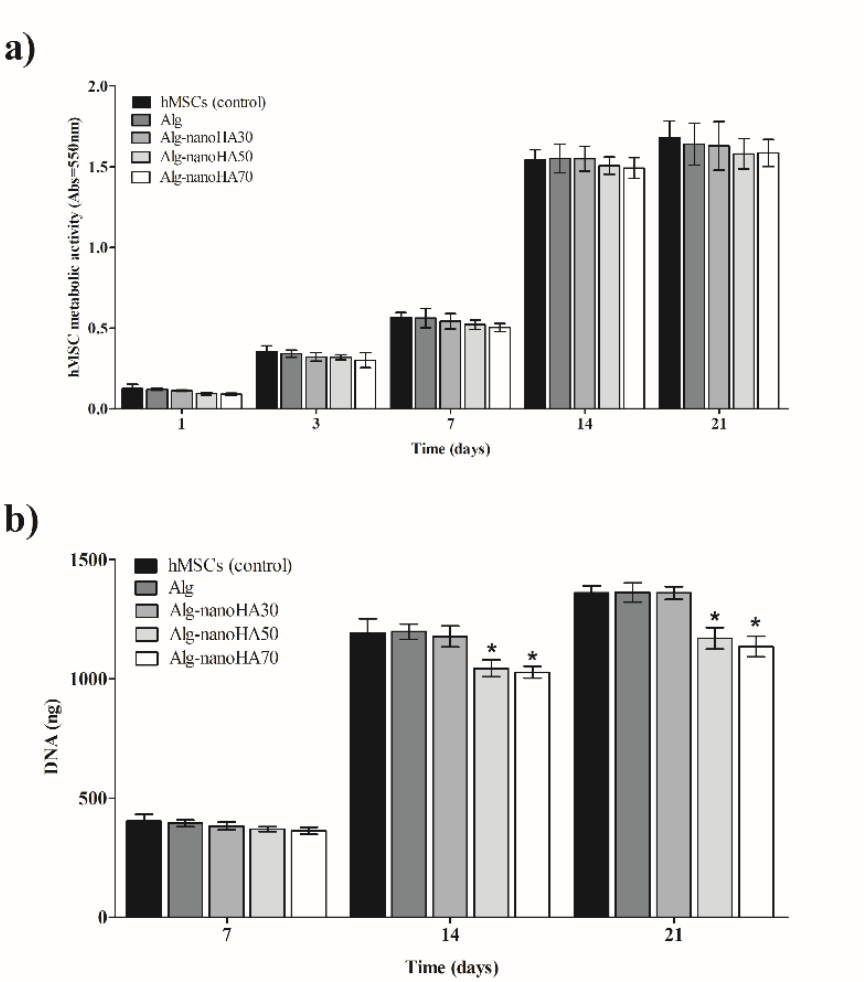

Figure 4 – (a) Metabolic activity and (b) proliferation of hMSCs cultured in the presence of hydrogels. *significant differences between hydrogels and hMSCs (control), for each time point, with $p < 0.05$, obtained by Tukey's post-hoc test. Data are expressed as mean ± SD (n=5).

3.2.3 Gene expression analysis

Gene expression analysis was carried out by quantitative RT-PCR in order to address the osteogenic activation of hMSCs, grown in the presence of developed composites (Fig. 6). hMSCs (control) were grown under basal and osteogenic inducing conditions and were assessed through the expression of the osteogenic transcription factors Runx2 and Sp7, as well as their downstream effectors Col1a1 and BGLAP.

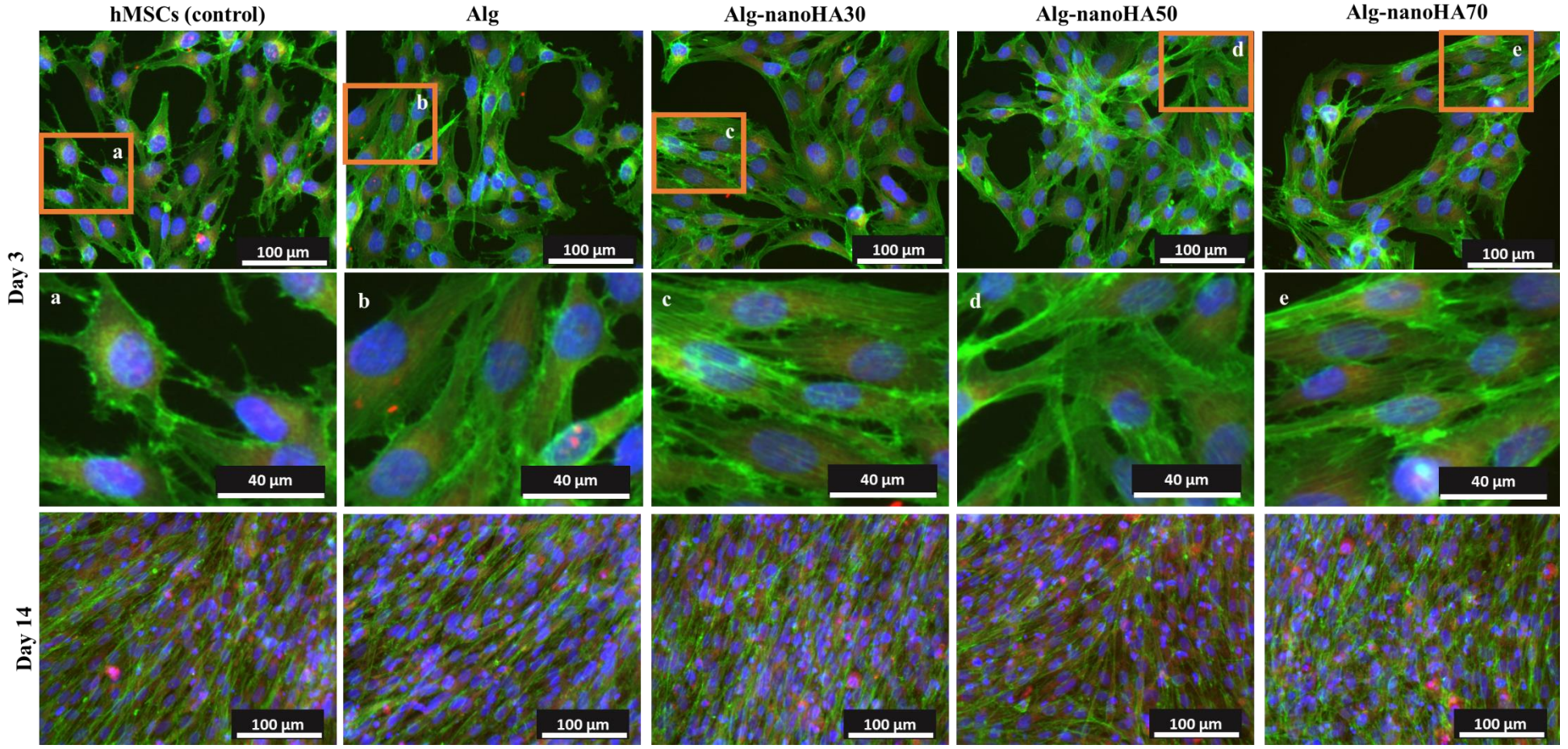

Figure 5 – Immunofluorescent images of hMSCs grown in the presence of hydrogels, at days 3 and 14. Cytoskeleton was stained green, nucleus counterstained in blue and mitochondria stained red. Scale bar corresponds to 40 and 100 µm.

Regarding the expression of Runx2, cultures grown in the presence of Alg presented a similar expression as compared to basal control. Cultures grown in the presence of Alg-nanoHA presented a significantly higher level than basal control and Alg, that, in the case of Alg-nanoHA30 and Alg-nanoHA50, were further found to be significantly higher than the osteogenic-induced control. Regarding Sp7, Col1a1 and BGLAP expression, cultures grown in the presence of Alg hydrogels presented significantly higher levels than basal control. Cultures grown in the presence of Alg-nanoHA hydrogels, particularly Alg-nanoHA30 and Alg-nanoHA50, significantly increased Sp7, Col1a1 and BGLAP expression to levels similar to those attained in osteogenic-induced cultures.

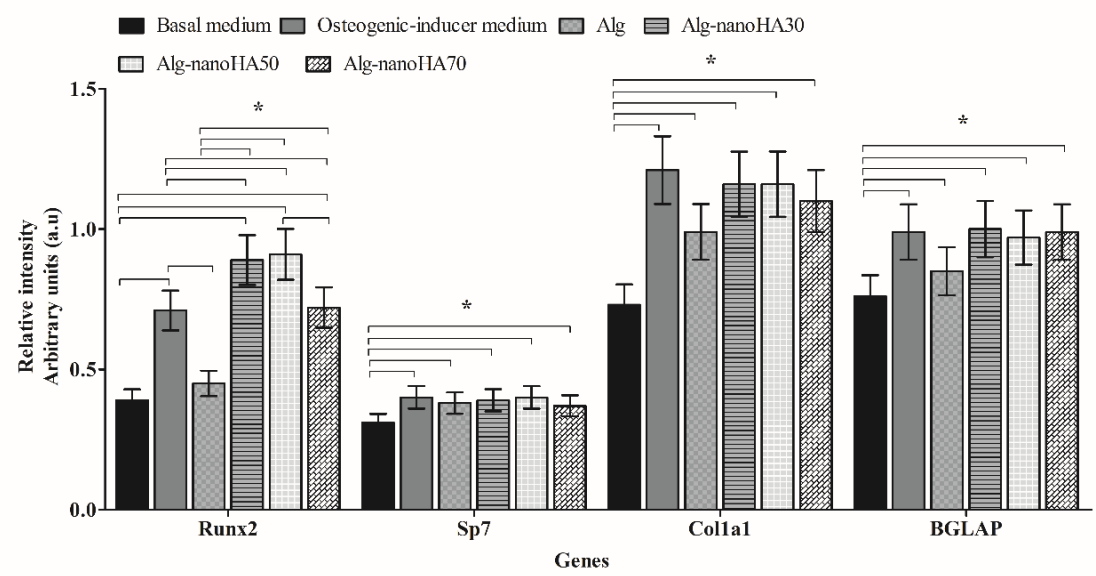

Figure 6 – Gene expression of hMSCs cultured in basal medium, osteogenic-inducer medium, Alg and Alg-nanoHA hydrogels. *Significant differences between all conditions used, with $p < 0.05$, obtained by Tukey's post-hoc test. The relative intensity of each target gene was normalized to beta-actin levels (ACTB), and calculated via the $2^{-\Delta\Delta Ct}$ method. Data are expressed as mean ± SD (n=3). Related transcription factor 2 (RUNX-2), Sp7 transcription factor (SP7), collagen type I (COL1A1) and bone gamma-carboxyglutamate protein (BGLAP).

3.3 *Ex vivo* functional assessment of bone formation

To address the biofunctionality of developed composites, these were implanted in segmental mid-diaphysis defects in embryonic chick femurs, grown for 11 days. Histological assessment of the implanted femurs is presented on Figure 7.

Femurs cultured in the absence (control) and presence of Alg hydrogels moderately induced the osteogenic activation, with evidence of collagen deposition at the defect margin, as observed by the red coloration in SR/AB staining and corresponding blue coloration within Masson's trichrome staining. Evidence of tissue mineralization was further attained at the developing bone collar within the peripheral structure of the tissue, as observed by von Kossa staining. Interestingly, Alg-nanoHA hydrogels induced a distinctive biological response. Alg-nanoHA30 and Alg-nanoHA50 enhanced the osteogenic response; both induced collagen deposition at the marginal bone collar and within the central region of the bone diaphysis, as sustained by the more intense collagen-positive matrix identified on histochemical staining. In addition, an organized pattern of thick mineralized *trabecula* was identified within the collar structure of the diaphysis. Comparatively, a significantly higher osteogenic activation was attained with Alg-nanoHA30, with a strong collagenous matrix being deposited within the central and marginal regions of the diaphysis, in close association with an organized and thick mineralized trabecular structure. Contrariwise, the implantation of Alg-nanoHA70 induced a reduced collagen deposition at the defect margin, as observed by both histochemical staining techniques. Furthermore, a thinner trabecular organization within the collar bone at the diaphysis was verified, with lessened mineralized trabecular organization.

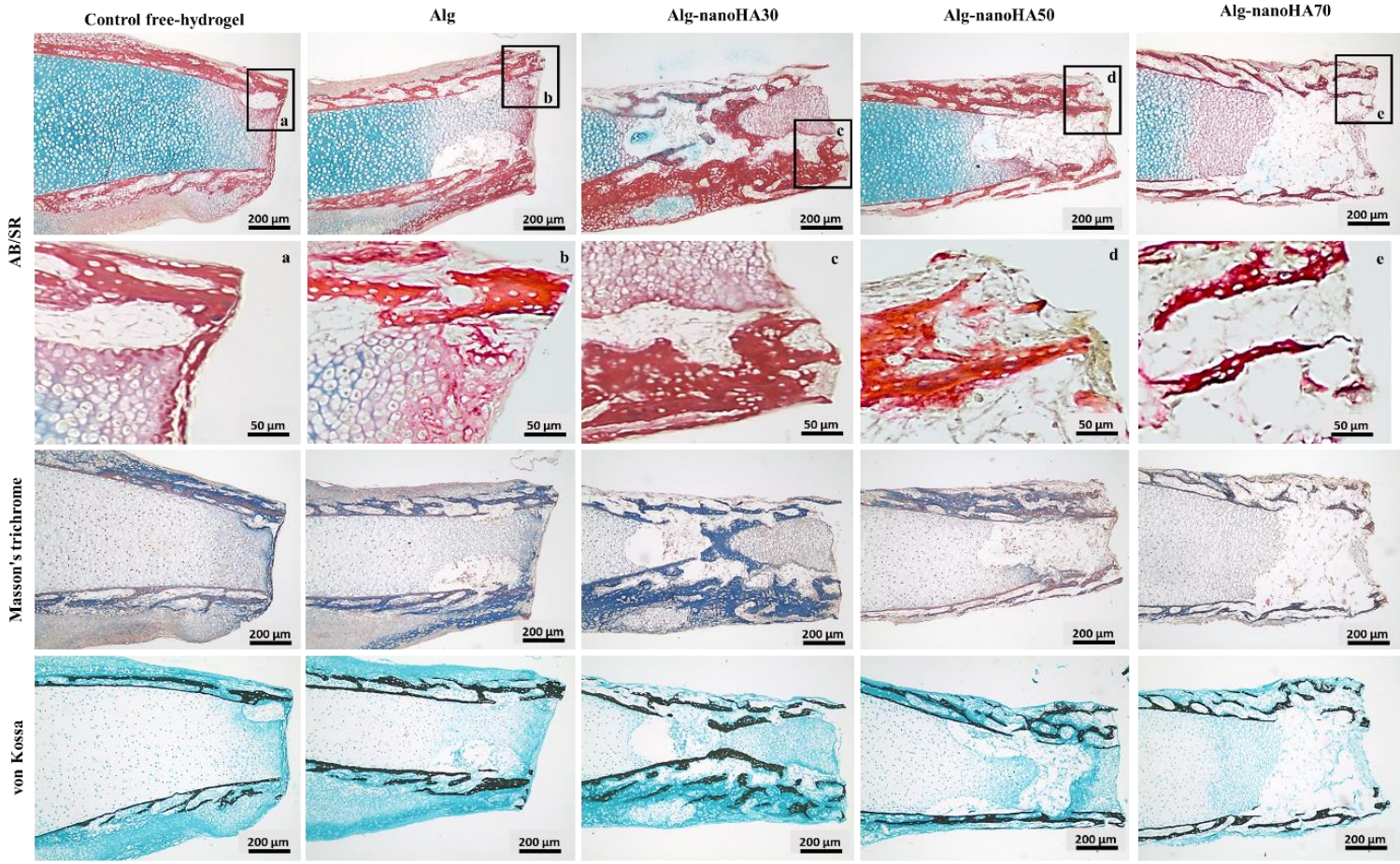

Figure 7 – Histological analysis of embryonic chick femurs implanted with developed composites and cultured for 11 days. Femurs were stained with Alcian blue/Sirius red, Masson's trichrome and von Kossa. Images depict the segmental defect region of the femur in contact with the composite that was lost during histological preparation. Alcian blue/Sirius red (AB/SR) staining marks the proteoglycan cartilage at blue, and the production of collagen at red. Masson's trichrome staining marks the collagen fibers at blue, and van Kossa staining marks the bone mineralization at black. Scale bars correspond to 50 and 200 µm.

4. DISCUSSION

Composites, combining ceramics and polymers, have emerged as potential biomaterials for the management of bone defects [6]. The osteoconductive/osteoinductive, biocompatibility and bioactivity properties of nanoHA materials [7, 28] combined with the injectability, biocompatibility and biodegradation properties of Alg polymers [29, 30] can improve the physic-chemical and cell adhesion/tissue development of the attained composites, enhancing bone tissue re-generation [31–33]. However, these properties could be dependent on the amount of ceramic nanoparticles used within the polymer-based composite, as observed by other authors [21–23]. In this context, in the present study, the influence of nanoHA content on an alginate-based hydrogel system was studied, regarding its physic-chemical and biological properties, within *in vitro* and *ex vivo* studies, aiming to optimize the combination of Alg and nanoHA within the established system for maximizing the bone regeneration process.

Initially, physic-chemical characteristics of Alg-nanoHA hydrogels were addressed. Alg-nanoHA hydrogels, regardless of the nanoHA content, showed a considerable matrix strength, stiffness and permeability, typical of this type of gelation [34]. The characteristic absorption bands of Alg and nanoHA can be clearly seen in the ATR-FTIR spectra, indicating a successful entrapment of nanoHA into the Alg matrix, without chemical reactions occurring between them. The entrapment of nanoHA increased the crosslinking of the polymeric network, mainly when nanoHA was added at 70%. This phenomenon was probably due to the ability of the Ca^{2+} ions, from the nanoHA particles, induces a specific and strong interaction with G-blocks of Alg, increasing the structural cohesion and leading to a stronger matrix with low solubility in water [35]. Moreover, nanoHA particles promoted the formation of rougher surfaces. Some authors have reported that rough implant surfaces, e.g. nanophase titania, zinc oxide or bioglass polymer composites, allow enhanced tissue ingrowth and improve the cell adhesion, proliferation and differentiation compared to smooth polymeric substrates [36, 37]. All Alg-nanoHA hydrogels showed interconnected pores, thus contributing to the retention of a large amount of water in the alginate matrix and further promoting diffusion of nutrients and macromolecules into the structure, following tissue implantation [23, 38].

Water-swelling characteristics of composites play an important role in the absorption of body fluids and transfer of cell nutrients and metabolites [39, 40]. The interactions of

carboxyl (-COOH) and hydroxyl (-OH) groups of the polymeric network with water molecules, leads to their diffusion into the hydrogel driven by the osmotic pressure [17]. However, the water-swelling content of composites decreased with the inclusion of nanoHA, with a significant impact when nanoHA was added at 70%. The presence of nanoHA, particularly at high level, could further contract and restrict the movability of the Alg polymeric chains, creating elastic forces within the hydrogel network, providing resistance to water diffusion and swelling tendencies [17, 39] and, consequently, affecting the diffusivity of nutrients, proteins and metabolites and cell-matrix interactions [17].

The balance between the attractive and repulsive forces in composites was determined by zeta potential measurements [9]. Several authors have shown that low zeta potential values in sodium alginate, carragennan, chitosan, and galactomannans might be associated with a higher concentration of Ca^{2+} ions [9,41,42]. Thereby, with the introduction of nanoHA, there was an increase of Ca^{2+} ions within the polymeric matrix, which could have contributed to increase the ionic strength of the network, consequently bringing zeta potential closer to the isoelectric point [42], which was particularly evident for Alg-nanoHA50 and Alg-nanoHA70. Some authors have reported that the negative surface charge of sheet-shaped hydrogels and calcium composites can positively affect the protein adsorption, osteoblast attachment and proliferation [43, 44].

The pH of tissue fluids undergoing repairing events may play a regulatory role in the healing and mineralization processes of bone since, at the early healing phase, tissue pH is lower than normal physiological pH (7.2), owing to accumulation of acidic metabolites in tissue fluids [45]. Furthermore, during the mineralization phase, an increase in tissue calcium content occurs due to the mineral deposition associated with new bone formation which promotes the increase in pH to reach more alkaline values [45]. The composites used in the present study showed to be stable at a large range of pH values, in which their behavior and stability were found to be influenced by the nanoHA content. At acidic conditions occurs the protonation of the COO^- groups of the Alg network [46], and the presence of nanoHA increases Ca^{2+} concentration and consequently the degree of network cross-linking, promoting the shrinkage of the composites. Under alkaline conditions occurs the ionization of COO^- groups of Alg and the diffusion of Ca^{2+} ions from gelling sites, endorsing the swelling of composites [46]. The high stability of Alg-nanoHA hydrogels at high pH values may be further related to the stability of nanoHA at neutral and alkaline environments [47].

Additionally, the bioactivity response of the composites was characterized regarding the apatite deposition on the materials' surface, upon immersion in SBF. The formation of bone-like mineral on the surfaces is correlated with an increase in the implant's calcium phosphate solubility [48] and is an essential property to indicate the bonding with living bone [48, 49]. No mineral layer was observed over Alg hydrogels, but the presence of nanoHA induced significantly the mineral layer growth with apatite structures developing on Alg-nanoHA hydrogels, which increased with increasing nanoHA content. This increase of apatite on Alg-nanoHA surfaces is probably due to the availability of negatively charged hydroxyl groups on nanoHA that acted as a nucleation site for crystal deposition [48, 49]. However, the observed Ca/P molar ratios were lower than that of stoichiometric hydroxyapatite (HAP), i.e. 1.67 [50]. Several authors have shown that apatite coatings via SBF incubation can have lower Ca/P ratios than stoichiometric HA [50, 51]. Once, the apatite's in vertebrate bone and enamel is not pure hydroxyapatite, it contains other ions, including, CO_3^{2-}, Cl^-, Mg^{2+}, Na^+, and K^+. Small amounts of some of these ions (i.e. Mg^{2+}, Na^+) can substitute for Ca^{2+} ions in the crystal lattice resulting in a lower Ca/P ratio [50].

In fact, the presence of nanoHA into Alg hydrogel increase the source of Ca^{2+} ions into the system, as observed by the released Ca^{2+} concentration from hydrogels detected by ICP-AES. The Ca^{2+} ions could affect the remineralization of demineralized areas, since Ca^{2+} concentration leads to a growth in the saturation of mineralized tissues with nanoHA, favoring the deposition of apatite in the lesions and eventually promoting remineralization [52]. Moreover, the amount of Ca^{2+} ions released from biomaterials can play a vital role in regulating of the chemotaxis, proliferation and osteogenic differentiation of osteoblast cells [49].

The obtained results showed that the nanoHA modified the physic-chemical characteristics of Alg-based hydrogel system. As described, these characteristics could play a vital role in the diffusivity of nutrients, proteins, and metabolites, cell-matrix interactions, chemotaxis, cell proliferation/differentiation, healing and mineralization, highlighting the importance of optimizing the synergism between biomaterials to be addressed in bone tissue regeneration.

The biological response of Alg-nanoHA hydrogel system was also evaluated trough *in vitro* cytocompatibility assessment with human osteoblastic cells and *ex vivo* functional assessment of bone formation. In the present study, hydrogels with nanoHA at 30% promoted higher cell proliferation when compared to those with higher nanoHA content

(50 and 70%), at 14 and 21 days, underlining the importance of nanoHA content for the bioactivity of the composite. Likewise, Eosoly et al found that MC3T3 cells proliferation was affected when high content of nanoHA was used within PCL composites [21]. One possible explanation is the optimal amount of Ca^{2+} ions released from composites, due to the solubility of nanoHA and of Alg hydrogel [53, 54]. Several authors have described that Ca^{2+} ions released from composites (e.g. calcium alginate, nanohydroxyapatite-chitosan, polysaccharide-enriched calcium sulfate) can affect significantly the metabolism of osteoblast cells and bone remodeling within the implantation site [28, 44, 49, 55]. The increase in Ca^{2+} ions concentration could lead to a disturb within the intracellular calcium homeostasis, which plays a vital role in cell proliferation and apoptosis [56, 57], for instance, calcium active calcium-dependent endonucleases that cleavage the DNA [56, 58, 59], and lead to a decrease of cell proliferation. Some authors pointed out that cell proliferation is hydroxyapatite nanoparticles dose-dependent [56, 59].

The cell morphology and cytoskeletal organization are important clues of cell homeostasis [60]. Some authors have described that more elongated cells present a higher degree of cytoskeletal tension (F-actin filaments) and differential expression of downstream effectors, such as RhoA and ROCK, which could enhance pathways associated with osteogenesis [60, 57]. In the present study, regardless of the composition of the composites, hMSCs presented elongated morphology with evident cytoplasmic extensions, indicating good cell functionality and osteogenic potential.

hMSCs cultures grown in the presence of composites were further characterized for the activation of the osteogenic program, with the assessment of Runx2, SP7, Col1a1, and BGLAP gene expression. Runx2 is a key transcriptional regulator for the osteogenic differentiation, directly and indirectly modulating the expression of osteoblastic-specific genes; SP7is also a transcription factor that acts downstream of Runx2, being necessary for the later differentiation of the osteogenic-committed cells into mature osteoblasts [61, 62]. Accordingly, hMSCs grown under osteogenic-stimulating conditions (i.e. in the presence of dexamethasone and ascorbic acid) presented significantly higher levels of both Runx2 and Sp7 transcription factors, a process that seems to result from the upregulation of distinct intracellular pathways, namely converging to the TAZ and MPK1 activation [63]. Comparatively, hMSCs cultures grown in the presence of Alg were found to display Runx2 levels similar to basal control, whether cultures established in the presence of Alg-nanoHA hydrogels presented significantly higher levels than basal

control, and further found to be similar (Alg-nanoHA70) or significantly higher (Alg-nanoHA30 and Alg-nanoHA50) than those attained in osteogenic-induced hMSCs. This suggests that Alg-nanoHA hydrogels are greatly effective on inducing osteogenesis *in vitro* through a significant induction of the master osteogenic regulator Runx2 [61]. Assayed hydrogels were also found to induce the expression of Sp7 to levels like to those attained in osteogenic-induced cultures, further sustaining the increased ability to promote the osteoblastic differentiation. Runx2 and Sp7 transcription factors may subsequently regulate the expression of osteoblastic matrix-related genes such as alkaline phosphatase, bone sialoprotein and, as presently evaluated, Col1a1 and BGLAP, by binding to specific enhancer regions [64]. Col1a1 is a major constituent of the organic extracellular matrix of bone tissue and its expression has been found to occur at high levels during the early stages of osteogenesis, considering an early osteogenic marker [65]. BGLAP codes a major non-collagenous protein of the extracellular matrix being regarded as a late marker of the osteogenic differentiation pathway with a high-level expression associated with the maturation and late differentiation of osteoblastic populations [65]. BGLAP product further contains a Gla (gamma carboxyglutamate) domain, which binds to calcium and hydroxyapatite, regulating bone mineral maturation [65]. Alg-nanoHA hydrogels, particularly Alg-nanoHA30 and Alg-nanoHA50, were found to significantly increase Col1a1 and BGLAP to levels similar to those attained in osteogenic-induced cultures, sustaining the increased osteogenic activation of hMSCs.

Ex vivo data underlined the *in vitro* findings, revealing an enhanced osteogenic response by Alg-nanoHA hydrogels, particularly the Alg-nanoHA30 composition. This condition induced a strong collagenous matrix deposition at the defect margin and stimulated the mineralized trabecular organization at the collar structure. Compositions with higher content of nanoHA (i.e. Alg-nanoHA50 and Alg-nanoHA70) presented an inferior osteogenic activation, whether Alg hydrogel induced the lowest osteogenic activation, in a way similar to control. Previous studies have demonstrated the osteogenic-inducing ability of chitosan/hydroxyapatite composite systems, in bone tissue-related applications [20, 66, 67]. Notwithstanding, no previous studies have addressed the development and biological evaluation of Alg hydrogels' loading with nanoHA particles at different ratios. In the present study, the ability of Alg-nanoHA composites to significantly induce the osteogenic activation in both *in vitro* and *ex vivo* systems was observed. Furthermore, a differential biological response was attained with the loading of distinct nanoHA particles' proportions.

5. CONCLUSIONS

This work denoted that the nanoHA concentration has a vital role in physic-chemical properties and biological response of the assayed composite. Broadly, physic-chemical features, like water-swelling ratio, stability at extreme pH conditions, apatite formation and Ca^{2+} release from Alg-nanoHA hydrogels were nanoHA dose-dependent. The biological response of composites was influenced by nanoHA content, in which Alg-based hydrogel with the nanoHA 30% content enhanced, *in vitro*, the osteoblastic cells' proliferation and osteogenic activation, and, in *ex vivo*, enhanced the collagenous deposition and trabecular bone formation, while those with higher concentrations (50 and 70%) impaired the biological response. The results showed the need to optimize the ratio of the composite's components in order to maximize bone tissue regeneration.

ACKNOLEDGMENTS

This work was financed by FEDER – Fundo Europeu de Desenvolvimento Regional funds through the COMPETE 2020 – Operacional Programme for Competitiveness and Internationalisation (POCI), Portugal 2020, by Portuguese funds through FCT/MCTES in the framework of the project "institute for Research and Innovation in Health Sciences (POCI-01-0145-FEDER-007274), by Project Biotherapies (NORTE-01-0145-FEDER-000012) and by Joana Barros' PhD grant (SFRH/BD/102148/2014). The authors would also like to acknowledge Rui Rocha (CEMUP), Rui Fernandes (HEMS), Rossana Correia (HEMS) and Liliana Grenho (FMDUP).

REFERENCES

1] P. Parhi, A. Ramanan, A.R. Ray, Preparation and characterization of alginate andhydroxyapatite-based biocomposite, J. Appl. Polym. Sci. 102 (2006) 5162–5165.

[2] G. Tozzi, A. De Mori, A. Oliveira, M. Roldo, Composite hydrogels for bone re-generation, Materials 9 (2016).

[3] M.C. Birt, D.W. Anderson, E.B. Toby, J.X. Wang, Osteomyelitis: recent advances in pathophysiology and therapeutic strategies, J. Orthop. 14 (2017) 45–52.

[4] X. Zhang, X. Yin, J. Luo, X. Zheng, H. Wang, J. Wang, et al., Novel hierarchical nitrogen-doped multiwalled carbon nanotubes/cellulose/nanohydroxyapatite nanocomposite as an osteoinductive scaffold for enhancing bone regeneration, ACS Biomaterials Science & Engineering 5 (2019) 294–307.

[5] M. Maisani, S. Ziane, C. Ehret, L. Levesque, R. Siadous, J.F. Le Meins, et al., A new composite hydrogel combining the biological properties of collagen with the mechanical properties of a supramolecular scaffold for bone tissue engineering, J.Tissue Eng. Regen. Med. 12 (2018) e1489–e1500.

[6] S. Obara, T. Yamauchi, N. Tsubokawa, Evaluation of the stimulus response of hydroxyapatite/calcium alginate composite gels, Polym. J. 42 (2010) 161–166.

[7] G. Turco, E. Marsich, F. Bellomo, S. Semeraro, I. Donati, F. Brun, et al., Alginate/hydroxyapatite biocomposite for bone ingrowth: a trabecular structure with high and isotropic connectivity, Biomacromolecules 10 (2009) 1575–1583.

[8] L. Chen, R. Shen, S. Komasa, Y. Xue, B. Jin, Y. Hou, et al., Drug-loadable calcium alginate hydrogel system for use in oral bone tissue repair, Int. J. Mol. Sci. 18(2017).

[9] F.O.M.S. Abreu, C. Bianchini, M.M.C. Forte, T.B.L. Kist, Influence of the composition and preparation method on the morphology and swelling behavior of alginate-chitosan hydrogels, Carbohyd Polym 74 (2008) 283–289.

[10] B. Sarker, R. Singh, R. Silva, J.A. Roether, J. Kaschta, R. Detsch, et al., Evaluation of fibroblasts adhesion and proliferation on alginate-gelatin crosslinked hydrogel, PLoS One 9 (2014) e107952.

[11] M.O. Dalheim, J. Vanacker, M.A. Najmi, F.L. Aachmann, B.L. Strand,B.E. Christensen, Efficient functionalization of alginate biomaterials, Biomaterials 80 (2016) 146–156.

[12] E.S. Place, L. Rojo, E. Gentleman, J.P. Sardinha, M.M. Stevens, Strontium- and zinc-alginate hydrogels for bone tissue engineering, Tissue Eng Part A 17 (2011) 2713–2722.

[13] Y. Luo, A. Lode, C. Wu, J. Chang, M. Gelinsky, Alginate/nanohydroxyapatite scaffolds with designed core/shell structures fabricated by 3D plotting and in situ mineralization for bone tissue engineering, ACS Appl. Mater. Interfaces 7 (2015) 6541–6549.

[14] S. Sancilio, M. Gallorini, C. Di Nisio, E. Marsich, R. Di Pietro, H. Schweikl, et al., Alginate/hydroxyapatite-based nanocomposite scaffolds for bone tissue engineering improve dental pulp biomineralization and differentiation, Stem Cells Int. 2018(2018) 9643721.

[15] K.Fox, P.A. Tran, N. Tran, Recent advances in research applications of nanophase hydroxyapatite, Chemphyschem 13 (2012) 2495–2506.

[16] J. Luo, X. Zhang, J. Ong'achwa Machuki, C. Dai, Y. Li, K. Guo, et al., Three-dimensionally N-doped graphene–hydroxyapatite/agarose as an osteoinductive scaffold for enhancing bone regeneration, ACS Applied Bio Materials 2 (2019) 299–310.

[17] M.C. Du, W.X. Song, Y. Cui, Y. Yang, J.B. Li, Fabrication and biological application of nano-hydroxyapatite (nHA)/alginate (ALG) hydrogel as scaffolds, J. Mater.Chem. 21 (2011) 2228–2236.

[18] Y. Cai, J. Yu, S.C. Kundu, J. Yao, Multifunctional nano-hydroxyapatite and alginate/gelatin based sticky gel composites for potential bone regeneration, Mater.Chem. Phys. 181 (2016) 227–233.

[19] M. Nabavinia, A.B. Khoshfetrat, H. Naderi-Meshkin, Nano-hydroxyapatite-alginate-gelatin microcapsule as a potential osteogenic building block for modular bone tissue engineering, Mater. Sci. Eng. C 97 (2019) 67–77.

[20] X.-F. Wang, P.-J. Lu, Y. Song, Y.-C. Sun, Y.-G. Wang, Y. Wang, Nano hydroxyapatite particles promote osteogenesis in a three-dimensional bio-printing construct consisting of alginate/gelatin/hASCs, RSC Adv. 6 (2016) 6832–6842.

[21] S. Eosoly, N.E. Vrana, S. Lohfeld, M. Hindie, L. Looney, Interaction of cell culture with composition effects on the mechanical properties of polycaprolactone-hydroxyapatite scaffolds fabricated via selective laser sintering (SLS), Mater. Sci. Eng. C 32 (2012) 2250–2257.

[22] S. Salmasi, L. Nayyer, A.M. Seifalian, G.W. Blunn, Nanohydroxyapatite effect on the degradation, osteoconduction and mechanical properties of polymeric bone tissue engineered scaffolds, Open Orthop J 10 (2016) 900–919.

[23] X. Zhang, W. Chang, P. Lee, Y. Wang, M. Yang, J. Li, et al., Polymer-ceramic spiral structured scaffolds for bone tissue engineering: effect of hydroxyapatite composition on human fetal osteoblasts, PLoS One 9 (2014) e85871.

[24] N. Mohammed, N. Grishkewich, R. Berry, K. Tam, Cellulose nanocrystal-alginate hydrogel beads as novel adsorbents for organic dyes in aqueous solutions, Cellulose 22 (2015) 3725–3738.

[25] T. Kokubo, H. Takadama, How useful is SBF in predicting in vivo bone bioactivity? Biomaterials 27 (2006) 2907–2915.

[26] C.F. dos Santos, P.S. Gomes, M.M. Almeida, M.G. Willinger, R.P. Franke, M.H. Fernandes, et al., Gold-dotted hydroxyapatite nanoparticles as multifunctional platforms for medical applications, RSC Adv. 5 (2015) 69184–69195.

[27] E.L. Smith, J.M. Kanczler, C.A. Roberts, R.O. Oreffo, Developmental cues for bone formation from parathyroid hormone and parathyroid hormone-related protein in an *ex vivo* organotypic culture system of embryonic chick femora, Tissue Eng Part C Methods 18 (2012) 984–994.

[28] N. Cao, X.B. Chen, D.J. Schreyer, Influence of calcium ions on cell survival and proliferation in the context of an alginate hydrogel, ISRN Chemical Engineering 2012 (2012) 9.

[29] G. Montalbano, S. Toumpaniari, A. Popov, P. Duan, J. Chen, K. Dalgarno, et al., Synthesis of bioinspired collagen/alginate/fibrin based hydrogels for soft tissue engineering, Mater. Sci. Eng. C 91 (2018) 236–246.

[30] Y.-W. Kim, J.E. Kim, Y. Jung, J.-Y. Sun, Non-swellable, cytocompatible pHEMAalginate hydrogels with high stiffness and toughness, Mater. Sci. Eng. C 95 (2019) 86–94.

[31] S. van Rijt, P. Habibovic, Enhancing regenerative approaches with nanoparticles, J. R. Soc. Interface 14 (2017).

[32] M. Biondi, A. Borzacchiello, L. Mayol, L. Ambrosio, Nanoparticle-integrated hydrogels as multifunctional composite materials for biomedical applications, Gels 1 (2015) 162.

[33] S. Pacelli, S. Basu, C. Berkland, J. Wang, A. Paul, Design of a cytocompatible hydrogel coating to modulate properties of ceramic-based scaffolds for bone repair, Cell. Mol. Bioeng. 11 (2018) 211–217.

[34] S. Ahirrao, P. Gide, B. Shrivastav, P. Sharma, Extended release of theophylline through sodium alginate hydrogel beads: effect of glycerol on entrapment efficiency, drug release, Particul Sci Technol 32 (2014) 105–111.

[35] M.J. Costa, A.M. Marques, L.M. Pastrana, J.A. Teixeira, S.M. Sillankorva, M.A. Cerqueira, Physicochemical properties of alginate-based films: effect of ionic crosslinking and mannuronic and guluronic acid ratio, Food Hydrocoll. 81 (2018) 442–448.

[36] M. Jager, H.P. Jennissen, F. Dittrich, A. Fischer, H.L. Kohling, Antimicrobial and osseointegration properties of nanostructured titanium orthopaedic implants, Materials (Basel, Switzerland) (2017) 10.

[37] S.K. Nishimoto, M. Nishimoto, S.W. Park, K.M. Lee, H.S. Kim, J.T. Koh, et al., The effect of titanium surface roughening on protein absorption, cell attachment, and cell spreading, Int. J. Oral Maxillofac. Implants 23 (2008) 675–680.

[38] N. Annabi, J.W. Nichol, X. Zhong, C. Ji, S. Koshy, A. Khademhosseini, et al., Controlling the porosity and microarchitecture of hydrogels for tissue engineering, Tissue Eng. B Rev. 16 (2010) 371–383.

[39] J. Zhang, Q. Wang, A. Wang, In situ generation of sodium alginate/hydroxyapatite nanocomposite beads as drug-controlled release matrices, Acta Biomater. 6 (2010) 445–454.

[40] L. Fan, J.P. Zhang, A.Q. Wang, *In situ* generation of sodium alginate/hydroxyapatite/ halloysite nanotubes nanocomposite hydrogel beads as drug-controlled release matrices, J. Mater. Chem. B 1 (2013) 6261–6270.

[41] M.G. Carneiro-da-Cunha, M.A. Cerqueira, B.W.S. Souza, J.A. Teixeira, A.A. Vicente, Influence of concentration, ionic strength and pH on zeta potential and mean hydrodynamic diameter of edible polysaccharide solutions envisaged for multinanolayered films production, Carbohyd Polym 85 (2011) 522–528.

[42] V. Uskokovic, R. Odsinada, S. Djordjevic, S. Habelitz, Dynamic light scattering and zeta potential of colloidal mixtures of amelogenin and hydroxyapatite in calcium and phosphate rich ionic milieus, Arch. Oral Biol. 56 (2011) 521–532.

[43] R. Smeets, A. Kolk, M. Gerressen, O. Driemel, O. Maciejewski, B. Hermanns-Sachweh, et al., A new biphasic osteoinductive calcium composite material with a negative zeta potential for bone augmentation, Head Face Med 5 (2009) 13.

[44] Y.M. Chen, J.P. Gong, M. Tanaka, K. Yasuda, S. Yamamoto, M. Shimomura, et al., Tuning of cell proliferation on tough gels by critical charge effect, J. Biomed. Mater. Res. A 88 (2009) 74–83.

[45] D.A. Chakkalakal, A.A. Mashoof, J. Novak, B.S. Strates, M.H. McGuire, Mineralization and pH relationships in healing skeletal defects grafted with demineralized bone matrix, J. Biomed. Mater. Res. 28 (1994) 1439–1443.

[46] M. Matyash, F. Despang, C. Ikonomidou, M. Gelinsky, Swelling and mechanical properties of alginate hydrogels with respect to promotion of neural growth, Tissue Eng Part C Methods 20 (2014) 401–411.

[47] C.S.D. Lee, H.R. Moyer, R.A. Gittens, J.K. Williams, A.L. Boskey, B.D. Boyan, et al., Regulating *in vivo* calcification of alginate microbeads, Biomaterials 31 (2010) 4926–4934.

[48] S. Bertazzo, W.F. Zambuzzi, D.D.P. Campos, T.L. Ogeda, C.V. Ferreira, C.A. Bertran, Hydroxyapatite surface solubility and effect on cell adhesion, Colloid Surface B 78 (2010) 177–184.

[49] S. Dhivya, S. Saravanan, T.P. Sastry, N. Selvamurugan, Nanohydroxyapatite reinforced chitosan composite hydrogel for bone tissue repair in vitro and in vivo, J Nanobiotechnol 13 (2015).

[50] D. Suarez-Gonzalez, K. Barnhart, E. Saito, R. Vanderby, S.J. Hollister, W.L. Murphy, Controlled nucleation of hydroxyapatite on alginate scaffolds for stem cell-based bone tissue engineering, J. Biomed. Mater. Res. A 95a (2010) 222–234.

[51] L. Jongpaiboonkit, T. Franklin-Ford, W.L. Murphy, Growth of hydroxyapatite coatings on biodegradable polymer microspheres, Acs Appl Mater Inter 1 (2009) 1504–1511.

[52] E. Pepla, L.K. Besharat, G. Palaia, G. Tenore, G. Migliau, Nano-hydroxyapatite and its applications in preventive, restorative and regenerative dentistry: a review of literature, Ann Stomatol (Roma) 5 (2014) 108–114.

[53] K.Y. Lee, D.J. Mooney, Alginate: properties and biomedical applications, Prog. Polym. Sci. 37 (2012) 106–126.

[54] Z.F. Chen, B.W. Darvell, V.W. Leung, Hydroxyapatite solubility in simple inorganic solutions, Arch. Oral Biol. 49 (2004) 359–367.

[55] G. Chan, D.J. Mooney, Ca(2+) released from calcium alginate gels can promote inflammatory responses in vitro and in vivo, Acta Biomater. 9 (2013) 9281–9291.

[56] R. Meena, K.K. Kesari, M. Rani, R. Paulraj, Effects of hydroxyapatite nanoparticles on proliferation and apoptosis of human breast cancer cells (MCF-7), J. Nanopart. Res. 14 (2012) 712.

[57] R. Zhao, P. Xie, K. Zhang, Z. Tang, X. Chen, X. Zhu, et al., Selective effect of hydroxyapatite nanoparticles on osteoporotic and healthy bone formation correlates with intracellular calcium homeostasis regulation, Acta Biomater. 59 (2017) 338–350.

[58] J. Zhang, X. Luo, D. Barbieri, A.M. Barradas, J.D. de Bruijn, C.A. van Blitterswijk, et al., The size of surface microstructures as an osteogenic factor in calcium phosphate ceramics, Acta Biomater. 10 (2014) 3254–3263.

[59] W. Tang, Y. Yuan, C. Liu, Y. Wu, X. Lu, J. Qian, Differential cytotoxicity and particle action of hydroxyapatite nanoparticles in human cancer cells, Nanomedicine (London, England) 9 (2014) 397–412.

[60] P.S. Mathieu, E.G. Loboa, Cytoskeletal and focal adhesion influences on mesenchymal stem cell shape, mechanical properties, and differentiation down osteogenic, adipogenic, and chondrogenic pathways, Tissue Eng. B Rev. 18 (2012) 436–444.

[61] E.D. Jensen, R. Gopalakrishnan, J.J. Westendorf, Regulation of gene expression in osteoblasts, BioFactors (Oxford, England) 36 (2010) 25–32.
[62] T. Komori, Regulation of bone development and extracellular matrix protein genes by RUNX2, Cell Tissue Res. 339 (2010) 189–195.
[63] F. Langenbach, J. Handschel, Effects of dexamethasone, ascorbic acid and β glycerophosphate on the osteogenic differentiation of stem cells in vitro, Stem Cell Res Ther 4 (2013) 117.
[64] H. Harada, S. Tagashira, M. Fujiwara, S. Ogawa, T. Katsumata, A. Yamaguchi, et al., Cbfa1 isoforms exert functional differences in osteoblast differentiation, J. Biol. Chem. 274 (1999) 6972–6978.
[65] G. Karsenty, Minireview: transcriptional control of osteoblast differentiation, Endocrinology 142 (2001) 2731–2733.
[66] Y. He, Y. Dong, F. Cui, X. Chen, R. Lin, Ectopic osteogenesis and scaffold biodegradation of nano-hydroxyapatite-chitosan in a rat model, PLoS One 10 (2015) e0135366.
[67] E. Chatzipetros, P. Christopoulos, C. Donta, K.I. Tosios, E. Tsiambas, D. Tsiourvas, et al., Application of nano-hydroxyapatite/chitosan scaffolds on rat calvarial critical-sized defects: a pilot study, Medicina oral, patologia oral y cirugia bucal 23 (2018) e625–e632.

CHAPTER 3

Lytic bacteriophages against multidrug-resistant *Staphylococcus aureus*, *Enterococcus faecalis* and *Escherichia coli* strains isolated from orthopaedic implant-associated infections

Joana Barros[a,b,c,*], Luís D.R. Melo[d], Patrícia Poeta[e,f], Gilberto Igrejas[f,g,h], Maria P. Ferraz[i], Joana Azeredo[d], Fernando J. Monteiro[a,b,c]

[a]i3S–Instituto de Investigação e Inovação em Saúde, Universidade do Porto, Rua Alfredo Allen 208, 4200-135 Porto, Portugal

[b]INEB–Instituto Nacional de Engenharia Biomédica, Porto, Portugal

[c]FEUP–Faculdade de Engenharia, Universidade do Porto, Porto, Portugal

[d]Laboratório de Investigação em Biofilmes Rosário Oliveira, Center of Biological Engineering, University of Minho, Braga, Portugal

[e]Department of Veterinary Sciences, University of Trás-os-Montes and Alto Douro, Vila Real, Portugal

[f]LAQV-REQUIMTE, Faculty of Science and Technology, Nova University of Lisbon, Lisbon, Portugal

[g]Department of Genetics and Biotechnology, University of Trás-os-Montes and Alto Douro, Vila Real, Portugal

[h]Functional Genomics and Proteomics Unit, University of Trás-os-Montes and Alto Douro, Vila Real, Portugal

[i]FP-ENAS/CEBIMED–University Fernando Pessoa Energy, Environment and Health Research Unit/Biomedical Research Center, Porto, Portugal

International Journal of Antimicrobial Agents, DOI: 10.1016/j.ijantimicag.2019.06.007

ABSTRACT

Orthopaedic implant-associated infections are a devastating complication of orthopaedic surgery with a significant impact on patients and healthcare systems. The aims of this work were to describe the patterns of antimicrobial resistance, pathogenicity and virulence of clinical bacterial isolates from orthopaedic implant-associated infections and to further isolate and characterise bacteriophages that are efficient in controlling these bacteria. *Staphylococcus aureus*, *Enterococcus faecalis* and *Escherichia coli* isolated from orthopaedic infections showed multiresistance patterns to the most frequently used antibiotics in clinical settings. The presence of mobile genetic elements (*mecA*, Tn*916*/Tn*1545* and *intl1*) and virulence determinants (*icaB*, *cna*, *hlb*, *cylLs*, *cylM*, *agg*, *gelE*, *fsr* and *fimA*) highlighted the pathogenicity of these isolates. Moreover, the isolates belonged to clonal complexes associated with the acquisition of pathogenicity islands and antimicrobial resistance genes by recombination and horizontal gene transfer. Bacteriophages vB_SauM_LM12, vB_EfaS_LM99 and vB_EcoM_JB75 were characterised and their ability to infect clinical isolates of *S. aureus*, *E. faecalis* and *E. coli*, respectively, was assessed. Morphological and genomic analyses revealed that vB_EfaS_LM99 and vB_EcoM_JB75 belong to the *Siphoviridae* and *Myoviridae* families, respectively, and no genes associated with lysogeny were found. The bacteriophages showed low latent periods, high burst sizes, broad host ranges and tolerance to several environmental conditions. Moreover, they showed high efficiency and specificity to infect and reduce clinical bacteria, including methicillin resistant *S. aureus* and vancomycin-resistant enterococci. Therefore, the results obtained suggest that the bacteriophages used in this work are a promising approach to control these pathogens involved in orthopaedic implant-associated infections.

Keywords: Implant-associated infection, Pathogenic bacteria, Multidrug resistant, Phage therapy, Efficiency, Specificity

GRAPHICAL ABSTRACT

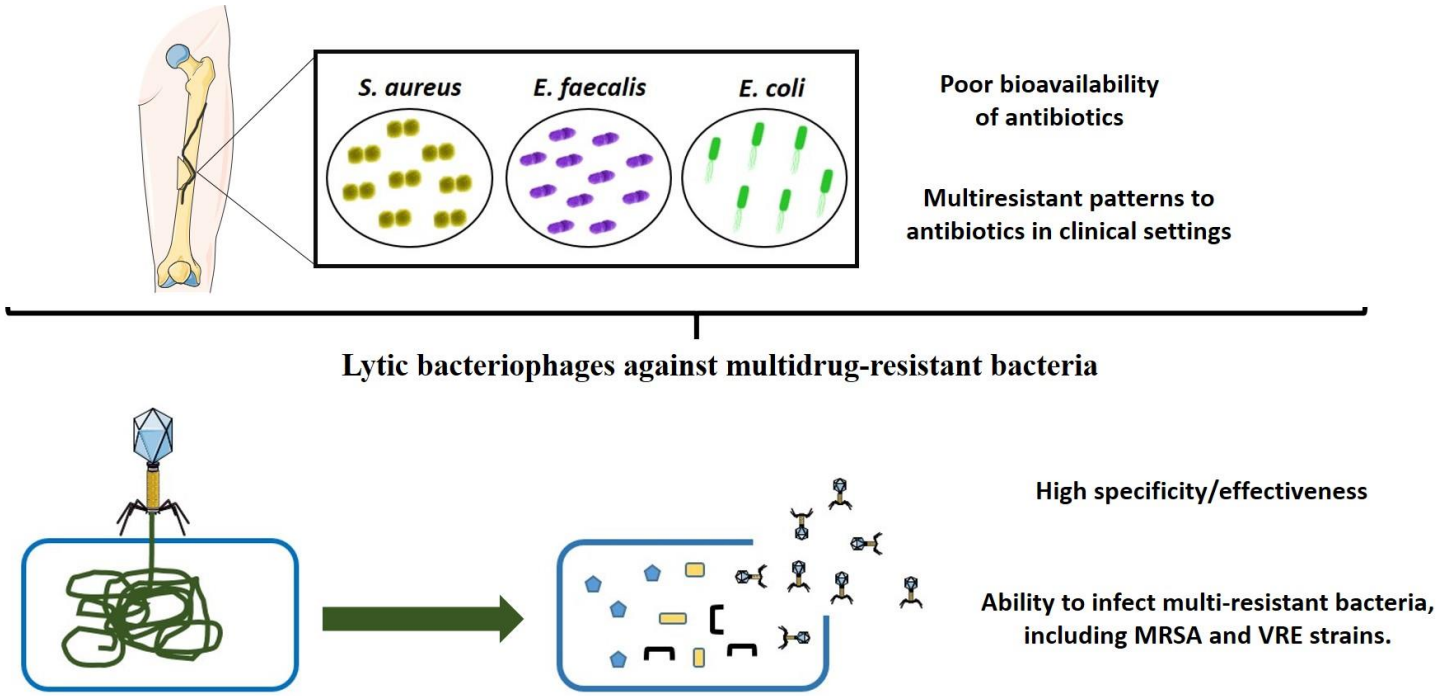

1. INTRODUCTION

Orthopaedic implant-associated infections are a devastating complication of orthopaedic surgery with a significant impact on patient quality of life and healthcare systems [1]. The most commonly isolated bacteria from these infections are *Staphylococcus aureus* (33–43%), *Staphylococcus epidermidis* (18–40%) and *Enterococcus* spp. (2.5–15%, mainly *Enterococcus faecalis*). However, Gram-negative bacilli, including *Escherichia coli* and *Pseudomonas aeruginosa*, are less frequent causes of implant-associated infection (4–7%) [2–4]. The emergence of antimicrobial-resistant bacteria and their ability to produce virulence factors have contributed to enhancing the pathogenicity and severity of orthopaedic implant associated infections [3,4–7]. According to the World Health Organization (WHO), these bacteria, namely methicillin-resistant *S. aureus* (MRSA) and vancomycin-resistant enterococci (VRE), are classified as a serious threat to public health owing to limited therapeutic options [8].

To address this situation, the use of bacteriophages (phages) has been extensively studied as an alternative therapeutic strategy [9]. Phages are bacterial viruses that specifically infect bacteria, hijacking their machinery, replicating intracellularly and finally lysing the host bacterium [7,10]. *In vitro* and *in vivo* studies have shown that for several situations, phage therapy is more specific, accurate and without adverse effects/local tissue toxicity compared with antibiotic therapy [7,10,11]. Characteristics such as bioavailability at the site of infection and migratory ability to other infection sites make this therapy more attractive. Therefore, phage therapy could be a promising alternative strategy to treat orthopaedic implant-associated infections. The purposes of this work were primarily to describe the patterns of antimicrobial resistance, pathogenicity and virulence of bacteria isolated from orthopaedic implant-associated infections and further to isolate and characterise phages that are efficient in controlling these pathogens.

2. MATERIAL AND METHODS

2.1 Characterisation of bacterial isolates

Bacterial isolates related to orthopaedic implant-associated infections were provided by Centro Hospitalar de Vila Nova de Gaia/Espinho, EPE (CHVNG) (Vila Nova de Gaia, Portugal) (Table 1). Over a 5-month period, 18 samples from osteoarticular infections were collected from patients at CHVNG. Biological samples were collected enabling the

isolation and identification of 19 bacterial isolates using VITEK®2 Compact Bacterial Identification and Monitoring System (bioMérieux Inc., Durham, NC) following standardised protocols implemented at CHVNG. The study was approved by the hospital ethics committee, and patient records were anonymised prior to analysis.

2.1.1 Antimicrobial resistance and genomic characterisation

Clinical isolates were subjected to antimicrobial susceptibility testing by the disk diffusion method according to European Committee on Antimicrobial Susceptibility Testing (EUCAST) and Clinical and Laboratory Standards Institute (CLSI) guidelines [12,13]. The antimicrobial classes, antibiotic concentration and zone diameter breakpoint for each bacterial species were defined according to EUCAST and CLSI recommendations following the disk diffusion antimicrobial susceptibility testing method. Genomic DNA of each isolate was extracted using specific methods: for S. *aureus*, lysostaphin/proteinase K/Tris–HCl [14]; for *E. faecalis*, InstaGeneTM matrix [15]; and for *E. coli*, boiling [15]. MRSA identification was performed by amplification of the *mecA* and *nucC* genes [16]. Detection of *tndX* and *int* genes in *E. faecalis* isolates was performed to demonstrate the presence of Tn*5397*-like and Tn*916*/Tn*1545*-like transposons, respectively [15]. The *intI1* and *intI2* genes, encoding class 1 and 2 integrases, respectively, were amplified in *E. coli* isolates [15]. For *E. coli*, the phylogenetic group (A, B1, B2 and D) was identified by amplification of the *chuA* and *yjaA* genes as well as DNA fragment TspE4.C2 [15,17,18]. Screening of virulence genes for *S. aureus* (*cna*, *eta*, *etb*, *tst*, *hlb*, *icaA*, *icaB* and *icaC*), *E. faecalis* (*ace*, *agg*, *gelE*, *esp*, *hyl*, *fsr* and *cylL$_L$L$_S$ABM*) and *E. coli* (*fimA*, *papGIII*, *stx*, *cnf1* and *papC*) was performed by PCR [14–18]. Positive and negative controls were used from the bacterial collection of the Medical Microbiology Laboratory of the Universidade de Trás-os-Montes e Alto Douro (UTAD) (Vila Real, Portugal). A list of the primers used is provided in the Supplementary material SS1.

2.1.2 Multilocus sequence typing (MLST)

Staphylococcus aureus and *E. faecalis* isolates were characterised by MLST. Internal fragments of seven housekeeping genes of *S. aureus* (*arcC*, *aroE*, *glpF*, *gmk*, *pta*, *tpi* and *yqiL*) and *E. faecalis* (*gdh*, *gyd*, *pstS*, *gki*, *aroE*, *xpt* and *yiqL*) were amplified using the primers listed in Supplementary material SS1 and were sequenced. The obtained

sequences were analysed by https://pubmlst.org/general.shtml and eBURST V3 to assign a specific sequence type (ST) and clonal complex (CC). Positive and negative controls were used from the bacterial collection of the Medical Microbiology Laboratory at UTAD.

2.2 Bacteriophage isolation/production and characterisation

A previously isolated phage from the Bacteriophage Biotechnology Group of the Centre for Biological Engineering (BBiG/CEB– Universidade do Minho, Braga, Portugal) was used to infect *S. aureus* isolates [19]. Specific new phages towards *E. faecalis* and *E. coli* strains were isolated from a wastewater treatment plant at Frossos (Braga, Portugal). A sample enrichment method was performed to isolate phages [20]. Briefly, centrifuged effluent was mixed with double-strength trypticase soy broth and exponentially grown *E. faecalis* and *E. coli* strains, respectively. The solution was then incubated at 37 °C and 120 rpm for 24 h and was further centrifuged and the supernatant was filtered through a PES 0.22 μM filter. Spot assays were performed against bacterial lawns to test for the presence of phages. Inhibition haloes were further purified and plaque picking was repeated until single-plaque morphology was observed. Phages were produced as previously described with some modifications [21]. Briefly, phage solutions were spread on lawns of their respective host strains (*S. aureus* 12, *E. faecalis* 99 and *E. coli* 2129975) using a paper strip and were incubated overnight at 37 °C. After full lysis, salt magnesium buffer was added to each plate and the plates were incubated at 4 °C and 120 rpm for 24 h. Subsequently, both liquid and top agar were collected and centrifuged and the supernatant was filtered. Chloroform was added to the filtered solution and the samples were stored at 4 °C for further use. Lytic spectra and efficiency of plating (EOP) were determined according to Kvachadze et al. [22]. In brief, phage suspensions were serially diluted and were placed over original or target host bacteria and the presence of a clear zone of lysis was examined following incubation at 37 °C for 16–18 h. The relative EOP was calculated as the ratio of the phage titre (PFU/mL) obtained in each isolate and that obtained in the propagating host. Three independent experiments were performed in duplicate.

2.2.1 Thermal and pH stability tests

To assess thermostability, phage solutions were incubated at different temperatures (–20 °C to 60 °C) for 24 h. To assess pH stability, phage suspensions were prepared at different pH values (pH 1–13) and were incubated at 4 °C for 24 h. In both cases, following incubation phages were titrated using the double-layer agar plate method to determine surviving phages. Three independent experiments were performed in duplicate.

2.2.2 Bacteriophages morphology

Phages were sedimented by centrifugation and the pellet was washed in tap water by repeating the centrifugation step [24]. Phages were deposited on copper grids with a carbon-coated Formvar film grid, were stained with 2% uranyl acetate (pH 4) and were examined using a JEOL JEM transmission electron microscope (TEM - Tokyo, Japan).

2.2.3 One-step Growth Curves

One-step growth curves were performed as previously described [21]. Briefly, host bacteria were grown to exponential phase and were then harvested and re-suspended in fresh medium. Respective phage solutions were added to exponential-phase cultures of host bacteria at a multiplicity of infection (MOI) of 0.01 and were allowed to adsorb for 5 min at 37 °C. The mixtures were centrifuged and the pellets were then re-suspended in fresh medium broth. Samples were taken at 10-min intervals and phage titration was performed by the double-layer agar plating method. Three independent experiments were performed in duplicate.

2.2.4 Genome sequencing analysis

Escherichia phage vB_EcoM_JB75 (JB75) and *Enterococcus* phage vB_EfaS_LM99 (LM99) genomic DNA was extracted essentially as previously described [24]. In brief, purified phages were treated with 0.016% (v/v) L1 buffer at 37 °C for 2 h. The enzymes were further thermally inactivated for 30 min at 65 °C. Then, phage proteins were digested with 50 μg/mL proteinase K, 20 mM ethylene diamine tetra-acetic acid (EDTA) and 1% sodium dodecyl sulfate (SDS) at 56 °C for 18 h. This was followed by phenol, phenol:chloroform (1:1, v/v) and chloroform extractions. DNA was precipitated with ice-cold absolute ethanol and 3 M sodium acetate (pH 4.6) and was then centrifuged. Pellets were washed in 70% ice-cold ethanol and were further air-dried and re-suspended in

nuclease-free water. Phage genomes were sequenced using an Illumina HiSeq system (Illumina Inc., San Diego, CA) with individual libraries of two non-homologous phages pooled together in equal amounts. Libraries were constructed using the KAPA DNA Library Preparation Kit Illumina (KAPA Biosystems, San Diego, CA) with the KAPA HiFi preparation protocol and were sequenced using 100-bp paired-end mode. The quality of the produced data was determined by Phred quality score at each cycle. Reads were demultiplexed and de novo assembled into a single contig with average coverage above 100 × using CLC Genomics Workbench v.7.0 (CLC Bio, Aarhus, Denmark) and were manually inspected. Phage genomes were first annotated using myRAST algorithm and were further manually inspected for potential alternative start codons or for the presence of non-annotated coding sequences (CDSs) using Geneious 9.1.4 (Biomatters Ltd., Auckland, New Zealand). Functions of the gene products were searched with BLASTp (coverage >80%; *E-value* $\leq 10^{-5}$) and Pfam programs (*E-value* $\leq 10^{-5}$). The presence of transmembrane domains was checked using TMHMM and Phobius, and membrane proteins were annotated when both tools were in concordance. Protein parameters (molecular weight and isoelectric point) were determined using ExPASy Compute pI/Mw tool. Moreover, transfer RNAs (tRNAs) were scanned using tRNAscan-SE and ARAGORN. Promoter regions were determined using PromoterHunter from the phiSITE database and were further checked manually. ARNold was used to predict rho-independent terminators, and the energy was calculated using Mfold.

2.3 Activity of bacteriophages against clinical bacteria

The activity of phages against the bacterial isolates from orthopaedic implant-associated infections was evaluated. Bacterial cultures were grown to exponential phase and were re-suspended in fresh medium. Phage solutions were added to bacterial cultures of each respective bacterium at a MOI of 10. These suspensions were incubated at 37 °C at 120 rpm for 2, 6 and 24 h. The number of cultivable cells was determined using the microdrop method. Three independent experiments were performed in duplicate.

2.4 Statistical analysis

Experimental data were analysed using IBM SPSS Statistics v.22.0 (IBM Corp., Armonk, NY). Results were reported as the mean ± standard deviation. One-way analysis

of variance (ANOVA) followed by post-hoc Turkey HSD multiple comparison test was used to determine significant differences ($P < 0.05$).

3. RESULTS

3.1 Antimicrobial resistance and genomic characterisation

A total of 19 clinical bacteria were isolated from orthopaedic implant-associated infections, showing resistance to several antibiotics (Table 1). Among these, 15 isolates were resistant to at least one antibiotic in three or more antimicrobial classes (Table 1), thus showing a multidrug-resistant (MDR) profile [25]. For further analysis, only isolates with a MDR profile were taken into consideration for further genomic characterisation as well as isolation and characterisation of phages against these target bacteria. This option was based on the therapeutic limitations for treating infections caused by MDR bacteria, with phage therapy being a possible solution.

Among six *S. aureus* isolates, four were MRSA and two isolates were methicillin-susceptible *S. aureus* (MSSA) (Table 1). All *S. aureus* isolates were shown to contain virulence determinants including polysaccharide intercellular adhesion gene (*icaB*), collagenbinding adhesin gene (*cna*) and haemolytic toxin β-haemolysin gene (*hlb*) (Table 1).

All seven *E. faecalis* isolates were vancomycin-resistant, three of which were also resistant to teicoplanin. The Tn*916*/Tn*1545* transposon was found in the latter isolates. Moreover, cytolysins (*cylLs* and *cylM*), aggregation protein (*agg*), gelatinase (*gelE*) and pheromone gelatinase biosynthesis-activating pheromone (*fsr*) virulence genes were found in the *E. faecalis* isolates (Table 1).

Lastly, the two *E. coli* isolates were classified into phylogenetic groups A and B1. The type 1 fimbriae gene (*fimA*) was detected in both isolates. Remarkably, the *E. coli* isolate classified into phylogenetic group B1 possessed the class 1 integron gene *intl1* (Table 1).

Table 1 | Antimicrobial resistance profile and genetic characterisation of bacteria isolated from orthopaedic implant-associated infections provided by the Centro Hospitalar de Vila Nova de Gaia/Espinho, EPE (Vila Nova de Gaia, Portugal).

Species	Strain	Source	Patient sex/age (years)	Antimicrobial resistance[a]	Genetic characterisation			
Enterobacter cloacae	2107408	Thigh bone	F/76	STR/CIP/FOX/CEF/AMX/SUL/MFX/TMP				
Klebsiella pneumoniae	2133201	Shoulder	M/39	AMX/NEO				
Acinetobacter lwoffii	2170401	Hip prosthesis	M/74	FEP				
Pseudomonas aeruginosa	209960	Lumbar arthrodesis	F/69	ATM/GEN/NET				
					Type	VFs	ST	CC
Staphylococcus aureus	2117045	Synovial fluid	F/72	ERY/FOX/CIP/GEN/AMP	MRSA	*icaB–cna–hlb*	239	8
	2093367	Knee	F/60	ERY/FOX/CIP/AMP	MRSA	*cna*	22	22
	2104780	Ankle	F/75	ERY/FOX/CIP/AMP	MRSA	*icaB–cna–hlb*	22	22
	2117741	Knee	M/70	ERY/FOX/CIP/GEN/AMP	MRSA	*icaB–cna–hlb*	22	22
	2106876	Hip prosthesis	F/53	GEN/AMP	MSSA	*icaB–hlb*	72	8
	2179342	Synovial fluid	M/42	GEN/AMK/AMP	MSSA	*icaB–cna–hlb*	72	8
					Transposon	VFs	ST	CC
Enterococcus faecalis	2099610	Lumbar arthrodesis	F/69	QDA/CIP/VAN	N/D	*cylLs*	117	21
	2105322	Septic arthritis	M/77	ERY/QDA/CIP/VAN	N/D	*agg–gelE–fsr–cylLs*	117	21
	2104780	Ankle	F/75	ERY/QDA/CIP/TET/NOR/VAN/TEC	Tn*916*/Tn*1545*	*agg–fsr–cylLs*	6	2
	2133201	Shoulder	M/39	ERY/QDA/CIP/TET/NOR/VAN/TEC	Tn*916*/Tn*1545*	*agg–cylM–fsr–cylLs*	16	58
	2084972	Soft foot bones	F/79	ERY/QDA/CIP/TET/NOR/VAN/TEC	Tn*916*/Tn*1545*	*agg–cylLs*	6	2
	2093926	Knee	M/76	ERY/QDA/CIP/VAN	N/D	*agg–fsr–cylLs*	117	21
	8105329	Knee prosthesis	M/75	ERY/QDA/VAN	N/D	*agg–gelE–fsr–cylLs*	117	21
					Phylogenetic group	VFs	Integron	
Escherichia coli	2129975	Iliac crest	M/86	CIP/CEF/MFX/TMP/NEO/NAL/OFX	B1	*fimA*	*intI1*	
	2154120	Hip prosthesis	M/47	CEF/TMP/NEO/NAL/OFX	A	*fimA*	N/D	

VF, virulence factor; ST, sequence type; CC, clonal complex; MRSA, methicillin-resistant S. aureus; MSSA, methicillin-susceptible S. aureus; N/D, not detected. [a]AMK, amikacin; AMP, ampicillin; AMX, amoxicillin; ATM, aztreonam; CEF, cefalotin; CIP, ciprofloxacin; ERY, erythromycin; FEP, cefepime; FOX, cefoxitin; GEN, gentamicin; MFX, moxifloxacin; NAL, nalidixic acid; NEO, neomycin; NET, netilmicin; NOR, norfloxacin; OFX, ofloxacin; QDA, quinupristin/dalfopristin; STR, streptomycin; SUL, sulfonamides; TEC, teicoplanin; TET, tetracycline; TMP, trimethoprim; VAN, vancomycin.

3.1.1 Multilocus sequence typing

The *S. aureus* isolates were divided into three STs, namely ST239, ST72 and ST22 (Table 1). The MRSA isolates belonged to ST239 and ST22, whilst the MSSA isolates belonged to ST72. According to eBURST V3 analysis, *S. aureus* isolates belonged to CC8 (ST239 and ST72) and CC22 (ST22), (Table 1; Supplementary Fig. S1). Isolates assigned to ST239 and ST72 (Table 1) belonged to the same cluster, having closely related genotypes (Supplementary Fig. S1). CC8 had a primary founder ST5, whilst CC22 had as the primary founder ST22. Regarding *E. faecalis*, the isolates were divided into three different STs belonging to three CCs: ST117 belonging to CC21; ST6 belonging to CC2; and ST16 belonging to CC58 (Table 1; Supplementary Fig. S1). CC21 had a primary founder ST21, whilst CC2 and CC58 had as the primary founders ST6 and ST16, respectively.

3.2 Bacteriophages isolation/production and characterisation

The phages used in this study were named vB_SauM_LM12 (LM12), vB_EfaS_LM99 (LM99), vB_EfaS_LM00I (LM00I), vB_EfaS_LM00II (LM00II), vB_EcoM_JB75 (JB75) and vB_EcoM_JB75I (JB75I) according to the recommendations of Kropinski et al. [26]. One phage (LM12) was used to infect *S. aureus* isolates (Table 2), whilst three phages (LM99, LM00I and LM00II) and two phages (JB75 and JB75I) were isolated to infect *E. faecalis* and *E. coli* isolates, respectively (Table 2). Phages LM12, LM99 and JB75 were able to lyse 91%, 64% and 55% of all *S. aureus*, *E. faecalis* and *E. coli* tested, respectively (Table 2). These phages were selected for further characterisation owing to their broad spectra of activity. The EOP was determined in bacterial isolates from orthopaedic implant-associated infections (Table 2). Phage LM12 was able to infect all *S. aureus* isolates, with a high EOP in five of six *S. aureus* isolates (Table 2). Phage LM99 was able to infect one *E. faecalis* isolate with high lytic efficiency and to promote lysis from without in another two isolates (Table 2). Furthermore, phage JB75 infected only one *E. coli* isolate with high EOP.

Table 2 | Lytic spectrum and efficiency of plating (EOP) of phages against *Staphylococcus aureus*, *Enterococcus faecalis* and *Escherichia coli* strains.

Species	Strain	Lytic spectrum[a]				EOP[b]
		Phage LM12				Phage LM12
Staphylococcus aureus	12	+				High
	ATCC 25923	+				
	ATCC 49230	H				
	ATCC 6538	–				
	ATCC 33591	H				
	2117045[c]	+				High
	2093367[c]	+				High
	2104780[c]	+				High
	2117741[c]	H				LFW
	2106876[c]	+				High
	2179342[c]	+				High
		LM09	LM99	LM00I	LM00II	LM99
Enterococcus faecalis	I899	+	+	+	+	High
	I900	+	+	+	+	
	I436	+	+	–	–	
	I980	H	+	+	+	
	2099610[c]	N/D	–	N/D	N/D	N/D
	2105322[c]	N/D	–	N/D	N/D	N/D
	2104780[c]	N/D	H	N/D	N/D	LFW
	2133201[c]	H	+	H	H	High
	2084972[c]	N/D	H	N/D	N/D	LFW
	2093926[c]	N/D	–	N/D	N/D	N/D
	8105329[c]	N/D	–	N/D	N/D	N/D
	JB75			JB75I		JB75
Escherichia coli	30	+		H		
	31	+		H		
	32	H		–		
	33	+		H		
	34	–		–		
	35	–		–		
	U923366	+		+		
	U924005	–		–		
	U923087	–		–		
	2129975[c]	+		+		High
	2154120[c]	–		–		N/D

LFW, lysis from without; N/D, not determined. [a]+, distinct clear plaques; –, plaques not formed; H, hazy plaques. [b]The EOP was recorded as high, low and LFW, representing >10, 0.1–1 and <0.1%, respectively. [c]Bacteria isolated from orthopaedic implant-associated infections.

3.2.1 Thermal and pH stability tests

The thermal stability of phage LM12 was assessed and a 100% survival rate was observed at 4 °C and 18 °C, whilst at 37 °C and 42 °C the survival rates were 98% and 94%, respectively (Fig. 1a). This phage was able to survive at –20 °C (42% survival rate), whereas it was killed at 60 °C (Fig. 1a). Regarding the thermal stability of phage LM99, a 100% survival rate was observed for a wide range of temperatures from –20 °C to 42

°C (Fig. 1a). Furthermore, the survival rate at 60 °C was approximately 39%. Phage JB75 was shown to be more sensitive to temperature, being stable from 4–42 °C. The survival rate was 75% at –20 °C, whilst no survival was detected at 60 °C (Fig. 1a). Regarding pH stability, the three phages were highly stable over a wide range of pH values (Fig. 1b). Phage LM12 showed a loss of stability at pH 10 (70% survival rate), whilst the stability of phage LM99 was affected at pH 4 and pH 12 (78% and 67% survival rates, respectively) (Fig. 1b). The phages were completely inactivated at extreme pH values (pH 1, 2 and 13) (Fig. 1b).

3.2.2 Phage morphology

Phage LM99 particles had an icosahedral head of 63 nm in diameter and a non-contractile tail of 212 nm in length and 9 nm in width (Fig. 1c), proving that it belongs to the *Siphoviridae* family. Phage JB75 revealed an isometric head of 73 nm diameter with a contractile tail 96 nm long and 24 nm wide, which is a morphology indicative of the *Myoviridae* family (Fig. 1c).

3.2.3 One-step growth curves

The latent and rise periods for phage LM12 were 20 min and 30 min, respectively. The burst size was 52 PFU/infected cell (Fig. 1d). Regarding phage LM99, the latent and rise periods were 10 min and 20 min, respectively, and the burst size was 107 PFU/infected cell (Fig. 1d). Regarding phage JB75, the latent and rise periods were 20 min and 30 min, respectively, and the burst size was 82 PFU/infected cell (Fig. 1d).

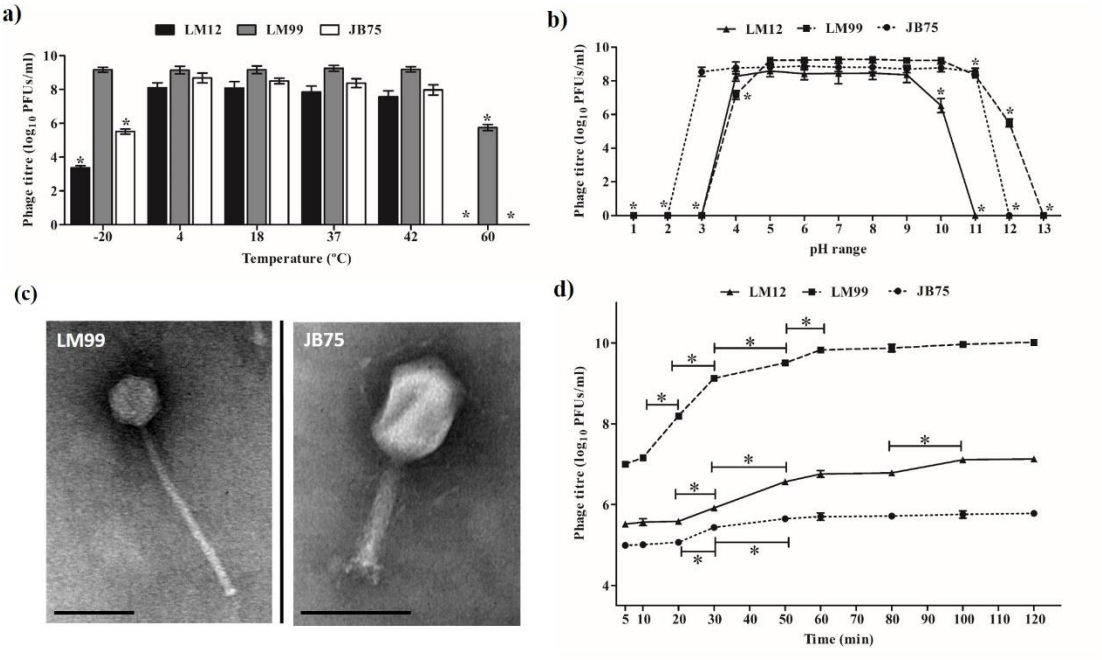

Figure 1 | (a,b) Stability of phages LM12, LM99 and JB75 at different temperatures (a) and pH values (b). (c) Morphology of phages LM99 and JB75 observed by transmission electron microscopy with uranyl acetate (2%) staining. Bar = 100 nm. (d) Curves for one-step growth of phages LM12, LM99 and JB75. *Statistically significant difference (P < 0.05).

3.2.4 Genomic sequencing analysis

The complete genomic sequences of phages LM99 and JB75 were deposited in GenBank under the accession nos. MH355583 and MH355584, respectively. Genome analysis revealed that both phages are virulent, not encoding any genes associated with lysogeny. However, phage LM99 encodes a gene homologous to a putative toxin gene (gp17 – haemolysin) and a metallo-βlactamase gene. *In silico* analysis showed that phage JB75 does not encode any known virulence-associated or toxin proteins. The genome of phage LM99 consists of a linear double-stranded DNA of 40 203 bp with a G+C% content of 30.5% (Fig. 2a). LM99 encodes 64 CDSs with an average length of 573 bp, tightly packed occupying 91% of its genome. Twenty-five of the predicted CDSs have an assigned function (39%) and two are unique (Supplementary Table S1). No tRNA genes were detected. The majority (97%) of the CDSs possess methionine as start codon, whilst CTG and GTG are the start codons of only one CDS each. Furthermore, 14 promoters and six rho-independent terminators were predicted. BLASTN search revealed high homology with enterococci siphoviruses vB_EfaS_AL3, LY0322, SHEF5, SHEF2,

PMBT2, SANTOR1 and EfaCPT1. Interestingly, these phages are not inserted in any genus.

The genome of phage JB75 consists of a linear double-stranded DNA of 167 208 bp with a G+C% content of 35% (Fig. 2b). This phage encodes 277 putative CDSs with an average length of 546 bp, also very tightly packed occupying approximately 94% of its genome. No unique proteins were detected and it was possible to predict a function for 134 CDSs (48%) (Supplementary Table S2). Unsurprisingly, 262 CDSs have methionine as start codon (95%), whilst two start with CTG, six with GTG and seven with TTG. Ten tRNA genes were predicted (tRNA-Arg, tRNA-Asn, tRNA-Gln, tRNAGly, tRNA-Leu, tRNA-Met, tRNA-Pro, tRNA-Ser, tRNA-Thr and tRNATyr). Moreover, 13 promoters and 26 rho-independent terminators were predicted. Homology searches revealed that JB75 has very high homologies with several E. coli myoviruses, namely YUEEL01, vB_EcoM-fHoEco02 and vB_EcoM-fFiEco06. These phages are inserted in the T4 virus genus.

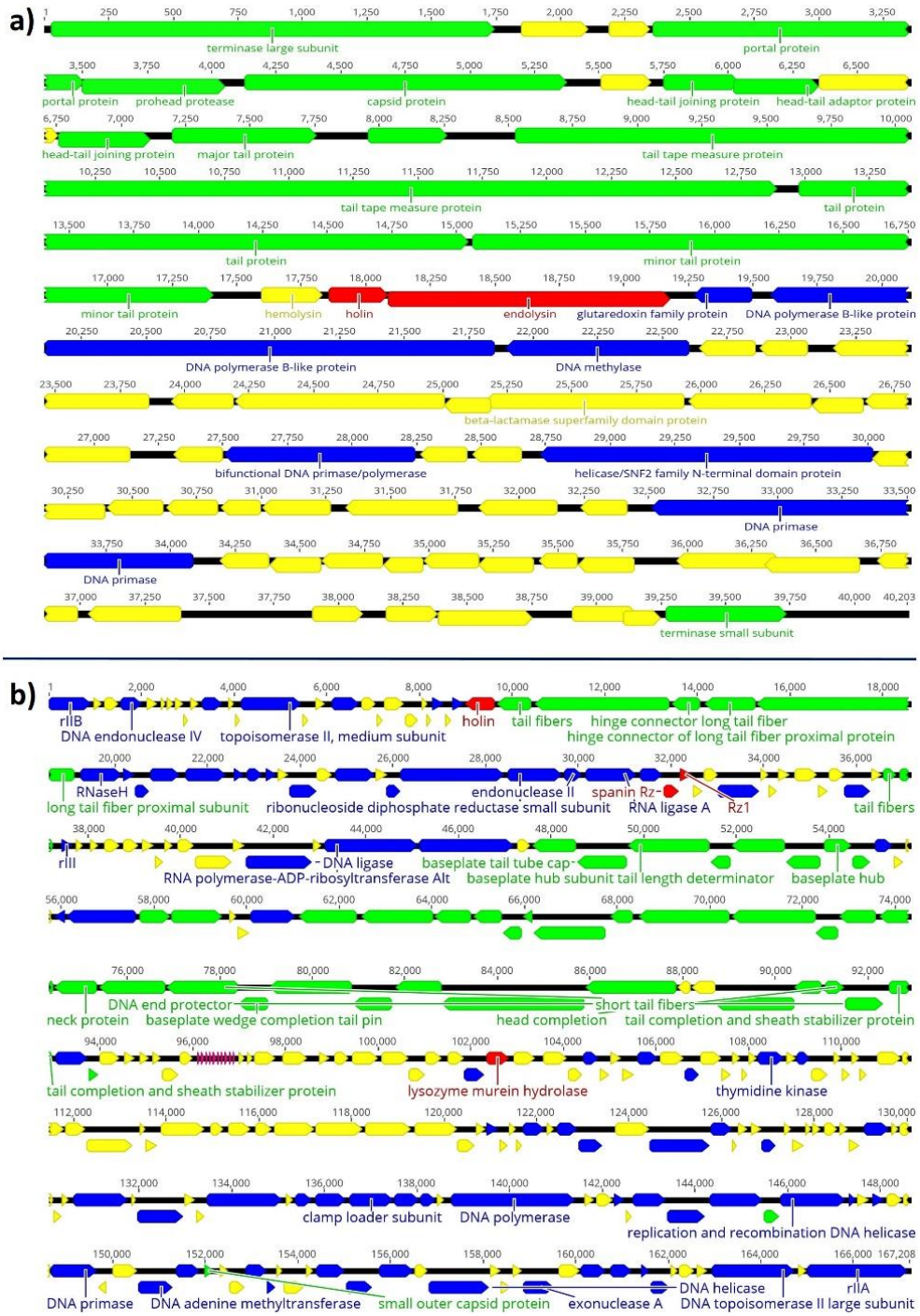

Figure 2 | Genome overview of (a) phage LM99 and (b) phage JB75. (a) The genome map of phage LM99 predicted 64 CDSs and (b) the genome map of phage JB75 predicted 277 CDSs. The CDSs are numbered and coloured according to their predicted function: yellow, hypothetical protein; blue, DNA replication and transcription gene; green, DNA packaging and phage morphogenesis gene; and red, cells lysis gene. Above the genomes, the nucleotide position (in kb) is given. The figure was created using Geneious 9.1.4. CDS, coding sequence.

3.3 Activity of bacteriophages against clinical bacteria

The antimicrobial activity of the phages was assessed against bacterial isolates with high EOP values (Table 2). In the control group (without phage), *S. aureus*, *E. faecalis* and *E. coli* bacterial counts increased continuously (Fig. 3, solid lines). However, when phages LM12, LM99 and JB75 were applied, significant reductions were observed in the tested isolates (Fig. 3, dotted lines). Noticeably, the phage effect varied according to the bacterial strain tested. Phage LM12 showed high antimicrobial activity for the four *S. aureus* isolates tested (Fig. 3a). Despite the slight increase in bacterial counts observed at 6 h and 24 h, bacterial counts were significantly lower compared with the controls ($P < 0.05$). Phage LM12 reduced the bacterial density of *S. aureus* 2093367 by 91%, 97% and 99% at 2, 6 and 24 h, respectively. Reductions of approximately 96%, 95% and 93% at 2, 6 and 24 h, respectively, were observed in *S. aureus* 2104780, *S. aureus* 2106876 (Fig. 3a). Regarding *S. aureus* 2117045 and *S. aureus* 2117741, the antimicrobial effect of LM12 decreased over time, showing a maximum effect at 2 h with a 77% reduction (Supplementary Fig. S2). Phage LM99 demonstrated significant antimicrobial activity against *E. faecalis* 2133201 (Fig. 3b). This phage was able to significantly reduce *E. faecalis* 2133201 density by 99% at 2, 6 and 24 h (Fig. 3b). The other *E. faecalis* isolates were not significantly affected by the presence of phage LM99 (Supplementary Fig. S2). Regarding *E. coli*, phage JB75 demonstrated a significant effect on *E. coli* 2129975 planktonic cells (Fig. 3c). The highest reduction was achieved at 6 h of incubation with a 96% reduction. At 2 h and 24 h, the phage was able to reduce the bacterium by 84% and 87%, respectively (Fig. 3c).

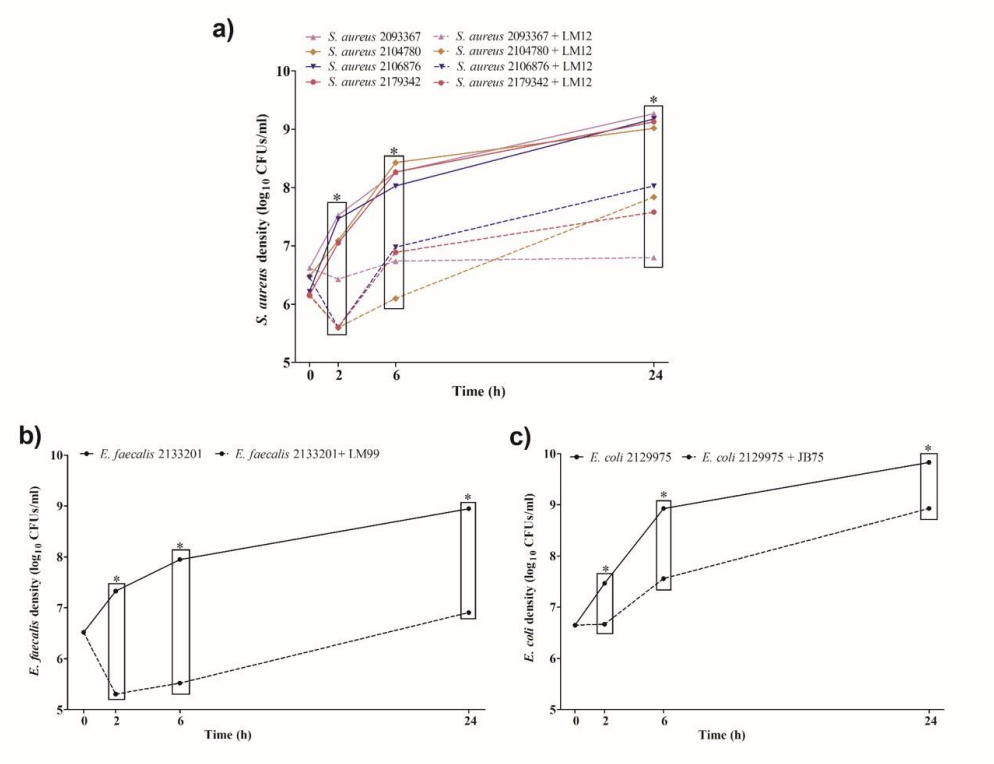

Figure 3 | Inhibitory effect of (a) phage LM12 on planktonic *Staphylococcus aureus*, (b) phage LM99 on planktonic *Enterococcus faecalis* and (c) phage JB75 on planktonic *Escherichia coli* isolated from orthopaedic implant-related infections. The solid lines represent the growth of bacteria without phages (control) and the dashed lines represent the growth of bacteria with phages. *Statistically significant difference ($P < 0.05$) between planktonic bacteria + phage and control densities for the same time of incubation.

4. DISCUSSION

Orthopaedic implant-related infections remain one of the major complications of orthopaedic clinical activity, causing a significant impact on patients and healthcare systems. In addition, the presence of MDR bacteria, namely MRSA and VRE, increases concern about these type of infections owing to limited therapeutic options [2,3]. The pathogenicity of these infections is even greater when the isolates possess mobile genetic elements (*mecA* in *S. aureus*, Tn*916*/Tn*1545* in *E. faecalis* and *intl1* in *E. coli*) and virulence elements (such as *icaB*, *hlb* and *cna* in *S. aureus*, *agg*, *gelE*, *cylM*, *cylL* and *fsr* in *E. faecalis* and *fimA* in *E. coli*) [6,27–30]. These mobile genetic elements can mediate the transfer and integration of resistance and virulence determinants into new host DNA [30]. The virulence elements can contribute to bacterial binding to host matrix proteins

and consequently bacterial adhesion to implants [6,27]. As observed by MLST and eBURST V3 analysis, both the phenotypic and genotypic profile obtained are in accordance with the findings of other authors [2,3,6,27,31], showing that these pathogens belong to lineages frequently involved in pandemic nosocomial infections [27,31]. Besides, intraspecies diversity between isolates was observed with different resistance and virulence patterns, increasing concern about the diagnosis and treatment of infections caused by these type of bacteria [6,31]. Considering the mentioned pathogenicity of bacterial strains and the poor bioavailability of antibiotics in bone tissue [32], there is an urgent need to develop novel therapeutic approaches to combat isolates involved in orthopaedic implant-associated infections. Phage therapy has long been shown to be a promising antibacterial strategy, mainly due to its high specificity and effectiveness in killing targeted pathogenic bacteria [7,10]. In the present study, three phages, namely LM12 (previously isolated), LM99 (isolated in this study) and JB75 (isolated in this study), were characterised in order to control bacterial pathogens previously isolated from orthopaedic implant-associated infections. The three phages presented outstanding characteristics such as broad bactericidal spectrum against the target pathogenic bacterium, short latent periods, large burst sizes and high stability to several environmental conditions. Furthermore, it is important to highlight the specificity of the phages used in this study. The characterised phages belong to the *Caudovirales* order, which are double stranded DNA viruses, having as a major advantage their inherent combined bacteriostatic and bacteriolytic mode of action [33]. By comparative genomics analysis, phage LM99 is not inserted in any genus, consequently a new genus should be created comprising LM99 and its closest relative. The homologies detected for phage JB75 and the more identic phages suggest the assignment of this phage to the T4 virus genus, which is one of the most well studied *Enterobacteriaceae* strictly lytic phages [34]. Furthermore, the phages are virulent and do not encode any genes associated with lysogeny. Genes homologous to a putative toxin gene (gp17 – haemolysin) and to a metallo-β-lactamase gene were detected in the genome of phage LM99. However, both genes are not homologous to genes found in bacteria, therefore their true function needs to be determined. All of these characteristics associated with the high efficiency of phages LM12, LM99 and JB75 in infecting bacteria, including MRSA and VRE isolated from orthopaedic implant-associated infections, make them potential candidates in therapeutic applications. Likewise, the three studied phages were efficient in reducing the number of

culturable bacterial cells over time compared with controls. Phage therapy studies with animal models have shown that, under certain circumstances, phages may help in reducing the density of the infecting bacterial population to a level that may allow the host immune response to mount a successful defence and clear the infection [7]. Recent studies have shown the efficacy and accuracy of phage therapy in the treatment of wound infections, diabetic foot ulcers, acute kidney injury, ulcers and chronic otitis caused by clinical pathogens [35–39]. In line with these potential clinical applications and considering the data obtained in the present work, phages LM12, LM99 and JB75 could be suitable to treat orthopaedic implant-associated infections.

5. CONCLUSIONS

Bacteria isolated from orthopaedic implant-associated infections showed patterns of multidrug resistance, virulence and pathogenicity. Bacteriophage therapy offers a possible alternative to classic antibiotic treatment to reduce bacterial colonisation. The studied phages were efficient in controlling clinical bacteria, suggesting that phage therapy could be suitable to treat pathogenic bacteria involved in orthopaedic implant-associated infections.

ACKNOLEDGMENT

The authors would also like to acknowledge Dr. Rui Fernandes (HEMS/i3S) for help electron microscopy analysis and PhD Margarida Sousa (UTAD) for support the experiments in Medical Microbiology Laboratory from UTAD. This work was supported by FEDER – Fundo Europeu de Desenvolvimento Regional funds through the COMPETE 2020 – Operacional Programme for Competitiveness and Internationalisation (POCI), Portugal 2020, by Portuguese funds through FCT/MCTES in the framework of the project “Institute for Research and Innovation in Health Sciences (POCI-01-0145-FEDER-007274), by Project Biotherapies (NORTE-01-0145-FEDER-000012) and by Joana Barros’ PhD grant (SFRH/BD/102148/2014).

REFERENCES

[1] Arciola CR, Campoccia D, Montanaro L. Implant infections: adhesion, biofilm formation and immune evasion. Nat Rev Microbiol 2018;16:397–409.

[2] Tande AJ, Patel R. Prosthetic joint infection. Clin Microbiol Rev 2014;27:302–45.

[3] Cremet L, Corvec S, Bemer P, Bret L, Lebrun C, Lesimple B, et al. Orthopaedic-implant infections by *Escherichia coli*: molecular and phenotypic analysis of the causative strains. J Infect 2012;64:169–75.

[4] Landraud L, Jaureguy F, Frapy E, Guigon G, Gouriou S, Carbonnelle E, et al. Severity of *Escherichia coli* bacteraemia is independent of the intrinsic virulence of the strains assessed in a mouse model. Clin Microbiol Infect 2013;19:85–90.

[5] Frank KL, Vergidis P, Brinkman CL, Greenwood Quaintance KE, Barnes AM, Mandrekar JN, et al. Evaluation of the *Enterococcus faecalis* biofilm-associated virulence factors AhrC and Eep in rat foreign body osteomyelitis and in vitro biofilm-associated antimicrobial resistance. PLoS One 2015;10:e0130187.

[6] Montanaro L, Arciola CR, Baldassarri L, Borsetti E. Presence and expression of collagen adhesin gene (*cna*) and slime production in *Staphylococcus aureus* strains from orthopaedic prosthesis infections. Biomaterials 1999;20:1945–9.

[7] Cheng M, Liang J, Zhang Y, Hu L, Gong P, Cai R, et al. The bacteriophage EF-P29 efficiently protects against lethal vancomycin-resistant *Enterococcus faecalis* and alleviates gut microbiota imbalance in a murine bacteremia model. Front Microbiol 2017;8:837.

[8] World Health Organization (WHO). WHO publishes list of bacteria for which new antibiotics are urgently needed. Geneva, Switzerland: WHO; 2017 https://www.who.int/news-room/detail/27-02-2017-who-publishes-listof-bacteria-for-which-new-antibiotics-are-urgently-needed [Accessed 25 July 2019].

[9] Pires DP, Vilas Boas D, Sillankorva S, Azeredo J. Phage therapy: a step forward in the treatment of *Pseudomonas aeruginosa* infections. J Virol 2015;89:7449–56.

[10] Oliveira A, Sillankorva S, Quinta R, Henriques A, Sereno R, Azeredo J. Isolation and characterization of bacteriophages for avian pathogenic *E. coli* strains. J Appl Microbiol 2009;106:1919–27.

[11] Capparelli R, Parlato M, Borriello G, Salvatore P, Iannelli D. Experimental phage therapy against *Staphylococcus aureus* in mice. Antimicrob Agents Chemother 2007;51:2765–73.

[12] European Committee on Antimicrobial Susceptibility Testing. Breakpoint tables for interpretation of MICs and zone diameters; 2015. Version 5.0 http://www. eucast.org [Accessed 26 July 2019].

[13] Clinical and Laboratory Standards Institute (CLSI). Performance standards for antimicrobial susceptibility testing; twenty-fifth informational supplement, Wayne, PA: CLSI; 2015. CLSI document M100-S25.

[14] Sousa M, Silva N, Igrejas G, Silva F, Sargo R, Alegria N, et al. Antimicrobial resistance determinants in *Staphylococcus* spp. recovered from birds of prey in Portugal. Vet Microbiol 2014;171:436–40.

[15] Goncalves A, Igrejas G, Radhouani H, Correia S, Pacheco R, Santos T, et al. Antimicrobial resistance in faecal enterococci and *Escherichia coli* isolates recovered from Iberian wolf. Lett Appl Microbiol 2013;56:268–74.

[16] Lozano C, Porres-Osante N, Crettaz J, Rojo-Bezares B, Benito D, Olarte I, et al. Changes in genetic lineages, resistance, and virulence in clinical methicillin-resistant *Staphylococcus aureus* in a Spanish hospital. J Infect Chemother 2013;19:233–42.

[17] Radhouani H, Pinto L, Coelho C, Sargo R, Araujo C, Lopez M, et al. MLST and a genetic study of antibiotic resistance and virulence factors in vanA-containing Enterococcus from buzzards (Buteo buteo). Lett Appl Microbiol 2010;50:537–41.

[18] Ruiz J, Simon K, Horcajada JP, Velasco M, Barranco M, Roig G, et al. Differences in virulence factors among clinical isolates of *Escherichia coli* causing cystitis and pyelonephritis in women and prostatitis in men. J Clin Microbiol 2002;40:4445–9.

[19] Melo LDR, Brandao A, Akturk E, Santos SB, Azeredo J. Characterization of a new *Staphylococcus aureus* kayvirus harboring a lysin active against biofilms. Viruses 2018;10 pii: E182. doi:10.3390/v10040182.

[20] van Belkum A, Goessens W, van der Schee C, Lemmens-den Toom N, Vos MC, Cornelissen J, et al. Rapid emergence of ciprofloxacin-resistant Enterobacteriaceae containing multiple gentamicin resistance-associated integrons in a Dutch hospital. Emerg Infect Dis 2001;7:862–71.

[21] Sillankorva S, Neubauer P, Azeredo J. Isolation and characterization of a T7-like lytic phage for *Pseudomonas fluorescens*. BMC Biotechnol 2008;8:80.

[22] Kvachadze L, Balarjishvili N, Meskhi T, Tevdoradze E, Skhirtladze N, Pataridze T, et al. Evaluation of lytic activity of staphylococcal bacteriophage Sb-1 against freshly isolated clinical pathogens. Microb Biotechnol 2011;4:643–50.

[23] Li B, Webster TJ. Bacteria antibiotic resistance: new challenges and opportunities for implant-associated orthopedic infections. J Orthop Res 2018;36:22–32.

[24] Melo LD, Sillankorva S, Ackermann HW, Kropinski AM, Azeredo J, Cerca N. Isolation and characterization of a new *Staphylococcus epidermidis* broad-spectrum bacteriophage. J Gen Virol 2014;95:506–15.

[25] Magiorakos AP, Srinivasan A, Carey RB, Carmeli Y, Falagas ME, Giske CG, et al. Multidrug-resistant, extensively drug-resistant and pandrug-resistant bacteria: an international expert proposal for interim standard definitions for acquired resistance. Clin Microbiol Infect 2012;18:268–81.

[26] Kropinski AM, Prangishvili D, Lavigne R. Position paper: the creation of a rational scheme for the nomenclature of viruses of bacteria and Archaea. Environ Microbiol 2009;11:2775–7.

[27] Quinones D, Kobayashi N, Nagashima S. Molecular epidemiologic analysis of Enterococcus faecalis isolates in Cuba by multilocus sequence typing. Microb Drug Resist 2009;15:287–93.

[28] Baldassarri L, Creti R, Recchia S, Pataracchia M, Alfarone G, Orefici G, et al. Virulence factors in enterococcal infections of orthopedic devices. Int J Artif Organs 2006;29:402–6.

[29] Montanaro L, Speziale P, Campoccia D, Ravaioli S, Cangini I, Pietrocola G, et al. Scenery of *Staphylococcus* implant infections in orthopedics. Future Microbiol 2011;6:1329–49.

[30] Malachowa N, DeLeo FR. Mobile genetic elements of *Staphylococcus aureus*. Cell Mol Life Sci 2010;67:3057–71.

[31] Ruiz-Garbajosa P, Bonten MJ, Robinson DA, Top J, Nallapareddy SR, Torres C, et al. Multilocus sequence typing scheme for *Enterococcus faecalis* reveals hospital-adapted genetic complexes in a background of high rates of recombination. J Clin Microbiol 2006;44:2220–8.

[32] Olson ME, Horswill AR. *Staphylococcus aureus* osteomyelitis: bad to the bone. Cell Host Microbe 2013;13:629–31.

[33] Roach DR, Leung CY, Henry M, Morello E, Singh D, Di Santo JP, et al. Synergy between the host immune system and bacteriophage is essential for successful phage therapy against an acute respiratory pathogen. Cell Host Microbe 2017;22:38–47 e4.

[34] Miller ES, Kutter E, Mosig G, Arisaka F, Kunisawa T, Ruger W. Bacteriophage T4 genome. Microbiol Mol Biol Rev 2003;67:86–156.

[35] Watanabe R, Matsumoto T, Sano G, Ishii Y, Tateda K, Sumiyama Y, et al. Efficacy of bacteriophage therapy against gut-derived sepsis caused by *Pseudomonas aeruginosa* in mice. Antimicrob Agents Chemother 2007;51:446–52.

[36] Biswas B, Adhya S, Washart P, Paul B, Trostel AN, Powell B, et al. Bacteriophage therapy rescues mice bacteremic from a clinical isolate of vancomycin-resistant *Enterococcus faecium*. Infect Immun 2002;70:204–10.

[37] Wang J, Hu B, Xu M, Yan Q, Liu S, Zhu X, et al. Therapeutic effectiveness of bacteriophages in the rescue of mice with extended spectrum β-lactamase-producing *Escherichia coli* bacteremia. Int J Mol Med 2006;17:347–55.

[38] Wills QF, Kerrigan C, Soothill JS. Experimental bacteriophage protection against *Staphylococcus aureus* abscesses in a rabbit model. Antimicrob Agents Chemother 2005;49:1220–1.

[39] Wright A, Hawkins CH, Anggard EE, Harper DR. A controlled clinical trial of a therapeutic bacteriophage preparation in chronic otitis due to antibiotic-resistant *Pseudomonas aeruginosa*; a preliminary report of efficacy. Clin Otolaryngol 2009;34:349–57.

CHAPTER 4

Encapsulated bacteriophages in alginate-nanohydroxyapatite hydrogel as a novel delivery system to prevent orthopedic implant-associated infections

Barros J MsC[1,2,3*], Melo LDR PhD[4], Silva RA MsC[5,6], Ferraz MP PhD[7], Azeredo J PhD[4], Pinheiro V PhD[8], Colaço B PhD[8,9], Fernandes MH PhD[5,6], Gomes PS PhD[5,6], Monteiro FJ PhD[1,2,3]

[1]I3S – Instituto de Investigação e Inovação em Saúde, Universidade do Porto;

[2]INEB – Instituto de Engenharia Biomédica, Universidade do Porto;

[3]FEUP – Faculdade de Engenharia, Universidade do Porto, Portugal;

[4]Laboratório de Investigação em Biofilmes Rosário Oliveira, Center of Biological Engineering, University of Minho, Braga, Portugal;

[5]Laboratory for Bone Metabolism and Regeneration – Faculty of Dental Medicine, University of Porto, Porto, Portugal;

[6]REQUIMTE/LAQV, University of Porto, Porto, Portugal.

[7]FP-ENAS/CEBIMED – University Fernando Pessoa Energy, Environment and Health Research Unit/Biomedical Research Center, Porto, Portugal;

[8]Departement of Animal Sciences, ECAV, University of Trás-os-Montes e Alto Douro, Vila Real, Portugal.

[9] Center for the Research and Technology of Agro-Environmental and Biological Sciences, University of Trás-os-Montes e Alto Douro, Vila Real, Portugal.

Nanomedicine: Nanotechnology, Biology and Medicine. ***Accepted for publication*****.**

ABSTRACT

An innovative delivery system based on bacteriophages-loaded alginate-nanohydroxyapatite hydrogel was developed as a multifunctional approach for local tissue regeneration and infection prevention and control. Bacteriophages were efficiently encapsulated, without jeopardizing phage viability and functionality, nor affecting morphology and chemical composition of the hydrogel. The bacteriophages delivery occurred by swelling-disintegration-degradation processes of the alginate's structure and was influenced by environmental pH. Good tissue response was observed following the implantation of bacteriophages-loaded hydrogels, sustaining their biosafety profile. Bacteriophages-loaded hydrogels did not affect the osteoblastic cells proliferation and morphology. A strong osteogenic and mineralization response was promoted through the implantation of the hydrogels system with nanohydroxyapatite. Lastly, bacteriophages-loaded hydrogel showed excellent antimicrobial activity inhibiting the attachment and colonization of multidrug-resistant vancomycin resistant *E. faecalis* surrounding and inside of the femoral tissues. This new local delivery approach could be a promising approach to prevent and control bacterial contamination during implantation and bone integration.

Keywords – Bacteriophages, Alginate-nanohydroxyapatite, Biocompatibility, Antimicrobial activity, Osteogenic differentiation

GRAPHICAL ABSTRACT

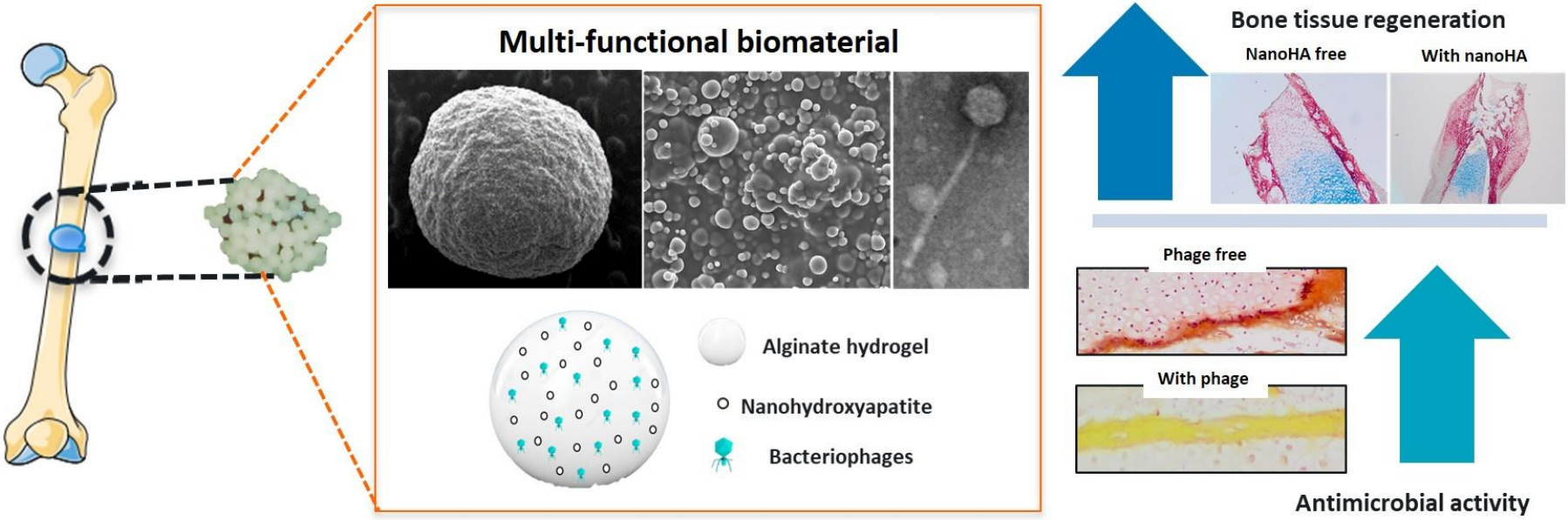

1. INTRODUCTION

Graft implantation is the most commonly used technique for bone loss repair and augmentation, in orthopedic surgical approaches [1]. However, the implantation procedure is highly susceptible to bacterial infection, due to either locally recruited microorganisms or hematogenous spread of existing pathogens [2, 3]. Current curative approaches, such as surgical debridement and prolonged systemic antibiotic therapy often translate into-high risk of life-long functional impairment and morbidity and contribute to the increase of the economic burden in healthcare systems [3-5]. Alternatively, the use of local strategies as vehicles for the delivery of antimicrobial agents has emerged as a regular adjunct in the prevention and treatment of bone graft-related infections [3, 6-8]. Local delivery systems have numerous advantages over systemic approaches, such as drug delivery at or close to the infection site, the increased efficacy and bioavailability of the antimicrobial agent, reduction of the dose administered and decrease systemic toxicity risks [8]. However, some limitations have been associated with these systems, namely the delivery of antimicrobial at sub-therapeutic levels, which could favor the development of bacterial resistance; limited antimicrobial diffusion into the peri-implant tissues; dose-dependent antimicrobial activity, and potential cytotoxicity of the antimicrobial agents [8, 9]. Additionally, the indiscriminate use of antibiotics in the clinical setting has vastly contributed to the emergence of antibiotic-resistant bacteria, thus increasing bacterial pathogenicity and defaulting the treatment of infections provoked by these bacteria [10, 11]. To overcome these limitations, new therapeutic approaches are urgently needed to prevent and manage local implant-related infections.

Bacteriophages (phages) have emerged as an alternative approach to current antimicrobial chemotherapy due to their capacity to infect and kill specific bacterial strains, without modifying the established commensal microbiome [9, 10, 12-15]. Phages are virulent viruses that recognize specific receptors in bacteria, being able to inject their genetic material and use the host biochemical machinery to replicate new phages' particles and enzymes, responsible for the subsequent lyse of bacteria. Furthermore, the newly formed phages particles are released and able to spread and infect other target bacteria nearby [10, 16]. The phages propagation and persistence depend always on its host bacterial pathogen presence, which contributes to regulate phages number in direct relation with pathogen level and facilitates diffusion into the surrounding areas in a gradient dependent on pathogen availability [9, 10, 12]. Likewise, phages are not

pathogenic for eukaryotic cells, despite being able to interact with phagocytic cells and be adsorbed through mammalian cells' surface receptors, being subsequently phagocytosed and degraded, they are not threatening [10, 12, 17].

Several studies have explored the potential of systemic phages administration for the treatment of implant-related infections [13-15, 18-21]. Nonetheless, experimental studies using phages-loaded biomaterials for local delivery approaches are scarce [9, 22, 23], and only focus on the phages release and antimicrobial activity, without exploring simultaneously the potential combination with a regeneration inductive biomaterial. Therefore, this work aims at developing a multi-functional regenerative biomaterial for local phage delivery, based on an alginate-nanohydroxyapatite (Alg-nanoHA) hydrogel system. To the best of our knowledge, the present work is the first to address the use of phage-loaded biomaterials as a novel local delivery system to, simultaneously, promote bone tissue regeneration, and prevent the development of local tissue infections. The efficacy and safety evaluation of this new system was evaluated both *in vitro*, *ex vivo* and *in vivo*.

2. METHODS

2.1 Preparation and physico-chemical characterization the hydrogel system

Initially, phage-free hydrogels were performed. Briefly, a 2 % (w/v) alginate solution (Alg) was prepared by dissolving sodium alginate powder in distilled water, at room temperature. Then, this solution was mixed with nanoHA powder (nanoXIM.HAp202, FLUIDINOVA®) at 30 wt %, during 1h at 60 rpm. After homogeneity, the mixture was dropped into a 250 mM calcium chloride ($CaCl_2$) solution and was allowed to harden for 30min. Afterward, hydrogels were rinsed twice with PBS and kept at 4°C. In order to disclose the relevance of nanoHA within the hydrogel system, Alg hydrogels were similarly prepared as above described, but in the absence of nanoHA.

Following, *E. faecalis* phages vB_EfaS_LM99 (LM99), previously described by Barros et al., Genbank accession number: MH355583, were encapsulated into hydrogel system. Briefly, phages LM99 solution (10^8 PFU/mL) was suspended in the Alg and Alg-nanoHA solutions. Then, Alg + phage LM99 and Alg-nanoHA + phage LM99 mixtures were dropped into a crosslinking solution to obtained hydrogels, under the same conditions above mentioned.

Hydrogels structure was observed by scanning electron microscopy (SEM). Briefly, samples were coated with a thin gold-palladium layer (SPI-Module) in an argon atmosphere and examined using an FEI Quanta 400FEG/ESEM microscope.

Hydrogels were further observed by transmission electron microscopy (TEM). In brief, samples were fixed in 2.5 % glutaraldehyde and 2 % paraformaldehyde in cacodylate Buffer 0.1 M (pH 7.4), dehydrated and embedded in Epon resin. Ultrathin sections were prepared and stained with uranyl acetate and lead citrate for 15 min each and examined under a JEOL JEM 1400 microscopy (TEM). Images were digitally recorded using a CCD digital camera Orious 1100W.

Chemical characterization of hydrogels was performed using attenuated total reflectance – Fourier transformed infrared spectroscopy (ATR – FTIR), using a Perkin – Elmer 2000 FTIR spectrometer. The samples were analyzed at a spectral resolution of 2 cm^{-1} and 100 scans were accumulated per sample.

2.2 Functional characterization

2.2.1 Encapsulation efficiency of the phages and shelf-life assessment of the hydrogel system

To evaluate the efficiency of phages' encapsulation, hydrogels were dissolved in a microsphere-broken solution (MBS) containing 50 mM sodium citrate, 0.2M sodium bicarbonate, and 50 mM Tris-HCl, pH 7.5, for 3 h under shaking at room temperature. The stability of phage LM99 in MBS was previously tested and validated. Phages encapsulation was quantified by the double-agar-layer plating method [24] and expressed in PFU/mL. The encapsulation efficiency (EE) of the phages was calculated as described in literature [25]. The shelf-life of the hydrogel system was assayed in Alg + phage LM99 and Alg-nanoHA + phage LM99 solutions, before crosslinking, and on Alg + phage LM99 and Alg-nanoHA + phage LM99 hydrogels, after crosslinking. From solutions stored at 4 °C, and after the dissolution of hydrogels in MBS, the phages titer was quantified and expressed in PFU/mL plotted against time. Three independent experiments were performed in triplicate.

2.2.2 Effect of pH on the structural behavior of hydrogels and influence on phages release

The effect of pH on the swelling behavior of the hydrogels and associated phages release was determined by the quantification of the swelling ratio and phages titer after

24 h. The swelling behavior was evaluated and calculated by measuring the changes in sample weight as a function of sample incubation in PBS at 37 ºC, for 24 h, as described in literature [26]. The phages released from hydrogels were quantified by the double-agar-layer plating method and expressed in PFU/mL. The results were taken as the mean values of eight measurements. The experiments were performed in triplicate.

2.2.3 Kinetic release of phages LM99

The kinetic release of phages from the hydrogels was assayed in dynamic conditions in PBS at 150 rpm and 37 °C. At predetermined time points, cumulative released phages were quantified using the double-agar-layer plating method. The cumulative amount of released phages was plotted against time. Three independent experiments were performed in triplicate.

2.3 Biological characterization

2.3.1 Inflammatory response – *in vivo* subcutaneous tissue implantation

The experiment was approved by the Local Ethics Committee and the national regulatory entity - *Direção Geral de Alimentação e Veterinária* (DGAV), observing the technical standards of protection for experimental animals, according to both policies and principles of laboratory animal care and with the European Union guidelines (European Directive 2010/63/EU and National Decree-Law 113/2013). Briefly, 16 New Zealand white rabbits, 18 weeks old and weighing between 3700-3900 g were used for the subcutaneous implantation of phages-loaded hydrogels and respective controls. Animals were maintained in cages, individually, in environmental conditions of 22 ºC and 55 % relative humidity with a ventilation rate of 18–20 times/h, and in a 12 h light/dark cycle. Water and food were available *ad libitum*. Prior to the experimental procedure, animals were acclimatized for 1 week.

Established surgical procedure was conducted under general anesthesia, achieved by animal sedation with diazepam (1 mg/kg), followed by the intramuscular (IM) injection of xylazine (5 mg/kg) and ketamine (35 mg/kg). Saline 0.9%, at 10 mL/kg/h of surgery was continuously administrated.

Following confirmation of the anesthesia, a cutaneous incision (about 3 cm long) was performed on the dorsal region for the implantation of phages-loaded hydrogels, and respective controls, following blunt subcutaneous dissection. Sample materials were randomly implanted and after hemostatic control, the surgical wound was terminated with

Polyglactin 910-4/0 restorable suture, with single stitches. In each animal, 3 hydrogels were implanted. The analgesic regimen was started post-operatively with buprenorphine 0.1 mg/kg IM 12/12 h and maintained for 72 h. Two and six weeks after implantation, the animals were euthanized with an anesthetic overdose. The subcutaneous tissue with hydrogel implants was collected by debridement and fixed for conventional histological preparation. Tissue samples were included in paraffin and, following section, stained with hematoxylin and eosin (H&E). Histological analyses were performed following image acquisition with an Olympus BX-51/22 dotSlide digital virtual microscope.

2.3.2 Osteogenic response

2.3.2.1 *In vitro* cytocompatibility assessment with human osteoblastic cells

In vitro cytocompatibility of phages-loaded hydrogels was studied with human osteoblast-like cells (MG63), following cell culture characterization in the presence of hydrogels' eluents. Briefly, eluents were collected under dynamic conditions, following hydrogels incubation in α-minimum essential medium (α-MEM), for 24 h, at 37 ºC, and at 150 rpm. Culture medium without hydrogels was used as control.

Cell cultures were grown in α-MEM supplemented with 10 % fetal bovine serum (FBS), 2.5 µg/mL amphotericin B, 100IU/mL penicillin and 100 µg/mL streptomycin at 37 °C, in a humidified atmosphere of 5 % CO_2 in the air. For subculture, adherent cells were enzymatically released with 0.05 % trypsin in 0.25 % EDTA, for 5min at 37 °C. and seeded at 10^4 cells/cm^2. After 24 h, cells were exposed to hydrogels' eluents for up to 7 days. Biologic response was evaluated in terms of cell morphology, metabolic activity and alkaline phosphatase (ALP) activity.

At each time-point, cultures' metabolic activity was evaluated using the MTT assay, based on the reduction of 3-(4,5- dimethylthiazol-2-yl)-2,5-diphenyltetrazolium bromide to a purple formazan product by viable cells, as previously described [27].

ALP activity determination was performed as described in literature [27]. ALP results were normalized to total protein content and expressed as nanomoles of p-nitrophenol produced per microgram of protein. Total protein content was quantified using the DC protein assay Kit (BioRad), according to the manufacturer's instructions.

Cell cytoskeleton filamentous actin (F-actin) organization and the morphology of the osteoblastic cells were assessed by immunofluorescence imaging. Briefly, cells were washed with PBS and fixed with 3.7 % paraformaldehyde for 15 min. Following cells' permeabilization with 0.1 % (v/v) Triton X-100, nonspecific binding sites were blocked

with 1% bovine serum albumin for 30 min. F-actin was stained with Alexa-Fluor 488 phalloidin-conjugated antibody (1:100, 30 min), and nucleus counterstaining with DAPI (1 µg/mL, 10 min). Images of fluorescent-labeled cells were obtained with a Celena S digital imaging system (Logos Biosystems). Three independent experiments were performed in quadruplicates.

2.3.2.2 *Ex vivo* functional assessment of bone formation

The osteogenic tissue response was assayed *ex vivo* within an embryonic chick femoral segmental defect model. This experiment was carried out in accordance with guidelines and regulations laid down in the Animals (Scientific procedures) act 1986 and with Home office approval UK (Project licence – PPL30/2762). Briefly, femurs were dissected from 11 day-old chick embryos (*Gallus domesticus*) and cut at middle diaphysis for the establishment of a segmental defect. Then, phages-loaded hydrogels and respective controls were implanted within the produced defects and were carefully placed into Netwell^{TM} Insert in 6 well-plates. Femurs, with implanted hydrogels, were for 11 days, in minimum essential medium (α-MEM), containing ascorbic acid (50 µg/mL), penicillin (100 units/mL)/streptomycin (100 µg/mL) and 2.5 µg/mL amphotericin B, at the liquid/gas interface, in a humidified atmosphere of 5 % CO_2 in air, and 37 °C. Culture media was changed daily. At the end of the experimental period, femurs were washed twice in PBS and fixed in 4 % paraformaldehyde. Histological analyses were performed following Alcian blue/Sirius red (AB/SR), von Kossa and Masson's trichrome staining. Images were captured with an Olympus BX-51/22 dotSlide digital virtual microscope. Three independent experiments were performed in quadruplicates.

2.3.3 Antimicrobial activity

2.3.3.1 *In vitro* characterization over planktonic and sessile bacteria

Antimicrobial activity of phages-loaded hydrogels was studied against pathogenic multidrug-resistant VRE *E. faecalis* 201. Briefly, exponential bacterial cultures (10^7 CFU/mL) were incubated with the hydrogels at 37 ºC, 150 rpm during 24 h. After incubation, the planktonic and sessile bacteria (on hydrogels and on tissue culture plates (TCPs)) were quantified by the colony forming units' (CFUs) method. Bacterial growth percentage was plotted against time. Alg and Alg-nanoHA hydrogels phages-free were used as controls. Three independent experiments were performed in triplicate.

2.3.3.2 *Ex vivo* antimicrobial assay in bacteria-infected femoral model

The antimicrobial activity was also evaluated within the *ex vivo* chicken femoral model. Briefly, embryonic femurs with established defect margins, as above described, were contaminated with exponential *E. faecalis* 201 (10^6 cell/mL), for 10 min, at room temperature, prior to hydrogels' implantation. Phages-loaded hydrogels and respective controls were implanted on previously contaminated femurs and were transferred to Netwell™ Insert in 6 well-plates, and incubated for 48 h. The bacterial colonization was characterized by histological analyses following Gram staining, after 48 h. Additionally, at 24 and 48h, the planktonic populations were quantified by CFUs method, with bacteria growth percentages being plotted against time. Three independent experiments were performed in quadruplicates.

2.4 Statistical analysis

All experiments were performed in triplicate as independent experiments. The results were reported as the arithmetic mean ± standard deviation. The experimental data were analyzed using IBM® SPSS® Statistics (vs. 22.0, Statistical Package for the Social Sciences Inc). The one-way analysis of variance (ANOVA) followed by the post hoc Turkey HSD multiple comparison tests were used to determine the significant difference ($p < 0.05$).

3. RESULTS

3.1 Physico-chemical characterization of the hydrogel system

Figure 1 shows the structure and network organization of hydrogels with and without encapsulated phages. Regardless of the encapsulated phages, Alg hydrogels showed a smooth surface, whereas Alg-nanoHA showed a rougher surface. The nanoHA particles were well embedded and homogeneously dispersed along the polymeric matrix (Fig. 1A). Moreover, all samples showed a typical Alg matrix, a network of fibril-like structures, (Fig. 1B). The phages LM99 were properly entrapped within the alginate matrix (Fig. 1B). The integrity of phages' structures (icosahedral head and long tail) were maintained after encapsulation, as observed in Fig. 1C.

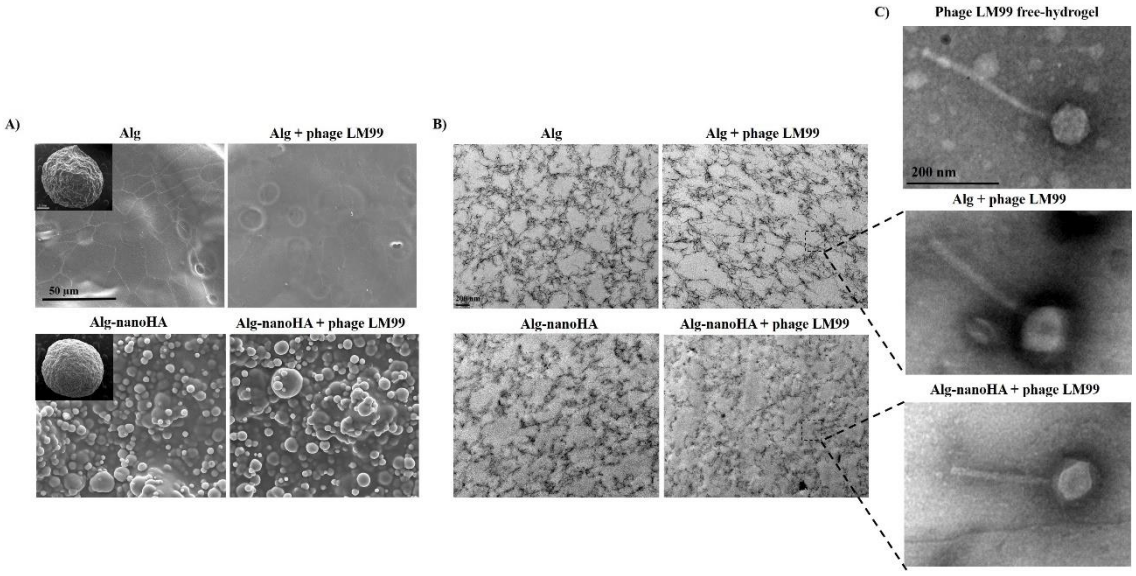

Figure 1 – A) SEM micrographs of hydrogels without and with encapsulated phages structure. Scale bar 1 mm and 50 µm. B) TEM micrographs of hydrogels without and with encapsulated phages network and C) phages structures-free hydrogels and encapsulated hydrogels, respectively. Scale bar 200 nm.

The ATR–FTIR spectra (Fig. 2A) show the chemical composition of the hydrogels without and with encapsulated phages. Regardless of phages encapsulation, Alg hydrogel displayed characteristic of carboxylic group (COO^-) at 1592 and 1417cm^{-1}, and of hydroxyl group (OH^-) over the range 3311 to 3307cm^{-1}. The bending of the OH^- group of the carboxyl is depicted at 819cm^{-1}. Alg-nanoHA hydrogels without and with encapsulated phages also showed similar ATR–FTIR spectra. The spectra displayed peaks corresponding to alginate matrix (COO^- bands), at the same wavelengths described for Alg hydrogels. Peaks corresponding to phosphate group (PO_4^{3-}) were observed at 1020cm^{-1} and 559cm^{-1}, that are attributed to the overlap of COO^- stretching of Alg and PO_4^{3-} stretching of nanoHA. The presence of bands at 3365cm^{-1} and 629cm^{-1} were assigned to OH^- group, corresponding to lattice water.

3.2 Functional characterization

3.2.1 Encapsulation efficiency of the phages and shelf-life assessment of the hydrogel system

A high amount of phages LM99 was encapsulated in both Alg and Alg-nanoHA hydrogels, with around 8.1 log_{10} PFU/mL, supporting a mean phages encapsulation

efficiency of 91 % (Fig. 2B). Furthermore, the encapsulation did not cause detrimental effects in phages' activity and replication ability.

The shelf-life of Alg + phage LM99 and Alg-nanoHA + phage LM99 in solutions (Fig. 2C), and on hydrogels (Fig. 2D) was studied over time. In solution, the phages titer remained constant (8.3 $\log_{10}$ PFU/mL) over 60 days, with no alteration in phages' stability and viability throughout time, or between Alg and Alg-nanoHA solutions (Fig. 2C). Regarding hydrogels, the amount of viable phages was also found to be broadly constant (6.9 $\log_{10}$ PFU/mL) during a 7-days, with no differences found between Alg and Alg-nanoHA (Fig. 2D).

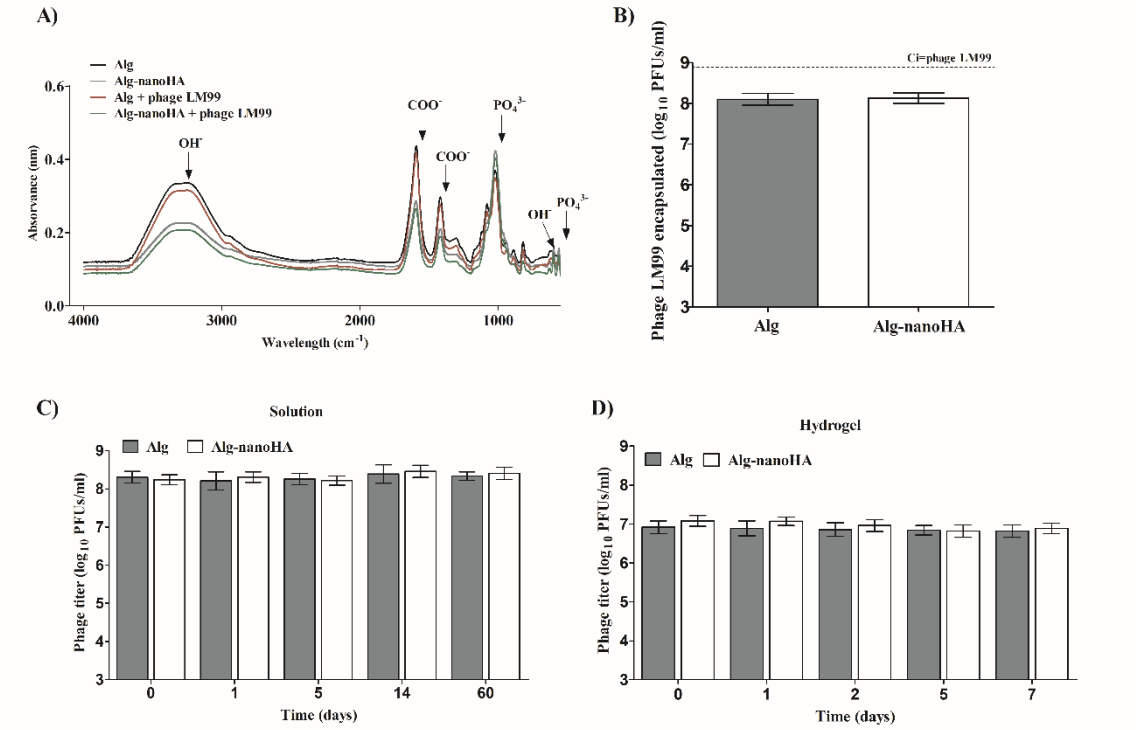

Figure 2 – A) ATR–FTIR spectra of the Alg + phage LM99 and Alg-nanoHA + phage LM99 hydrogels. B) Encapsulation efficiency of phages on Alg and Alg-nanoHA hydrogels. C) Phages titer into Alg and Alg-nanoHA solution and (D) into hydrogels.

3.2.2 Effect of pH on swelling behavior and associated phages release from the hydrogel system

The effect of different pH values in the hydrogels' swelling behavior and consequent phages release is shown in Figure 3A. At pH 3, a shrinkage of Alg and Alg-nanoHA hydrogels matrix was observed, and no phages were detected. With the increase of pH value, a progressive swelling behavior was observed, with disintegration occurring at

alkaline pH values. At pH 5, the swelling ratio was 130 %, allowing the release of 40 % of the encapsulated phages in Alg and in Alg-nanoHA hydrogels. At pH 7, the swelling ratio was 230 % and 95 % of encapsulated phages released from Alg and Alg-nanoHA hydrogels, respectively. Finally, at pH 9, a breakdown of the Alg hydrogels was observed, while the Alg-nanoHA30 continued to swell. The released phages titer from Alg-nanoHA at pH 9 was 95% (Fig. 3A). No differences on the swelling behavior between the hydrogels with and without phages were found and a correlation between the swelling ratio and released phages was observed (Fig. 3A). Overall, the phages LM99 showed higher stability at the pH range 5-9, with 100 % of survival rate, while, at pH 3 phages were completely inactivated, evidencing an established correlation between the swelling behavior of the hydrogels and the amount of phages released, at different pH values.

3.2.3 Kinetic release of phages LM99

In Figure 3B is shown the kinetics release of the phages LM99 from hydrogels. No differences of released phages titer between Alg and Alg-nanoHA hydrogels were observed over time. A gradual increase in the phage titer was observed during 24 h. After 30 min, 40 % of encapsulated phages were released and after 6 and 24 h of incubation, 88 % and 97 % of phages release were observed, respectively. After this time point, no differences in terms of the amount of phages were observed, with almost all phages being released from Alg and Alg-nanoHA hydrogels (Fig. 3B).

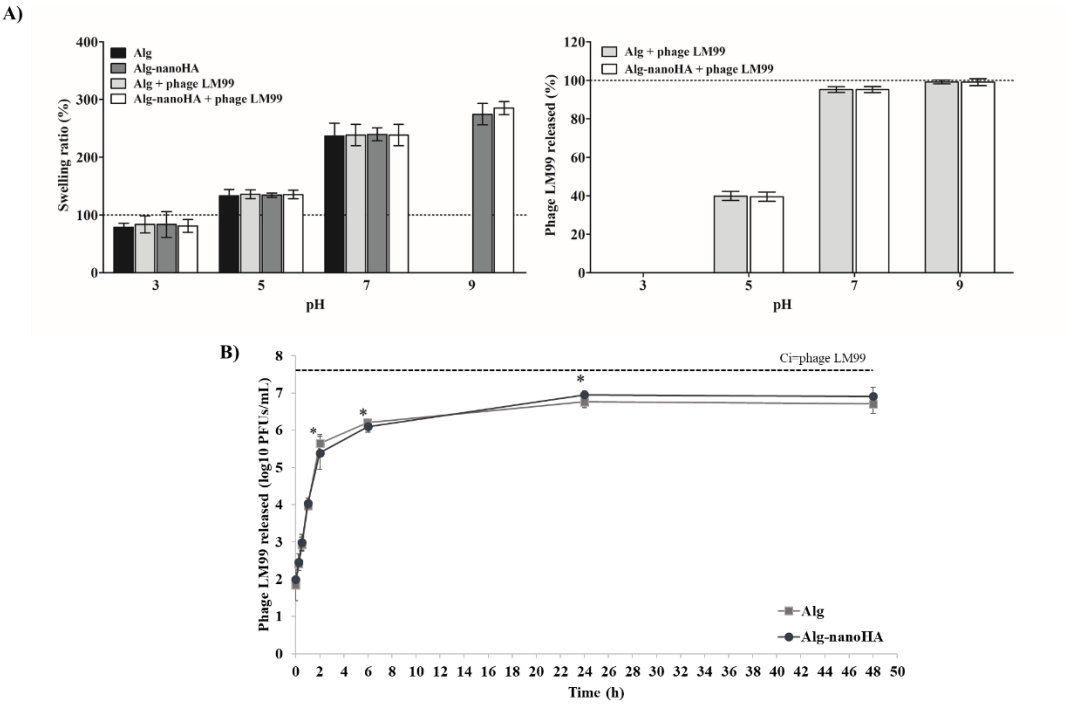

Figure 3 – A) The swelling behavior and releasing of phages from hydrogels without and with encapsulated phages at different pH values. B) Kinetics of phages release from Alg and Alg-nanoHA hydrogels. *significant differences of number phages released over time, for the same material, with $p < 0.05$.

3.3 Biological characterization

3.3.1 Inflammatory response – *in vivo* subcutaneous tissue implantation

Throughout the follow-up period, no post-operative complications as tissue infection or other adverse host reactions were identified (Fig. 4). At the defined time points, animals were euthanized and a systematic necropsy was carried out, revealing no macroscopic alterations of the internal organs. Also, at the implantation site, no significant inflammatory reaction or cellular exudate were identified.

After 2 weeks, the tissue surrounding implants displayed symptoms of a mild immune activation. Moreover, implanted hydrogels were embraced by a capsular organized structure, rich in fibroblasts and collagen fibers. The population of cells within the hydrogels at 2 weeks consisted mainly of polymorphonuclear leukocytes, lymphocytes, and macrophages, with no evidence of bleeding, intercellular edema, or vascular congestion (Fig. 4). Comparatively, no differences on the immune response, recruited cell populations, and tissue infiltration were observed between all conditions at 6 weeks, while an increased hydrogel fragmentation was observed, with tissue infiltration established throughout the fragments of the implanted biomaterials. Again, phages encapsulation was not found to modify the obtained cell response on both Alg and Alg-nanoHA hydrogels (Fig. 4).

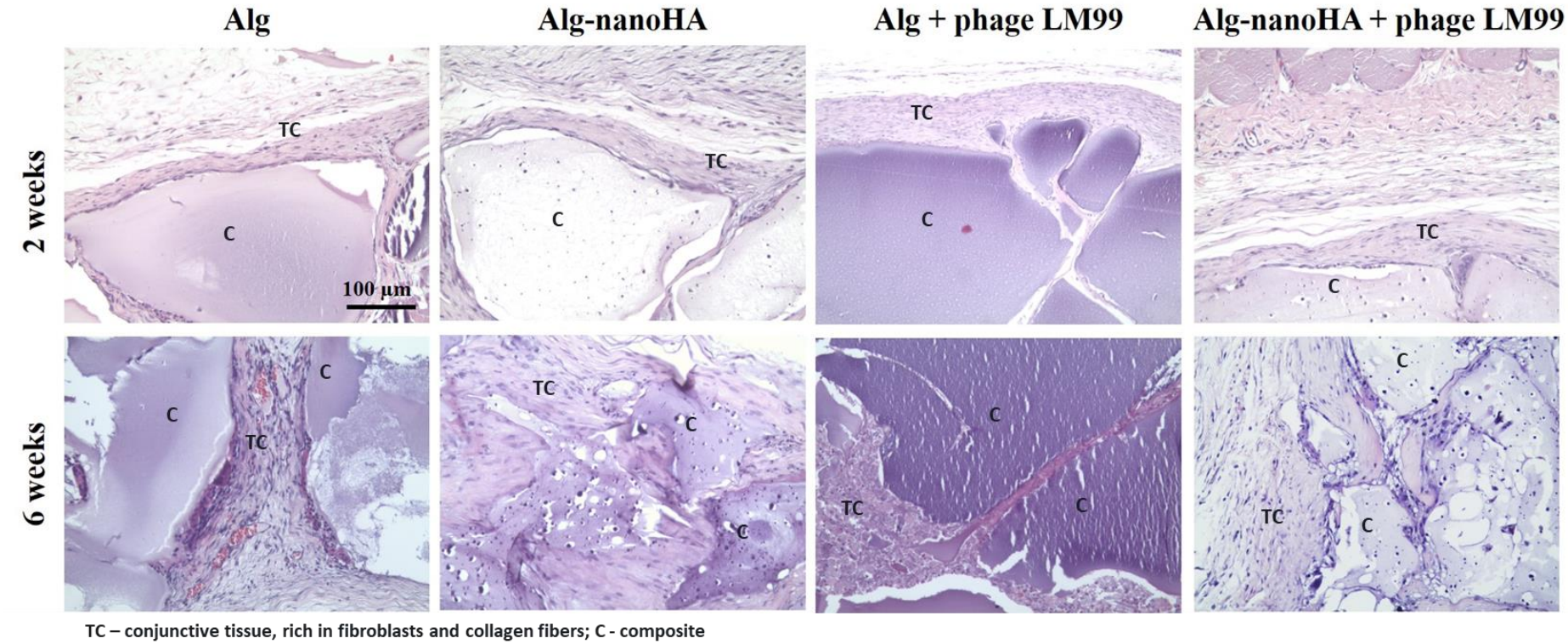

Figure 4 – Histological images of subcutaneous tissue with implanted hydrogels without and with phages encapsulated stained with H&E, at 2 and 6 weeks of implantation. Hematoxylin stains cell nuclei at blue and eosin stains the extracellular matrix and cytoplasm at pink. Scale bars 100 µm.

3.4 Osteogenic response

3.4.1 *In vitro* cytocompatibility assessment with human osteoblastic cells

An increase of MTT reduction values was observed in the control, throughout the 7-days' culture period. Comparatively, no significant differences were found between cells exposed to hydrogels eluents, with or without phages, and no differences were found between them and the established control (free-hydrogel eluents) (Fig. 5A).

Functional activity of grown osteoblastic cultures determined by ALP activity was found to increase between day 3 and 7 of culture, with high levels being obtained at day 7, in cultures grown on control (Fig. 5B). Cultures grown in the presence of hydrogels eluents, with or without phages, presented similar results, and no significant differences were found between the several conditions.

Cells were found to massively adhere to culture substrates, presenting an elongated and spread morphology with evident cell-to-cell contact being established since day 1 (Fig. 5C). Cells further exhibited well-organized F-actin cytoskeletons and prominent central nuclei, with philopodia extending at the cell margins. Representative images at day 3 revealed an active proliferation, which further increased until day 7, when organized cell layers could be depicted, with high confluent zones. The cells exposed to hydrogels eluents, with or without phages, showed similar morphological organization within the established cultures.

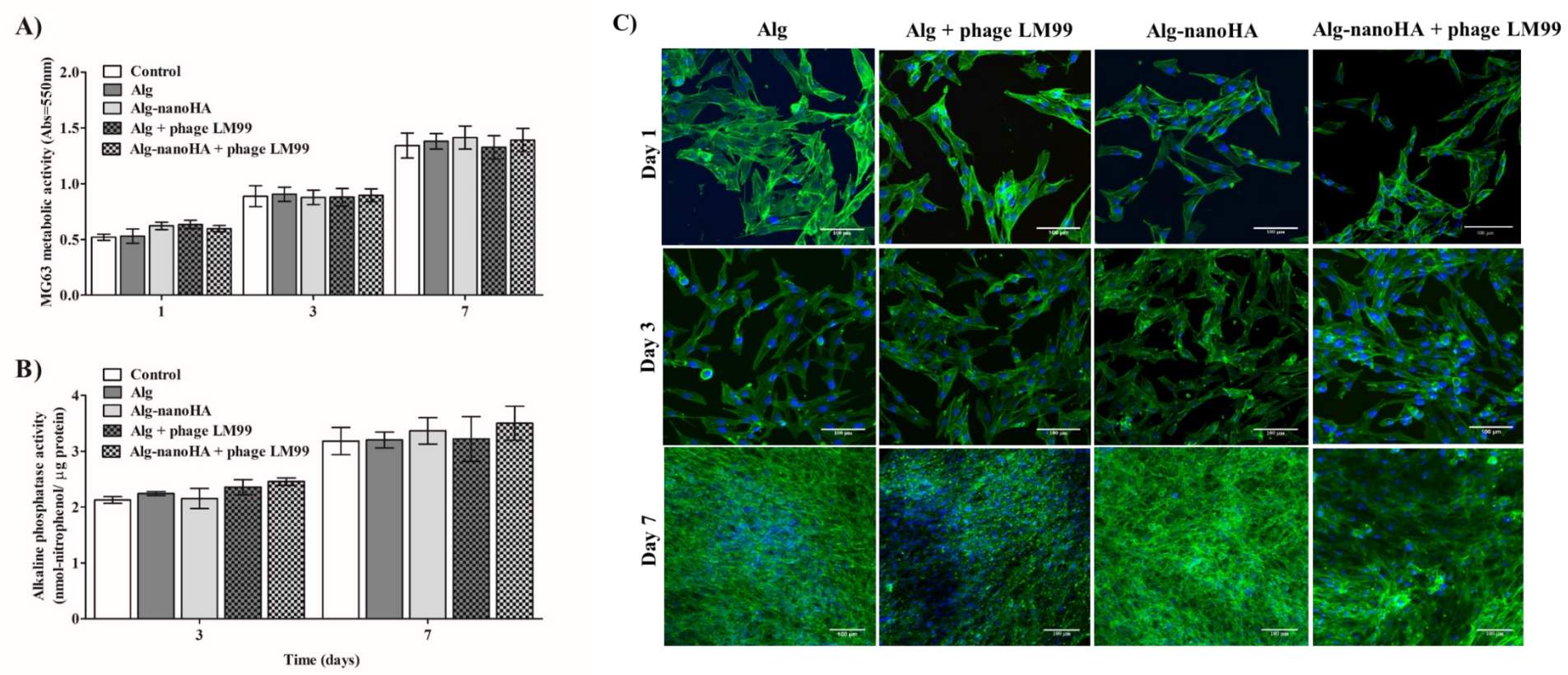

Figure 5 – (A) Cell metabolic activity, (B) ALP activity and (C) F-actin cytoskeletons and nuclei of MG63 cells cultured in the presence of hydrogels' eluents. Cytoskeleton was stained green and nucleus counterstained in blue. Scale bar 100 µm.

3.4.1 *Ex vivo* functional assessment of bone formation

Phages-free and phages-loaded Alg hydrogels induced a moderate osteogenic activation at the margin of the established segmental defect, and also at the bone collar formed within the peripheral structure of the tissue (Fig. 6). Comparatively, an increased osteogenic response was observed for Alg-nanoHA hydrogels, regardless of the presence of phages. The implantation of Alg-nanoHA enhanced significantly the collagenous matrix deposited within the central and marginal regions of the diaphysial structure and an organized and thick trabecular structure was formed. Masson's trichrome staining further corroborated the increased collagenous deposition obtained with Alg-nanoHA hydrogels. An increased mineral deposition within the developed trabecular structure was also evidenced by the von Kossa staining. It should be noticed that phages encapsulation seems not to have interfered with the enhanced osteogenic capability of Alg-nanoHA hydrogels.

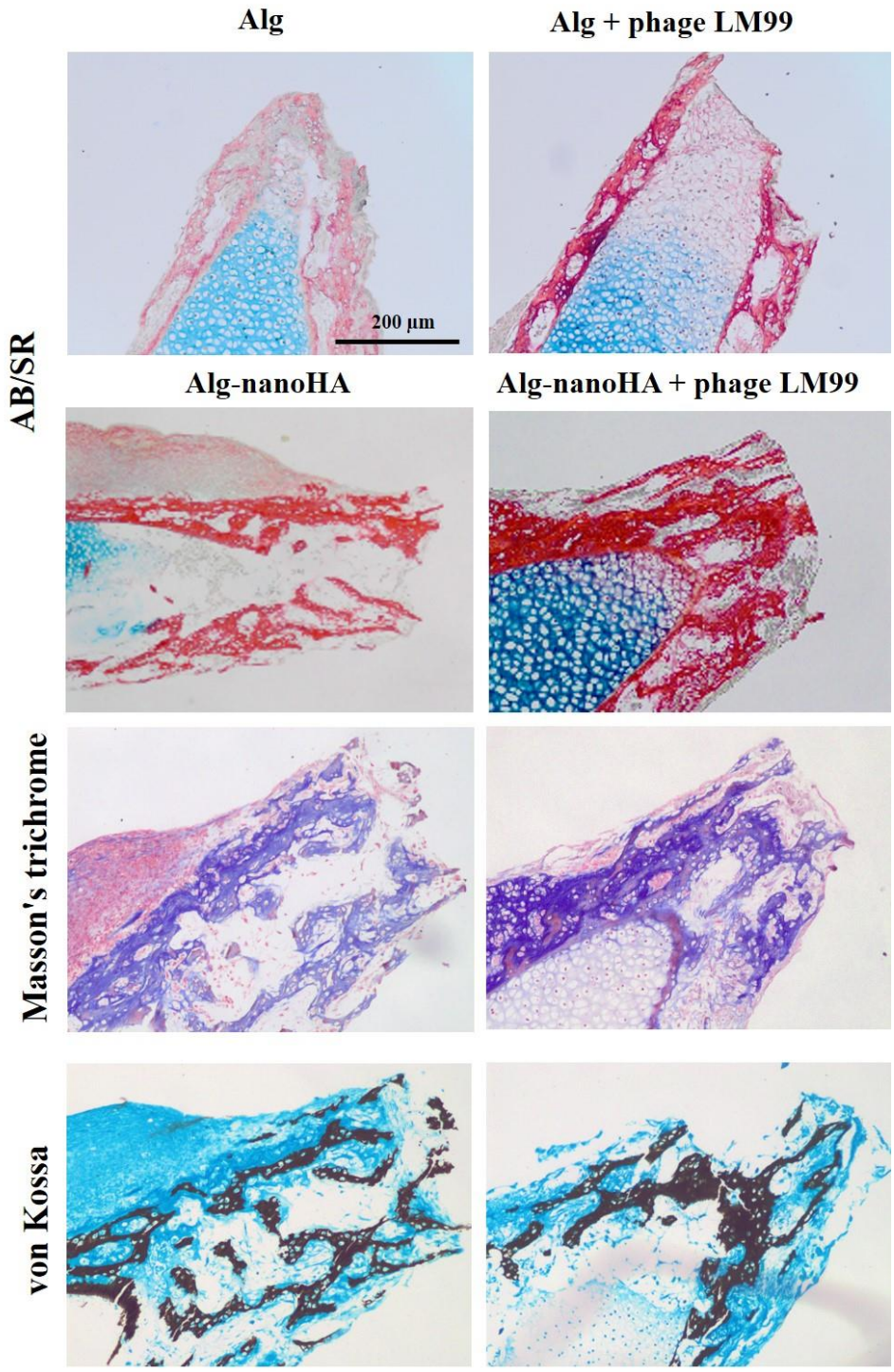

Figure 6 – Histological analysis of embryonic femurs implanted with developed hydrogels and cultures for 11 days. Images depict the segmental defect region of the femur in contact with the composite that was lost during histological preparation. Femurs were stained with AB/SR, Masson's trichrome and von Kossa. AB/SR staining marks the proteoglycan cartilage at blue, and the production of collagen at red. Masson's trichrome staining marks the collagen fibers at blue, and van Kossa staining marks the bone mineralization at black. Scale bar at 200 µm.

3.5 Antimicrobial activity

3.5.1 *In vitro* characterization over planktonic and sessile bacteria

The antimicrobial activity of phages-loaded hydrogels against planktonic and sessile bacteria is depicted in Figure 7.

Regarding planktonic bacteria, an increase of *E. faecalis* 201 density was observed after 24 h for Alg and Alg-nanoHA hydrogels, and no significant differences between these biomaterials could be found. In the presence of Alg + phages LM99 and Alg-nanoHA + phages LM99 hydrogels, bacterial growth was significantly inhibited (around 99 %), after 24 h of incubation (Fig. 7A).

Concerning sessile bacteria, both phages-loaded Alg and Alg-nanoHA hydrogels prevented the establishment of a sessile population, being able to avoid 98 % of bacterial attachment during the first 24 h, when compared to phages-free hydrogels (Fig. 7B).

When compared to the sessile population on TCPs, hydrogels with encapsulated phages were further able to reduce the bacterial attachment in 92 %, during the first 24 h (Fig. 7B), as compared to the respective phage-free hydrogels.

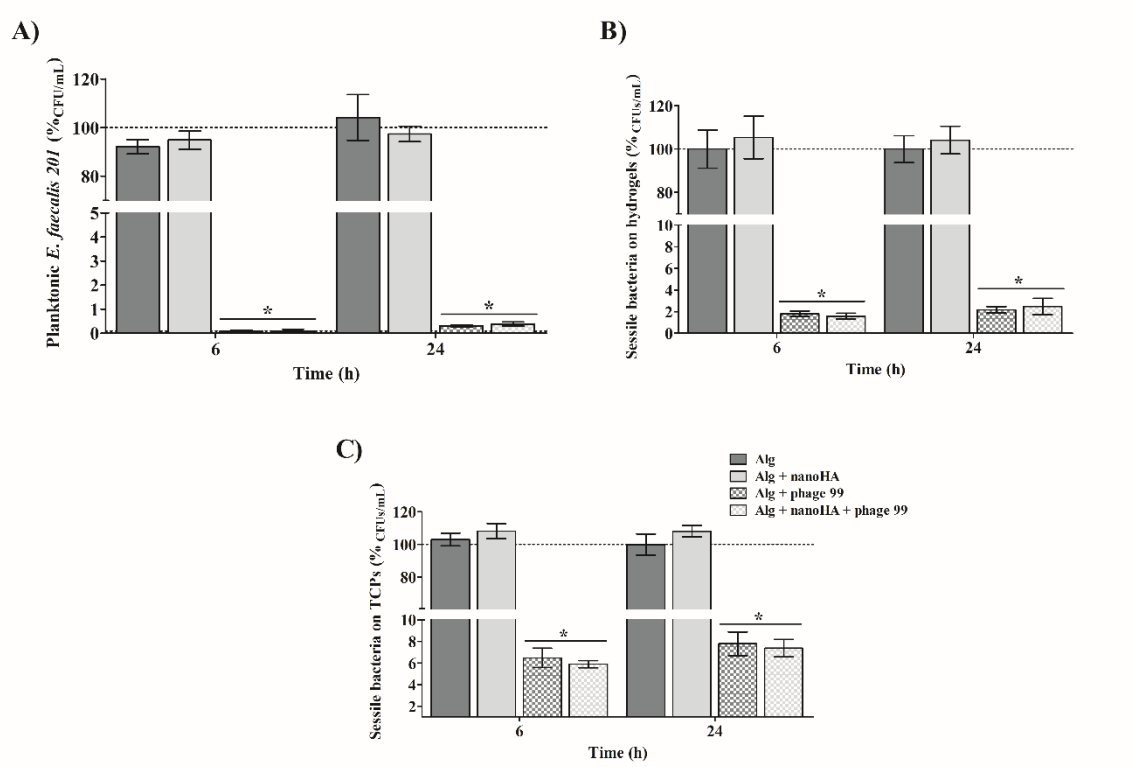

Figure 7 – (A) Percentage of planktonic *E. faecalis* 201 growth; (B) Sessile bacteria on Alg and Alg-nanoHA hydrogels without and with phages encapsulated and (C) Sessile bacteria on TCPs. *****statistically significant differences between phages-free Alg and phages-loaded Alg and between Alg-nanoHA and Alg-nanoHA + phage LM99 hydrogels, for the same time-point, with $p < 0.05$.

3.5.2 *Ex vivo* antimicrobial assay in bacteria-infected femoral model

The antibacterial activity was also evaluated using *ex vivo* chicken femoral model, previously infected with multidrug-resistant *E. faecalis* 201 strain (Fig. 8).

In the presence of phages-loaded Alg and Alg + nanoHA hydrogels, the bacterial density was three orders-of-magnitude lower in terms of CFUs when compared to phage-free hydrogels, corresponding to inhibition of 99.6 % and 99.9 % after 24 and 48 h, respectively (Fig. 8A). No differences in the antimicrobial activity were found between both hydrogels' formulations with phages.

Bacterial colonization within femurs was dependent on the hydrogels implanted within a segmental defect (Fig. 8B). With Alg or Alg-nanoHA implantation, bacterial colonies were identified within the tissue structure of the femurs, as revealed by Gram staining. Contrariwise, no bacterial growth was noticed when Alg + phages LM99 and Alg-nanoHA + phages LM99 hydrogels were implanted.

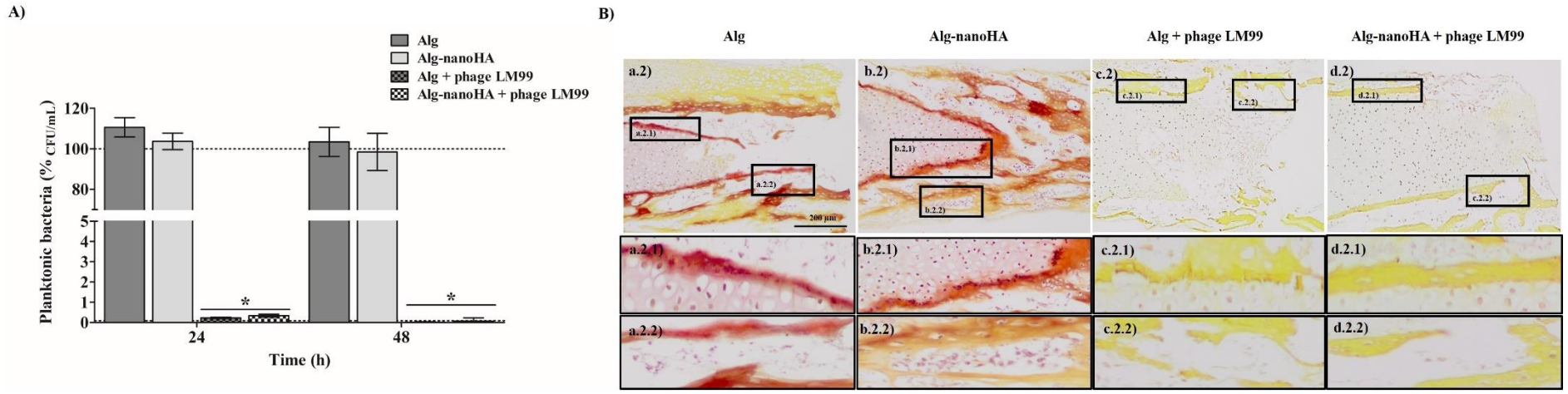

Figure 8 – A) Percentage of planktonic *E. faecalis* 201 growth in the surrounding implants; ***** statistically relevant differences between phages-free and phages-loaded hydrogels, for the same time-point, with $p < 0.05$. (B) Histological analysis of bacterial colonization within the femurs, following Gram staining. In a.2.1, b.2.1, c.2.1 and d.2.1 bacterial clusters were observed in the trabeculae and in a.2.2, b.2.2, c.2.2 and d.2.2 bacterial clusters were found in the underlying spaces. Scale bar at 200 µm.

4. DISCUSSION

Any surgical intervention, in particular when including the implantation of biomaterials, has a high risk of infections associated, which can be devastating for the patients and cause problems to the healthcare systems [28]. Antimicrobial-loaded biomaterials, as delivery systems, have received special attention in applications for the prevention and treatment of implant-related infections [9, 28]. However, the limited antimicrobial diffusion, sub-therapeutic levels of the antimicrobial agent, dose-dependent antimicrobial activity, antimicrobials' toxicity, and the spread of antibiotic-resistant bacteria, underscore the need for new approaches to control these bacterial infections [7, 9, 29, 30].

In the present study, a new drug-delivery system based on encapsulated phages on Alg-nanoHA hydrogels was assessed as a multifunctional approach. This system has three components with specific and complementary functionalities: 1) Alg hydrogel is responsible for the transport and delivery of the therapeutic agents to the local target, 2) the stimulation of the osteo-regeneration is endorsed by the presence of bioactive and osteoconductive nanoHA, and, 3) the prevention of bacterial colonization and proliferation is addressed by the local delivery of phages.

Firstly, phages were encapsulated into developed hydrogels and their influences on the material morphology, structure, chemical composition, encapsulation efficiency and shelf-life were evaluated. The phages were entrapped into a three-dimensional network of hydrogel, by ionic cross-linking, with no chemical reactions being detected between materials and phages. The encapsulation method did not affect the structure of hydrogels, neither nanoHA dispersion nor Alg matrix. The phages LM99 were efficiently encapsulated on Alg and Alg-nanoHA hydrogels, without jeopardizing phage morphology, viability and functionality. Other authors also reported the encapsulation of phages FelixO1 and phages UAB_Phi20 into Alg hydrogels with similar behavior and efficiency [25, 31]. A remarkable shelf-life of encapsulated phages on Alg or Al-nanoHA solutions was observed, whereas the shelf-life of phages into hydrogels was also broadly unaltered up to 7 days.

The Alg solubility and its swelling-disintegration-erosion process could explain the release profiles obtained for the hydrogel system. Several authors have reported the importance of pH-dependence and hydrophilic behavior of Alg network, on drug release mechanisms [31-33]. For instance, at basic pH, the swelling of Alg network occurs, due

to the ionization of the carboxylate groups (COO^-) and diffusion of Ca^{2+} ions from gelling sites [31-33], allowing thereby the phages permeability. Whereas, under acid conditions the Alg network shrinks, due to the protonation of the COO^- groups and increase of cross-linking degree [31-33], holding the phages entrapped in Alg matrices. It should be noted that no detrimental effects on phages viability were observed after phages delivery at pH 5, 7 and 9, which could be a promising feature for phages delivery at the site of bone infection, where the normal pH is 6.8[34].

From Alg and Alg-nanoHA hydrogels almost all entrapped phages were delivered, in a process expectedly modulated by a swelling-disintegration-erosion process, due to ion-exchange between medium and Alg hydrogel walls [31-33]. Similar phages release profiles were reported from hydroxypropylmethylcellulose, alginate/$CaCO_3$ or Eudragit® hydrogels for targeted delivery of phages [9, 23, 31, 33], suggesting that, in fact, Alg-nanoHA hydrogels could be used as a controlled phages release delivery system.

Secondly, the biological interaction of encapsulated phages in hydrogel systems was evaluated in terms of *in vivo* inflammatory response, osteogenic response and antimicrobial activity, both within *in vitro* and *ex vivo* assays.

Good biocompatibility and safety profiles were observed for all hydrogels subcutaneously implanted in a rabbit model. Adequate cell invasion and extracellular matrix deposition overall conditions (phages-free and -loaded) were observed, accompanied by low inflammatory response and absence of implant rejection (i.e., absence of edema, exudate, necrosis or degenerative alterations). Some reports have shown the efficiency of phages therapy in medical, veterinary, agricultural, and aquaculture applications without adverse safety concerns for eukaryotic cells [13, 35, 36]. Phages administration has shown to stimulate the host immune response, depending on the route of administration, e.g., oral and topical administrations may induce the production of anti-phages neutralizing antibodies, while intravenous administration of phages has the potential to stimulate innate and adaptive immune responses [13, 37]. No significant differences were identified on the local tissue response following the implantation of phages-loaded hydrogels, sustaining their biosafety profile.

Moreover, by *in vitro* cytocompatibility, it was observed that phages and hydrogels' leachable products did not interfere with osteoblastic cells' viability, proliferation and morphology, indicating that the phage-loaded biomaterial systems could allow for bone cells spreading and growth. Chung *et al* demonstrated that the incorporation of phages into tissue engineering fibers did not interfere with cell behavior [38]. Furthermore, the

cytocompatibility of Alg and nanoHA materials has been previously described in several studies [32, 39].

The osteogenic response of hydrogel systems was emphasized by *ex vivo* functionality of bone formation results. The osteogenic and mineralization response was broadly influenced by Alg-nanoHA hydrogels implantation, noticing that the increase of collagenous deposition, trabecular bone formation and mineralization was promoted by nanoHA. These data evidence the potential osteoconductive and osteoinductive activities of nanoHA, feature already described by other authors [40, 41], suggesting that, in fact, Alg-nanoHA + phage LM99 hydrogels could be used to improve bone tissue regeneration at the local bone defect.

Finally, the antimicrobial activity of encapsulated phages in hydrogel systems was evaluated against a multidrug-resistant VRE *E. faecalis* strain, under both *in vitro* and *ex vivo* conditions. Under *in vitro* conditions, an effective antimicrobial activity and a large diffusion of phages from hydrogels were observed, inhibiting attachment and growth of planktonic and sessile bacteria on biomaterials and surrounding media. Additionally, by *ex vivo* assessment, it was observed that phages-loaded hydrogels were able to prevent the proliferation and colonization of the bacterial strain in the surroundings of the implant and within the femoral tissues. The antimicrobial results obtained indicate that this approach can be used as an alternative local delivery system to prevent infection and eradicate bacteria strains, even those showing multidrug resistance profiles, at the implant area, before they adhere and create a biofilm.

Overall, in the present study, a new multifunctional drug-delivery system based on encapsulated phages on Alg-nanoHA hydrogels was developed and showed to be a promising and efficient approach to prevent and control bacterial contamination, given the local delivery of phages and their ability to replicate at the site of infection, during the implantation and bone integration, promoted by nanoHA particles.

ACKNOWLEDGMENTS

The authors gratefully acknowledge the technical support provided by Rui Fernandes (HEMS), Rossana Correia (HEMS) for histological and TEM analysis. The help of PhD Liliana Grenho (FMDUP) for *in vivo* and *in vitro* biocompatibility analysis and *ex vivo* analysis is also deeply appreciated. This work was supported by FEDER – Fundo Europeu de Desenvolvimento Regional funds through the COMPETE 2020 – Operacional

Programme for Competitiveness and Internationalisation (POCI), Portugal 2020, by Portuguese funds through FCT/MCTES in the framework of the project "institute for Research and Innovation in Health Sciences (POCI-01-0145-FEDER-007274), by Project Biotherapies (NORTE-01-0145-FEDER-000012) and by Joana Barros' PhD grant (SFRH/BD/102148/2014).

REFERENCES

[1] Wang W, Yeung KWK. Bone grafts and biomaterials substitutes for bone defect repair: A review. Bioact Mater 2017;2:224-47.

[2] Zimmerli W, Moser C. Pathogenesis and treatment concepts of orthopaedic biofilm infections. FEMS Immunol Med Microbiol 2012;65:158-68.

[3] Gimeno M, Pinczowski P, Perez M, Giorello A, Martinez MA, Santamaria J, et al. A controlled antibiotic release system to prevent orthopedic-implant associated infections: An *in vitro* study. Eur J Pharm Biopharm 2015;96:264-71.

[4] Street TL, Sanderson ND, Atkins BL, Brent AJ, Cole K, Foster D, McNally MA, Oakley S, Peto L, Taylor A, Peto TEA, Crook DW, Eyre DW. Molecular Diagnosis of Orthopedic-Device-Related Infection Directly from Sonication Fluid by Metagenomic Sequencing. J Clin Microbiol 2017;55:2334-47.

[5] Junka A, Szymczyk P, Ziolkowski G, Karuga-Kuzniewska E, Smutnicka D, Bil-Lula I, Bartoszwicz M, Mahabady S, Sedghizadeh PP. Bad to the Bone: On *In Vitro* and *Ex Vivo* Microbial Biofilm Ability to Directly Destroy Colonized Bone Surfaces without Participation of Host Immunity or Osteoclastogenesis. Plos One 2017;12:e0169565.

[6] Qiu Y, Zhang N, An YH, Wen X. Biomaterial strategies to reduce implant-associated infections. Int J Artif Organs 2007;30:828-41.

[7] Silva T, Silva JC, Colaco B, Gama A, Duarte-Araujo M, Fernandes MH, Bettencourt A, GomesP. *In vivo* tissue response and antibacterial efficacy of minocycline delivery system based on polymethylmethacrylate bone cement. J Biomater Appl 2018;33:380-91.

[8] Francolini I, Vuotto C, Piozzi A, Donelli G. Antifouling and antimicrobial biomaterials: an overview. Apmis 2017;125:392-417.

[9] Kaur S, Harjai K, Chhibber S. Bacteriophage Mediated Killing of *Staphylococcus aureus In Vitro* on Orthopaedic K Wires in Presence of Linezolid Prevents Implant Colonization. Plos One 2014;9.

[10] Loc-Carrillo C, Abedon ST. Pros and cons of phage therapy. Bacteriophage 2011;1:111-4.
[11] Edgar R, Friedman N, Molshanski-Mor S, Qimron U. Reversing Bacterial Resistance to Antibiotics by Phage-Mediated Delivery of Dominant Sensitive Genes. Appl Environ Microb 2012;78:744-51.
[12] Nobrega FL, Costa AR, Kluskens LD, Azeredo J. Revisiting phage therapy: new applications for old resources. Trends Microbiol 2015;23:185-91.
[13] Morris J, Kelly N, Elliott L, Grant A, Wilkinson M, Hazratwala K, McEwen P. Evaluation of Bacteriophage Anti-Biofilm Activity for Potential Control of Orthopedic Implant-Related Infections Caused by *Staphylococcus Aureus*. Surg Infect 2018.
[14] Yilmaz C, Colak M, Yilmaz BC, Ersoz G, Kutateladze M, Gozlugol M. Bacteriophage Therapy in Implant-Related Infections An Experimental Study. J Bone Joint Surg Am 2013;95a:117-25.
[15] Trampuz A, Klatt A, Luca MD. Isolation of a new lytic bacteriophages for treatment of prosthetic joint infection. Orthopaedic Proceedings 2017;99-B:36.
[16] Oliveira H, Sillankorva S, Merabishvili M, Kluskens LD, Azeredo J. Unexploited opportunities for phage therapy. Front Pharmacol 2015;6.
[17] Gorski A, Jonczyk-Matysiak E, Miedzybrodzki R, Weber-Dabrowska B, Lusiak-Szelachowska M, Baginska N, et al. Phage Therapy: Beyond Antibacterial Action. Front Med-Lausanne 2018;5.
[18] Fish R, Kutter E, Bryan D, Wheat G, Kuhl S. Resolving Digital Staphylococcal Osteomyelitis Using Bacteriophage-A Case Report. Antibiotics (Basel) 2018;7.
[19] Kishor C, Mishra RR, Saraf SK, Kumar M, Srivastav AK, Nath G. Phage therapy of staphylococcal chronic osteomyelitis in experimental animal model. Indian J Med Res 2016;143:87-94.
[20] Dublanchet A, Patey O. Phage therapy for bone and joint infections: report of french cases. Orthopaedic Proceedings 2017;99-B:35.
[21] Chan BK, Turner PE, Kim S, Mojibian HR, Elefteriades JA, Narayan D. Phage treatment of an aortic graft infected with *Pseudomonas aeruginosa*. Evolution, Medicine, and Public Health 2018;2018:60-6.
[22] Meurice E, Rguiti E, Brutel A, Hornez JC, Leriche A, Descamps M, Bouchart F. New antibacterial microporous CaP materials loaded with phages for prophylactic treatment in bone surgery. J Mater Sci-Mater M 2012;23:2445-52.

[23] Kaur S, Harjai K, Chhibber S. *In Vivo* Assessment of Phage and Linezolid Based Implant Coatings for Treatment of Methicillin Resistant *S. aureus* (MRSA) Mediated Orthopaedic Device Related Infections. Plos One 2016;11.

[24] Melo LDR, Sillankorva S, Ackermann HW, Kropinski AM, Azeredo J, Cerca N. Characterization of *Staphylococcus epidermidis* phage vB_SepS_SEP9-a unique member of the *Siphoviridae* family. Res Microbiol 2014;165:679-85.

[25] Ma Y, Pacan JC, Wang Q, Xu Y, Huang X, Korenevsky A, Sabour PM. Microencapsulation of bacteriophage felix O1 into chitosan-alginate microspheres for oral delivery. Appl Environ Microbiol 2008;74:4799-805.

[26] Mohammed N, Grishkewich N, Berry RM, Tam KC. Cellulose nanocrystal–alginate hydrogel beads as novel adsorbents for organic dyes in aqueous solutions. 2015;22:3725-38.

[27] Gomes PS, Fernandes MH. Effect of therapeutic levels of doxycycline and minocycline in the proliferation and differentiation of human bone marrow osteoblastic cells. Arch Oral Biol 2007;52:251-9.

[28] Orapiriyakul W, Young PS, Damiati L, Tsimbouri PM. Antibacterial surface modification of titanium implants in orthopaedics. Journal of Tissue Engineering 2018;9.

[29] Qiu Y, Zhang N, An YH, Wen X. Biomaterial strategies to reduce implant-associated infections. J Artif Organs 2007;30:828-41.

[30] Siljander MP, Sobh AH, Baker KC, Baker EA, Kaplan LM. Multidrug-Resistant Organisms in the Setting of Periprosthetic Joint Infectiond-Diagnosis, Prevention, and Treatment. J Arthroplasty 2018;33:185-94.

[31] Colom J, Cano-Sarabia M, Otero J, Arinez-Soriano J, Cortes P, Maspoch D, Llagostera M. Microencapsulation with alginate/$CaCO_3$: A strategy for improved phage therapy. Sci Rep-Uk 2017;7.

[32] Jain D, Bar-Shalom D. Alginate drug delivery systems: application in context of pharmaceutical and biomedical research. Drug Development and Industrial Pharmacy 2014;40:1576-84.

[33] Vinner GK, Vladisavljevic GT, Clokie MRJ, Malik DJ. Microencapsulation of Clostridium difficile specific bacteriophages using microfluidic glass capillary devices for colon delivery using pH triggered release. Plos One 2017;12.

[34] Kinnari TJ, Esteban J, Martin-De-Hijas NZ, Sanchez-Munoz O, Sanchez-Salcedo S, Colilla M, et al. Influence of surface porosity and pH on bacterial adherence to

hydroxyapatite and biphasic calcium phosphate bloceramics. J Med Microbiol 2009;58:132-7.
[35] Cisek AA, Dabrowska I, Gregorczyk KP, Wyzewski Z. Phage Therapy in Bacterial Infections Treatment: One Hundred Years After the Discovery of Bacteriophages. Curr Microbiol 2017;74:277-83.
[36] Kazmierczak Z, Gorski A, Dabrowska K. Facing Antibiotic Resistance: Staphylococcus aureus Phages as a Medical Tool (vol, 6, pg 2551, 2014). Viruses-Basel 2015;7:1667-.
[37] Zimecki M, Artym J, Kocieba M, Weber-Dabrowska B, Borysowski J, Gorski A. Effects of prophylactic administration of bacteriophages to immunosuppressed mice infected with Staphylococcus aureus. BMC microbiology 2009;9:169.
[38] Chung W-J, Merzlyak A, Lee S-W. Fabrication of engineered M13 bacteriophages into liquid crystalline films and fibers for directional growth and encapsulation of fibroblasts. Soft Matter 2010;6:4454-9.
[39] Teotia AK, Raina DB, Singh C, Sinha N, Isaksson H, Tagil M, Lidgren L, Kumar A. Nano-Hydroxyapatite Bone Substitute Functionalized with Bone Active Molecules for Enhanced Cranial Bone Regeneration. Acs Appl Mater Inter 2017;9:6816-28.
[40] Cunniffe GM, Curtin CM, Thompson EM, Dickson GR, O'Brien FJ. Content-Dependent Osteogenic Response of Nanohydroxyapatite: An *In Vitro* and *In Vivo* Assessment within Collagen-Based Scaffolds. ACS Appl Mater Interfaces 2016;8:23477-88.
[41] Martinelli NM, Ribeiro MJG, Ricci R, Marques MA, Lobo AO, Marciano FR. I*n Vitro* Osteogenesis Stimulation via Nano-Hydroxyapatite/Carbon Nanotube Thin Films on Biomedical Stainless Steel. Materials 2018;11.

CHAPTER 5

GENERAL DISCUSSION AND FUTURE PERSPECTIVES

GENERAL DISCUSSION

Bone is a complex and dynamic tissue, which has self-remodeling capability [1]. However, in cases of non-self-healable extensive damages (e.g. degenerative disease, prosthetic revisions, resection of bone tumors or complex fractures or defects above critical size) the use of bone material substitutes is mandatory. Moreover, these biomaterials may contain therapeutic agents (e.g. growth factors, hormones, nucleic acids, antimicrobial and anti-inflammatory agents, biomodulators) or specific therapeutic cells to regulate and promote bone tissue regeneration [1, 2].

Composites, based on the combination of different materials, such as polymers, ceramics or metals, have emerged as bone graft substitutes and as drug delivery vehicles, for the management of bone defects [3, 4]. In the present work, a bioactive alginate-nanoHA hydrogel for bone regeneration was developed, and the influence of nanoHA content on an alginate-based hydrogel was optimized within the established system to maximize bone regeneration capacity. Previous reports have shown that nanoHA content could affect hardness and stiffness, water-swelling ratio, bone-like apatite layer formation, and further modulate biological response, as cell attachment, proliferation and differentiation and bone growth rate [5-7]. Accordingly, in the present study, nanoHA concentration had a vital role in the modulation of the physico-chemical properties and biological response of the assayed composite. The presence of nanoHA, particularly at high levels, contracted and restricted the mobility of the Alg polymeric chains [8, 9], providing resistance to water diffusion and swelling tendencies. Furthermore, the composites' stability at different pH conditions were also affected by the presence of nanoHA particles, that allowed the shrinkage and swelling of composites in the presence of strongly acid and alkaline environments. All these phenomena can be explained by the increasing presence of Ca^{2+} concentration, deriving from nanoHA particles, that induced a specific and strong interaction with G-blocks of Alg and consequently increased its crosslinking degree [10].

After implantation, biomaterials undergo numerous dissolution/precipitation processes induced by biological fluids. The dissolution of nanoHA releases Ca^{2+} and PO_4^{3-} ions, that can modulate cellular behavior within the microenvironment, and lead to bone integration and mineralization [5]. The formation of bone-like mineral on the surfaces, when immersed in simulated body fluids, may be correlated with an increase in the implant's calcium phosphate solubility, and is an essential property to indicate the

bonding with living bone [11, 12]. The Ca^{2+} released from composites was proportional to nanoHA content and it contributed to increase apatite deposition on the surface of hydrogels with nanoHA. This increase of apatite on Alg-nanoHA surfaces was probably due to the availability of negatively charged hydroxyl groups on nanoHA that acted as nucleation sites for crystal deposition [11, 12]. Furthermore, the amount of Ca^{2+} released from biomaterials can play a vital role in regulating the chemotaxis, proliferation and osteogenic differentiation of osteoblastic cells [12-14]. The biological response of composites was also influenced by nanoHA content, as Alg-based hydrogels with 30% nanoHA content enhanced mesenchymal cells' proliferation and osteogenic activation, increasing the expression of Runx2, Col1a1 and BGLAP levels. Composites with high nanoHA content (50 and 70 %) lead to a decrease of cell proliferation and osteogenic cell response, probably due to excessive Ca^{2+} being released, that could lead to a disturbance within the intracellular calcium homeostasis, known to play a vital role in cell proliferation and apoptosis [15, 16]. *Ex vivo* data underlined the *in vitro* findings, revealing an enhanced collagenous deposition, trabecular bone formation and matrix mineralization with Alg-nanoHA30 hydrogels, while composites with higher nanoHA content impaired the biological response, in the assayed chick femoral model. No previous studies have addressed the development and biological evaluation of Alg hydrogels loaded with nanoHA particles at different ratios. In fact, the nanoHA content played a major role in some relevant physico-chemical properties and biological response of the composite system, emphasizing the need to optimize the ratio of the composite's components in order to maximize bone tissue regeneration. The Alg-based hydrogel with 30% of nanoHA showed a good functional synergism that culminated in the enhancement of bone regeneration.

Biomaterials' implantation poses a serious risk of bacterial infection, that can be, in some cases, devastating for the patients and a burden for the healthcare systems [17, 18]. This susceptibility for infection appears to be partly due to a localized deficiency in phagocytosis of bacteria in the vicinity of an implant, and to the growth of bacterial aggregates leading to biofilm formation on the surface of the implanted devices [19]. Most infections related to orthopedic implants are caused by opportunistic pathogens that colonize the implant or tissues, leading to implant failure or bone destruction [19]. In the present work, fifteen clinical bacterial strains were isolated from orthopedic implant-related infections, showing resistance to several antibiotics, such as glycopeptides, aminoglycosides and penicillins, the most common antibiotics used in clinical [20, 21],

increasing the concern about these type of infections, due to confining the therapeutic options [2, 3]. The presence of mobile genetic (*mec*A*S. aureus*, *Tn916/Tn1545E. faecalis* and *intl*1*E. coli*) and virulent elements (such as *ica*B*S. aureus*, *hlbS. aureus*, *cnaS. aureus*, *agg E. faecalis*, *gel*E *E. faecalis* *cyl*M*E. faecalis*, *cyl*L*E. faecalis*, *fsrE. faecalis* and *fim*A*E. coli*) increases the pathogenicity and severity of these infections [22-25]. Once, the mobile genetic elements can mediate the resistance and virulence determinants transfer and integrate into a new host DNA [26]. On the other hand, the virulent elements can favor bacterial binding to host matrix proteins, and consequently increase bacterial adhesion to implants [7, 28]. Besides, these pathogens belong to lineages frequently involved in pandemic nosocomial infections [23, 27], with different resistance and virulence patterns, increasing the concern about diagnosis and treatment of infections caused by these type of bacteria [22, 27].

Therefore, considering the mentioned pathogenicity and severity of these pathogens and the poor bioavailability of antibiotics in bone tissue [28], there is an urgent need to develop alternative therapeutic approaches to fight and control isolates involved in orthopedic implant-associated infections. Phages therapy have long shown to be a promising anti-infective strategy, mainly due to its high specificity and effectiveness in killing targeted pathogenic bacteria [29-35]. Phages have capacity to infect and kill specific bacterial strains, without modifying the established commensal microbiome. Despite they are able to interact with phagocytic cells and be adsorbed through mammalian cells' surface receptors, they are not pathogenic for eukaryotic cells since are subsequently eliminated by them [33-35]. Phages present a good therapeutic bioavailability, since they replicate within the host bacterium, that is, at the local of infection, and are always available in the doses required for the treatment, and it is not necessary to repeat the delivery. This phenomenon is referred to as ''auto-dosing'' whereby, phages themselves, by exponential growth, contribute to establish a high titer at the site of infection. Moreover, they have good migration capacity - the release of the new progeny of phages and afterlife cycle – assists on the spreading and infection of other target bacteria nearby [33-35]. Phages propagation and persistence depend always on the presence of their host bacterial pathogens, which contributes to regulate phages number in direct relation with pathogen level and facilitates diffusion into the surrounding areas, in a gradient dependent on pathogen availability [33-35]. Despite the great advantages of phages, phage therapy also presents some drawbacks such as the requirement to determine which bacteria are causing the disease (due to their specificity) and the emergence of phage-resistant bacterial strains. An interesting way to increase phage fitness against

bacteria and to reduce or delay the emergence of resistance is to use adequate phage cocktail to treat clinical strains. Nevertheless, their application can be challenging in terms of regulatory approval due to phage structures, life cycles, and genome organization. Besides, there are no consensual and validated guidelines for the selection of individual or multiple therapeutic phages that target a specific pathogen. In the present study, three phages, *S. aureus* – phage LM12, *E. faecalis* – phage LM99 and *E. coli* – phage JB75, were characterized in order to control and kill the pathogens isolated from orthopedic implant-related infections. All phages presented outstanding characteristics as bactericidal activity, good broad spectrum against the target pathogenic bacteria, short latent periods, large burst sizes, and high stability to several environmental conditions. Besides, these virulent phages did not encode any genes associated with lysogeny. Furthermore, it is important to highlight the high specificity of the phages used in this work that was dependent of bacterial strain tested. All these characteristics associated to their high efficiency to infect the multidrug resistant bacteria, make them potential candidates for prophylaxis and treatment of infections provoked by these pathogens. Individual phage therapy was used to prove the efficacy of phage as therapeutic agents to fight bacteria involved in implant-related infections.

Several studies have explored the efficacy and precision of phage therapy in the treatment of orthopedic infections based on systemic administration of phage solution [30, 36-41]. Nonetheless, experimental studies using phages-loaded biomaterials for local delivery approaches are scarce [42-44], and focused only on the phages releasing and their antimicrobial activity, without exploring simultaneously the potential combination with a regeneration inductive biomaterial. To the best of our knowledge, the present work is the first to address the use of phages-loaded biomaterials as a novel local delivery system to, simultaneously, promote bone tissue regeneration, and prevent the development of local infection. Therefore, a new drug-delivery system based on encapsulated phages into Alg-nanoHA hydrogel was developed, where each component endorses a specific and complementary function: 1) Alg hydrogel is responsible for the transport and delivery of the therapeutic agent to the local target; 2) the stimulation for osteo-regeneration is endorsed by nanoHA; and, 3) the prevention of bacterial colonization and proliferation is addressed by the local phages delivery.

Local delivery systems have numerous advantages over systemic approaches, such as therapeutic agents' delivery at or close to the defect site, the increased efficacy and bioavailability of the therapeutic agents, reduction of the dose administered and decrease

systemic toxicity risks [45]. In the present work, it was shown that the local phage release was due to Alg solubility capacity [46, 47]. When phage-loaded hydrogels are exposed to an aqueous medium, a successive progression of swelling-disintegration-erosion occurs at the Alg network by ion-exchange with the medium [48], allowing phages to diffuse out of the hydrogel. The pH-responsive character and hydrophilic nature of Alg matrix endorses the potentiality of this system for drug delivery during the healing and mineralization processes. At the early healing phase, tissue pH is lower than normal physiological pH 7.2, owing to accumulation of acidic metabolites in tissue fluids [49]. In acidic environment the Alg network shrinks, due to the protonation of the COO^- groups and increase of cross-linking degree [50-52], holding the phages entrapped in Alg matrices. During the mineralization phase, an increase in tissue calcium content occurs due to the mineral deposition associated with new bone formation, which promotes the increase in pH to reach more alkaline values [53]. In this environment, the swelling of Alg network occurs, due to the ionization of the carboxylate groups (COO^-) and diffusion of Ca^{2+} ions from gelling sites [50-52], allowing thereby the phages permeability. It should be noted that no detrimental effects on phages viability and functionally were observed after phages delivery at broad range of pH 5 – 9, which could be a promising feature for phages delivery at the site of bone infection, where the normal pH is 6.8 [54]. Furthermore, the presence of nanoHA did not affect the kinetic phage release from hydrogels, with almost all phages being released from the composites, suggesting Alg-nanoHA hydrogels could be used as a suitable phages release delivery system.

Biocompatibility and safety are important requirements for local drug delivery systems and their tissue engineering applications [2, 19]. Several authors have shown the efficiency of phages therapy in medical, veterinary, agricultural, and aquaculture applications without adverse safety concerns for eukaryotic cells [36, 55, 56] [57]. In the present work, phage-loaded hydrogels showed a good cytocompatibility, biocompatibility and biosafety profiles, indicating that phage-loaded hydrogel systems could allow for bone cells dissemination, growth and differentiation, without cause relevant inflammatory or immune activation.

Hydrogels are increasingly employed in regenerative medicine due to their favorable biocompatibility and they can be surgically implanted or injected into defective tissues in a minimally invasive manner due to their *in situ* gelation capability [58, 59]. As a result, hydrogels fill the volume and take the shape of the available space at the implantation or injection site. In the present work, the regenerative potential of hydrogels was underlined

by Alg-nanoHA hydrogels implantation, highlighting the osteoconductive and osteoinductive character of nanoHA [60, 61]. Besides, it should be noticed that the phages encapsulation did not interfere with bone regeneration, indicating that the phage-loaded Alg-nanoHA hydrogels could be used to improve bone tissue regeneration at the local bone defect.

The local strategies, as vehicles for the delivery of antimicrobial agents, has emerged as a regular adjunct in the prevention and treatment of bone graft-related infections [45, 62-64]. In the present work, encapsulated phages on Alg-nanoHA hydrogels showed an effective antimicrobial activity and a large diffusion from hydrogels, inhibiting attachment, proliferation and colonization of planktonic (see SS2) and sessile bacteria with multidrug resistance profiles on biomaterials and in their surrounding media. Moreover, this system was able to prevent the proliferation and colonization of the virulent pathogens in the surroundings and within the femoral tissues. The data indicate that this approach could be used as an alternative local delivery system to prevent infection and eradicate clinical bacterial strains, even those showing multidrug resistance profiles, at the implant area, before they adhere and create a biofilm.

Overall, this new drug-delivery system based on encapsulated phages on Alg-nanoHA hydrogels showed to be a promising and efficient approach to promote bone tissue regeneration, promoted by nanoHA particles, and to prevent the bacterial contamination during implantation and bone integration, given the local delivery of phages and their ability to replicate at the site of infection.

FUTURE WORK

The present study consisted on the development of a new drug-delivery system based on encapsulated phages on Alg-nanoHA hydrogel, as proof of concept for preventing and control bacterial contamination during the implantation and bone integration. However, additional experiments should be performed in order to strengthen the potentiality of this concept.

Since the physico-chemical properties of hydrogel and viability and functionality of phages can be affected by current conventional technologies (steam/dry heat, ethylene oxide, and gamma irradiation), future studies must be performed to find the right sterilization method for the final product. The sterilization treatment using supercritical carbon dioxide ($scCO_2$) could be a possibility to be applied in this system. Once, this method is a green and sustainable technology able to reach the sterility levels required by regulation for medical devices, without altering the original properties of even highly sensitive materials. Detailed parameters such processing temperature, pressure, time, presence of additives (hydrogen peroxide/water/peracetic acid) should be studied, with the intent of evaluating possible interferences of the method on physico-chemical, mechanical and biological properties of this system.

To improve the phages spectrum of action and, simultaneously, attenuate the development of phage-resistant bacterial mutants, the isolation and characterization of new phages should be performed, with the intent of developing adequate phages cocktail. All phages used in the cocktail should be studied individually and mixed since some interference phenomena between different phages types may occur. Their antimicrobial activity should be tested against a panel of bacterial strains, also individually and mixed, to confirm the efficiency of phage cocktail. After phages cocktail encapsulation into hydrogel system, all experiments related to phages delivery, cytocompatibility, biocompatibility, osteogenicity and antimicrobial activity should be also performed, in order to prove the phage cocktail applicability on biomaterials for bone tissue regeneration.

Finally, adequate *in vivo* antimicrobial and osteogenic experiments should be designed and performed in order to evaluate the potential anti-infective and regenerative of the biomaterial implanted under *in vivo* conditions.

REFERENCES

[1] Cao B, Li Y, Yang T, Bao Q, Yang M, Mao C. Bacteriophage-based biomaterials for tissue regeneration. Adv Drug Deliv Rev 2018.

[2] Dang M, Saunders L, Niu X, Fan Y, Ma PX. Biomimetic delivery of signals for bone tissue engineering. Bone Res 2018;6:25.

[3] Nabavinia M, Khoshfetrat AB, Naderi-Meshkin H. Nano-hydroxyapatite-alginate-gelatin microcapsule as a potential osteogenic building block for modular bone tissue engineering. Mat Sci Eng C-Mater 2019;97:67-77.

[4] Chen LY, Shen RZ, Komasa S, Xue YX, Jin BY, Hou YP, Okazaki J, Gao J. Drug-Loadable Calcium Alginate Hydrogel System for Use in Oral Bone Tissue Repair. Int J Mol Sci 2017;18.

[5] Eosoly S, Vrana NE, Lohfeld S, Hindie M, Looney L. Interaction of cell culture with composition effects on the mechanical properties of polycaprolactone-hydroxyapatite scaffolds fabricated via selective laser sintering (SLS). Mat Sci Eng C-Mater 2012;32:2250-7.

[6] Salmasi S, Nayyer L, Seifalian AM, Blunn GW. Nanohydroxyapatite Effect on the Degradation, Osteoconduction and Mechanical Properties of Polymeric Bone Tissue Engineered Scaffolds. Open Orthop J 2016;10:900-19.

[7] Zhang X, Chang W, Lee P, Wang Y, Yang M, Li J, et al. Polymer-ceramic spiral structured scaffolds for bone tissue engineering: effect of hydroxyapatite composition on human fetal osteoblasts. Plos One 2014;9:e85871.

[8] Du MC, Song WX, Cui Y, Yang Y, Li JB. Fabrication and biological application of nano-hydroxyapatite (nHA)/alginate (ALG) hydrogel as scaffolds. J Mater Chem 2011;21:2228-36.

[9] Zhang J, Wang Q, Wang A. *In situ* generation of sodium alginate/hydroxyapatite nanocomposite beads as drug-controlled release matrices. Acta Biomater 2010;6:445-54.

[10] Costa MJ, Marques AM, Pastrana LM, Teixeira JA, Sillankorva SM, Cerqueira MA. Physicochemical properties of alginate-based films: Effect of ionic crosslinking and mannuronic and guluronic acid ratio. Food Hydrocolloids 2018;81:442-8.

[11] Bertazzo S, Zambuzzi WF, Campos DDP, Ogeda TL, Ferreira CV, Bertran CA. Hydroxyapatite surface solubility and effect on cell adhesion. Colloids Surf B 2010;78:177-84.

[12] Dhivya S, Saravanan S, Sastry TP, Selvamurugan N. Nanohydroxyapatite-reinforced chitosan composite hydrogel for bone tissue repair *in vitro* and *in vivo*. J Nanobiotechnol 2015;13.

[13] Chen YM, Gong JP, Tanaka M, Yasuda K, Yamamoto S, Shimomura M, Osada Y. Tuning of cell proliferation on tough gels by critical charge effect. J Biomed Mater Res A 2009;88a:74-83.

[14] Chan G, Mooney DJ. Ca^{2+} released from calcium alginate gels can promote inflammatory responses *in vitro* and *in vivo*. Acta Biomater 2013;9:9281-91.

[15] Meena R, Kesari KK, Rani M, Paulraj R. Effects of hydroxyapatite nanoparticles on proliferation and apoptosis of human breast cancer cells (MCF-7). J Nanopart Res 2012;14.

[16] Zhao R, Xie PF, Zhang K, Tang ZR, Chen XN, Zhu XD, Fan Y, Yang X, Zhang X. Selective effect of hydroxyapatite nanoparticles on osteoporotic and healthy bone formation correlates with intracellular calcium homeostasis regulation. Acta Biomater 2017;59:338-50.

[17] De Witte TM, Fratila-Apachitei LE, Zadpoor AA, Peppas NA. Bone tissue engineering via growth factor delivery: from scaffolds to complex matrices. Regen Biomater 2018;5:197-211.

[18] Chocholata P, Kulda V, Babuska V. Fabrication of Scaffolds for Bone-Tissue Regeneration. Materials (Basel) 2019;12.

[19] ter Boo GJ, Grijpma DW, Moriarty TF, Richards RG, Eglin D. Antimicrobial delivery systems for local infection prophylaxis in orthopedic- and trauma surgery. Biomaterials 2015;52:113-25.

[20] Arciola CR, Campoccia D, Ehrlich GD, Montanaro L. Biofilm-Based Implant Infections in Orthopaedics. Biofilm-Based Healthcare-Associated Infections, Vol I 2015;830:29-46.

[21] Kaufman MG, Meaike JD, Izaddoost SA. Orthopedic Prosthetic Infections: Diagnosis and Orthopedic Salvage. Seminars in Plastic Surgery 2016;30:66-72.

[22] Montanaro L, Arciola CR, Baldassarri L, Borsetti E. Presence and expression of collagen adhesin gene (*cna*) and slime production in *Staphylococcus aureus* strains from orthopaedic prosthesis infections. Biomaterials 1999;20:1945-9.

[23] Quinones D, Kobayashi N, Nagashima S. Molecular Epidemiologic Analysis of *Enterococcus faecalis* Isolates in Cuba by Multilocus Sequence Typing. Microb Drug Resist 2009;15:287-93.

[24] Baldassarri L, Creti R, Recchia S, Pataracchia M, Alfarone G, Orefici G, Campoccia D, Montanaro L, Arciola CR. Virulence factors in enterococcal infections of orthopedic devices. Int J Artif Organs 2006;29:402-6.

[25] Montanaro L, Speziale P, Campoccia D, Ravaioli S, Cangini I, Pietrocola G, Giannini S, Arciola CR. Scenery of *Staphylococcus* implant infections in orthopedics. Future Microbiol 2011;6:1329-49.

[26] Maslanova I, Doskar J, Varga M, Kuntova L, Muzik J, Maluskova D, RuzixkovaV, Pantucek R. Bacteriophages of *Staphylococcus aureus* efficiently package various bacterial genes and mobile genetic elements including SCCmec with different frequencies. Env Microbiol Rep 2013;5:66-73.

[27] Ruiz-Garbajosa P, Bonten MJM, Robinson DA, Top J, Nallapareddy SR, Torres C, Cantón R, Baquero F, Murray BE, del Campo R, Willems RJ. Multilocus sequence typing scheme for *Enterococcus faecalis* reveals hospital-adapted genetic complexes in a background of high rates of recombination. J Clin Microbiol 2006;44:2220-8.

[28] Olson ME, Horswill AR. *Staphylococcus aureus* osteomyelitis: bad to the bone. Cell Host Microbe 2013;13:629-31.

[29] Kaur S, Harjai K, Chhibber S. Bacteriophage mediated killing of *Staphylococcus* aureus *in vitro* on orthopaedic K wires in presence of linezolid prevents implant colonization. Plos One 2014;9:e90411.

[30] Fish R, Kutter E, Bryan D, Wheat G, Kuhl S. Resolving Digital Staphylococcal Osteomyelitis Using Bacteriophage-A Case Report. Antibiotics (Basel) 2018;7.

[31] Meurice E, Rguiti E, Brutel A, Hornez JC, Leriche A, Descamps M, Bouchart F. New antibacterial microporous CaP materials loaded with phages for prophylactic treatment in bone surgery. J Mater Sci Mater Med 2012;23:2445-52.

[32] Kaur S, Harjai K, Chhibber S. *In Vivo* Assessment of Phage and Linezolid Based Implant Coatings for Treatment of Methicillin Resistant *S. aureus* (MRSA) Mediated Orthopaedic Device Related Infections. Plos One 2016;11:e0157626.

[33] Nobrega FL, Costa AR, Kluskens LD, Azeredo J. Revisiting phage therapy: new applications for old resources. Trends Microbiol 2015;23:185-91.

[34] Oliveira H, Sillankorva S, Merabishvili M, Kluskens LD, Azeredo J. Unexploited opportunities for phage therapy. Front Pharmacol 2015;6:180.

[35] Gorski A, Jonczyk-Matysiak E, Miedzybrodzki R, Weber-Dabrowska B, Lusiak-Szelachowska M, Baginska N, Borysoski J, Lobocka MB, Wegrzyn A, Wegrzyn G. Phage Therapy: Beyond Antibacterial Action. Front Med (Lausanne) 2018;5:146.

[36] Morris J, Kelly N, Elliott L, Grant A, Wilkinson M, Hazratwala K, McEwen P. Evaluation of Bacteriophage Anti-Biofilm Activity for Potential Control of Orthopedic Implant-Related Infections Caused by *Staphylococcus Aureus*. Surg Infect 2018.

[37] Yilmaz C, Colak M, Yilmaz BC, Ersoz G, Kutateladze M, Gozlugol M. Bacteriophage Therapy in Implant-Related Infections An Experimental Study. J Bone Joint Surg Am 2013;95a:117-25.

[38] Trampuz A, Klatt A, Luca MD. Isolation of new lytic bacteriophages for treatment of prosthetic joint infection. Orthopaedic Proceedings 2017;99-B:36.

[39] Kishor C, Mishra RR, Saraf SK, Kumar M, Srivastav AK, Nath G. Phage therapy of staphylococcal chronic osteomyelitis in experimental animal model. Indian J Med Res 2016;143:87-94.

[40] Dublanchet A, Patey O. Phage therapy for bone and joint infections: report of french cases. Orthopaedic Proceedings 2017;99-B:35.

[41] Chan BK, Turner PE, Kim S, Mojibian HR, Elefteriades JA, Narayan D. Phage treatment of an aortic graft infected with *Pseudomonas aeruginosa*. Evolution, Medicine, and Public Health 2018;2018:60-6.

[42] Meurice E, Rguiti E, Brutel A, Hornez JC, Leriche A, Descamps M, Bouchart F. New antibacterial microporous CaP materials loaded with phages for prophylactic treatment in bone surgery. J Mater Sci-Mater M 2012;23:2445-52.

[43] Kaur S, Harjai K, Chhibber S. Bacteriophage Mediated Killing of *Staphylococcus aureus In Vitro* on Orthopaedic K Wires in Presence of Linezolid Prevents Implant Colonization. Plos One 2014;9.

[44] Kaur S, Harjai K, Chhibber S. *In Vivo* Assessment of Phage and Linezolid Based Implant Coatings for Treatment of Methicillin Resistant *S. aureus* (MRSA) Mediated Orthopaedic Device Related Infections. Plos One 2016;11.

[45] Francolini I, Vuotto C, Piozzi A, Donelli G. Antifouling and antimicrobial biomaterials: an overview. Apmis 2017;125:392-417.

[46] Veiga AS, Schneider JP. Antimicrobial hydrogels for the treatment of infection. Biopolymers 2013;100:637-44.

[47] Gao P, Nie X, Zou M, Shi Y, Cheng G. Recent advances in materials for extended-release antibiotic delivery system. J Antibiot (Tokyo) 2011;64:625-34.

[48] Mohammed N, Grishkewich N, Berry R, Tam K. Cellulose nanocrystal-alginate hydrogel beads as novel adsorbents for organic dyes in aqueous solutions. Cellulose 2015;22:3725-38.

[49] Chakkalakal DA, Mashoof AA, Novak J, Strates BS, McGuire MH. Mineralization and pH relationships in healing skeletal defects grafted with demineralized bone matrix. J Biomed Mater Res B 1994;28:1439-43.
[50] Jain D, Bar-Shalom D. Alginate drug delivery systems: application in context of pharmaceutical and biomedical research. Drug Dev Ind Pharm 2014;40:1576-84.
[51] Colom J, Cano-Sarabia M, Otero J, Arinez-Soriano J, Cortes P, Maspoch D, Llagostera M. Microencapsulation with alginate/CaCO3: A strategy for improved phage therapy. Sci Rep-Uk 2017;7.
[52] Vinner GK, Vladisavljevic GT, Clokie MRJ, Malik DJ. Microencapsulation of Clostridium difficile specific bacteriophages using microfluidic glass capillary devices for colon delivery using pH triggered release. Plos One 2017;12.
[53] Chakkalakal DA, Mashoof AA, Novak J, Strates BS, McGuire MH. Mineralization and pH relationships in healing skeletal defects grafted with demineralized bone matrix. Journal of biomedical materials research 1994;28:1439-43.
[54] Kinnari TJ, Esteban J, Martin-De-Hijas NZ, Sanchez-Munoz O, Sanchez-Salcedo S, Colilla M, Valler-Regí M, Gomez-Barrena E. Influence of surface porosity and pH on bacterial adherence to hydroxyapatite and biphasic calcium phosphate bloceramics. J Med Microbiol 2009;58:132-7.
[55] Cisek AA, Dabrowska I, Gregorczyk KP, Wyzewski Z. Phage Therapy in Bacterial Infections Treatment: One Hundred Years After the Discovery of Bacteriophages. Curr Microbiol 2017;74:277-83.
[56] Kazmierczak Z, Gorski A, Dabrowska K. Facing Antibiotic Resistance: Staphylococcus aureus Phages as a Medical Tool (vol, 6, pg 2551, 2014). Viruses-Basel 2015;7:1667.
[57] Chung W-J, Merzlyak A, Lee S-W. Fabrication of engineered M13 bacteriophages into liquid crystalline films and fibers for directional growth and encapsulation of fibroblasts. Soft Matter 2010;6:4454-9.
[58] Chen L, Shen R, Komasa S, Xue Y, Jin B, Hou Y, Okazaki J, Gao J. Drug-Loadable Calcium Alginate Hydrogel System for Use in Oral Bone Tissue Repair. Int J Mol Sci 2017;18.
[59] Li J, Mooney DJ. Designing hydrogels for controlled drug delivery. Nat Rev Mater 2016;1.
[60] Cunniffe GM, Curtin CM, Thompson EM, Dickson GR, O'Brien FJ. Content-Dependent Osteogenic Response of Nanohydroxyapatite: An *in Vitro* and *in Vivo*

Assessment within Collagen-Based Scaffolds. ACS Appl Mater Interfaces 2016;8:23477-88.

[61] Martinelli NM, Ribeiro MJG, Ricci R, Marques MA, Lobo AO, Marciano FR. In Vitro Osteogenesis Stimulation via Nano-Hydroxyapatite/Carbon Nanotube Thin Films on Biomedical Stainless Steel. Materials 2018;11.

[62] Qiu Y, Zhang N, An YH, Wen X. Biomaterial strategies to reduce implant-associated infections. Int J Artif Organs 2007;30:828-41.

[63] Gimeno M, Pinczowski P, Perez M, Giorello A, Martinez MA, Santamaria J, Arruebo M, Luján L. A controlled antibiotic release system to prevent orthopedic-implant associated infections: An *in vitro* study. Eur J Pharm Biopharm 2015;96:264-71.

[64] Silva T, Silva JC, Colaco B, Gama A, Duarte-Araujo M, Fernandes MH, Bettencourt A, Gomes P. *In vivo* tissue response and antibacterial efficacy of minocycline delivery system based on polymethylmethacrylate bone cement. J Biomater Appl 2018;33:380-91.

SUPPLEMENTARY MATERIAL

SULLPLEMENTATY 1 – CHAPTER 3

Supplementary support 1| Primers used in the PCR analyses carried out in this study

Primer1	Sequence (5′- 3′)	Product (pb)
MRSA		
mecA - F	GGGATCATAGCGTCATTATTC	532
mecA - R	AACGATTGTGACACGATAGCC	
nucC - F	TCAGCAAATGCATCACAAACAG	255
nucC - R	CGTAAATGCACTTGCTTCAGG	
Tn*5397*-like and Tn*916*/Tn*1545*-like transposons		
tndX - F	ATGATGGGTTGGACAAAGA	1500
tndX - R	CTTTGCTCGATAGGCTCTA	
int - F	GCGTGATTGTATCTCACT	1028
Int - R	GACGCTCCTGTTGCTTCT	
Integrases for *E. coli*		
intI1 - F	GGGTCAAGGATCTGGATTTCG	483
intI1 - R	GGGTCAAGGATCTGGATTTCG	
intI2 - F	CACGGATATGCGACAAAAAGGT	788
intI2 - R	GTAGCAAACGAGTGACGAAATG	
Phylogenetic groups		
chuA-F	GACGAACCAACGGTCAGGAT	279
chuA-R	TGCCGCCAGTACCAAAGACA	
YjaA-F	TGAAGTGTCAGGAGACGCTG	211
YjaA-R	ATGGAGAATGCGTTCCTCAAC	
TspE4C2 - F	GAGTAATGTCGGGGCATTCA	152
TspE4C2 -R	CGCGCCAACAAAGTATTACG	
Virulence genes for *S. aureus*		
cna - F	CGGTTCCCCCATAAAAGTGAAG	372
cna - R	CCCATAGCCTTGTGGATTTG	
ETA - F	ACTGTAGGAGCTAGTGCATTTGT	190

ETA - R	TGGATACTTTTGTCTATCTTTTTCATCAAC	
etb - F	CAGATAAAGAGCTTTATACACACATTAC	612
etb - R	AGTGAACTTATCTTTCTATTGAAAAACACTC	
tst - F	TTCACTATTTGTAAAAGTGTCAGACCCACT	180
tst - R	TACTAATGAATTTTTTTATCGTAAGCCCTT	
hlb - F	GTTGGTGCTCTTACTGACAA	309
hlb - R	TGTGTACCGATAACGTGAAC	
icaA - F	ACAGTCGCTACGAAAAGAAA	103
icaA - R	GGAAATGCCATAATGACAAC	
icaB - F	CTGATCAAGAATTTAAATCACAAA	302
icaB - R	AAAGTCCCATAAGCCTGTTT	
icaC - F	TAACTTTAGGCGCATATGTTTT	400
icaC - R	TTCCAGTTAGGCTGGTATTG	
Virulence genes for *E. faecalis*		
ace - F	AAAGTAGAATTAGATCCACAC	248
ace - R	TCTATCACATTCGGTTGCG	
agg - F	AAGAAAAAGAAGTAGACCAAC	1553
agg - R	AAACGGCAAGACAAGTAAATA	
gelE - F	AGT TCA TGT CTA TTT TCT TCA C	403
gelE - R	CTT CAT TAT TTA CAC GTT TG	
esp - F	CTTTGATTCTTGGTTGTCGGATAC	475
esp - R	TTCAACTACCACGGTTTGTTTATC	
hyl - F	GAGTAGAGGAATATCTTAGC	661
hyl - R	AGGCTCCAATTCTGT	
fsr - F	AAC CAG AAT CGA CCA ATG AAT	3268
fsr - F	GCC CCT CAT AAC TCA ATA CC	
cylA - F	TGG ATG ATA GTG ATA GGA AGT	517
cylA - R	TCT ACA GTA AAT CTT TCG TCA	
cylB - F	AAT CCT ACC TAT GTT CTG TTA	843
cylB - R	AAT AAA CTC TTC TTT TCC AAC	
cylM - F	CTGATGGAAAGAAGATAGTAT	832

cylM - R	TGAGTTGGTCTGATTACATTT	
cylLL - F	GATGGAGGGTAAGAATTATGG	253
cylLL - F	GCTTCACCTCACTAAGTTTTATAG	
cylLS - F	GAAGCACAGTGCTAAATAAGG	240
cylLS - R	GTATAAGAGGGCTAGTTTCAC	
Virulence genes for *E. coli*		
fimA - F	GTTGTTCTGTCGGCTCTGTC	447
fimA - R	ATGGTGTTGGTTCCGTTATTC	
papGIII - F	CATTTATCGTCCTCAACTTAG	482
papGIII - R	AAGAAGGGATTTTGTAGCGTC	
stx - F	CTT CGG TAT CCT ATT CCC GG	484
stx - F	GGA TGC ATC TCT GGT CAT TG	
cnf - F	AAGATGGAGTTTCCTATGCAGGAG	498
cnf - R	CATTCAGAGTCCTGCCCTCATTATT	
papC - F	GACGGCTGTACTGCAGGGTGTGGCG	328
papC - R	ATATCCTTTCTGCAGGGATGCAATA	
Genes housekeeping for *S. aureus*		
arcC - F	TTG ATT CAC CAG CGC GTA TTG TC	~500
arcC - R	AGG TAT CTG CTT CAA TCA GCG	
aroE - F	ATC GGA AAT CCT ATT TCA CAT TC	~500
aroE - R	GGT GTT GTA TTA ATA ACG ATA TC	
glpF - F	CTA GGA ACT GCA ATC TTA ATC C	~500
glpF - R	TGG TAA AAT CGC ATG TCC AAT TC	
gmk - F	ATC GTT TTA TCG GGA CCA TC	~500
gmk - R	TCA TTA ACT ACA ACG TAA TCG TA	
pta - F	GTT AAA ATC GTA TTA CCT GAA GG	~500
pta - R	GAC CCT TTT GTT GAA AAG CTT AA	
tpi - F	TCG TTC ATT CTG AAC GTC GTG AA	~500
tpi - F	TTT GCA CCT TCT AAC AAT TGT AC	
yqiL - F	CAG CAT ACA GGA CAC CTA TTG GC	~500
yqiL - R	CGT TGA GGA ATC GAT ACT GGA AC	

Genes housekeeping for *E. faecalis*		
gdh - F	GGCGCACTAAAAGATATGGT	530
gdh - R	CCAAGATTGGGCAACTTCGTCCCA	
gyd - F	CAAACTGCTTAGCTCCAATGGC	395
gyd - R	CATTTCGTTGTCATACCAAGC	
pstS - F	CGGAACAGGACTTTCGC	583
pstS - R	ATTTACATCACGTTCTACTTGC	
gki - F	GATTTTGTGGGAATTGGTATGG	438
gki - R	ACCATTAAAGCAAAATGATCGC	
aroE - F	TGGAAAACTTTACGGAGACAGC	459
aroE - R	GTCCTGTCCATTGTTCAAAAGC	
xpt - F	AAAATGATGGCCGTGTATTAGG	456
xpt - R	AACGTCACCGTTCCTTCACTTA	
yiqL - F	CAGCTTAAGTCAAGTAAGTGCCG	436
yiqL - R	GAATATCCCTTCTGCTTGTGCT	

MRSA, methicillin-resistant *Staphylococcus aureus*.

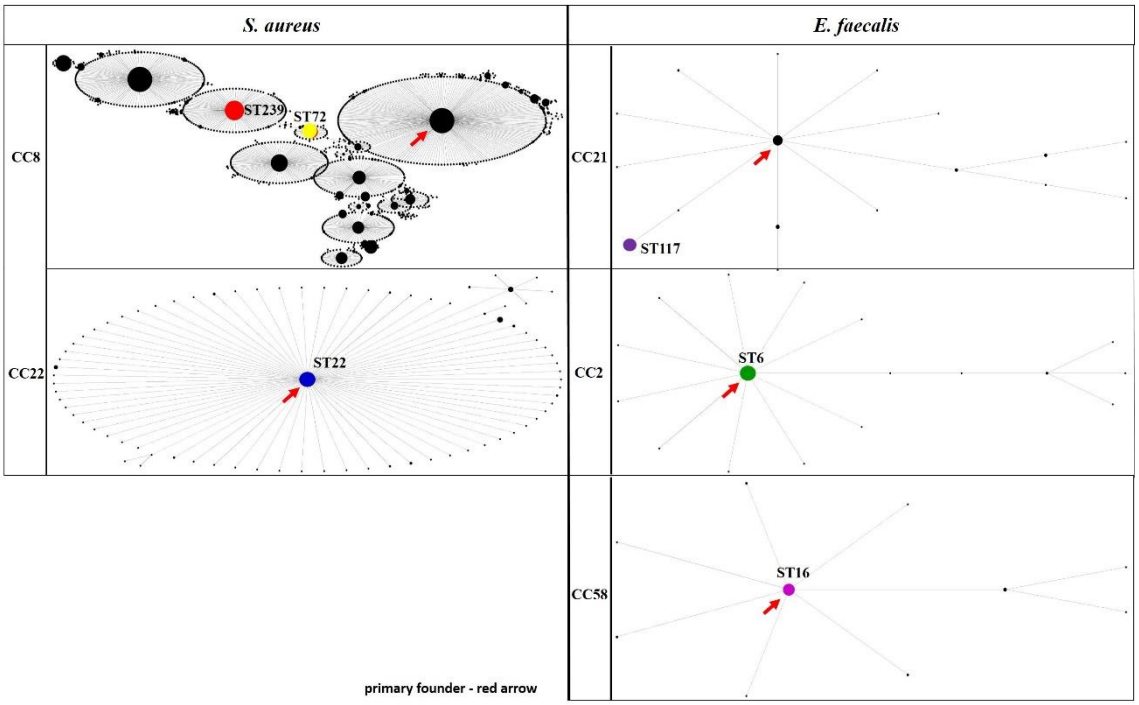

Figure S1 | eBURST V3 diagram of clonal complexes (CCs) and sequences types (STs) of *Staphylococcus aureus* and *Enterococcus faecalis* isolates.

Table S1 | Features of the predicted CDSs of bacteriophage LM99. - https://portal.i3s.up.pt/docs/joana.barros/1563900088293TableS1LM99pdf.pdf

Table S2 | Features of the predicted CDSs of bacteriophage JB75. - https://portal.i3s.up.pt/docs/joana.barros/1563900101506TableS2JB75pdf.pdf

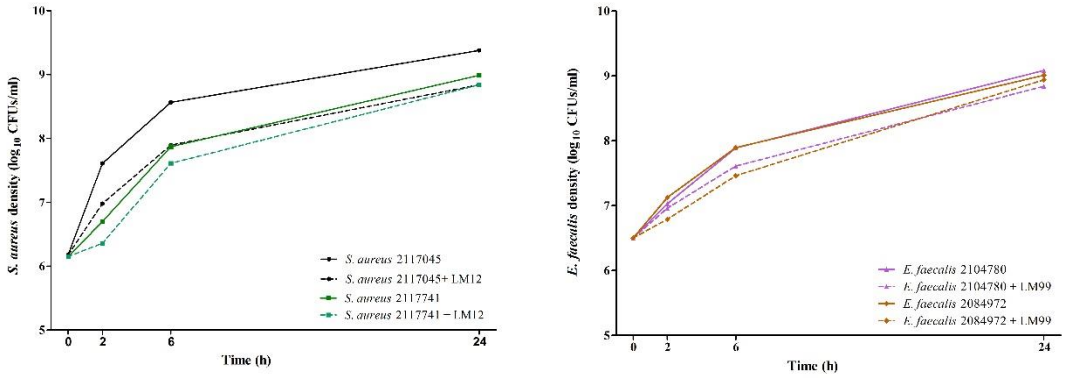

Figure S2 | Inhibitory effect of phages LM12 and LM99 on planktonic *Staphylococcus aureus* and *Enterococcus faecalis* isolates from orthopaedic implant-related infections. The solid lines represent growth of bacteria without phage (control) and the dashed lines represent growth of bacteria with phage. No significant differences were observed between control and bacterial + phage densities for the same time of incubation.

SULLPLEMENTATY 2 – CHAPTER 5

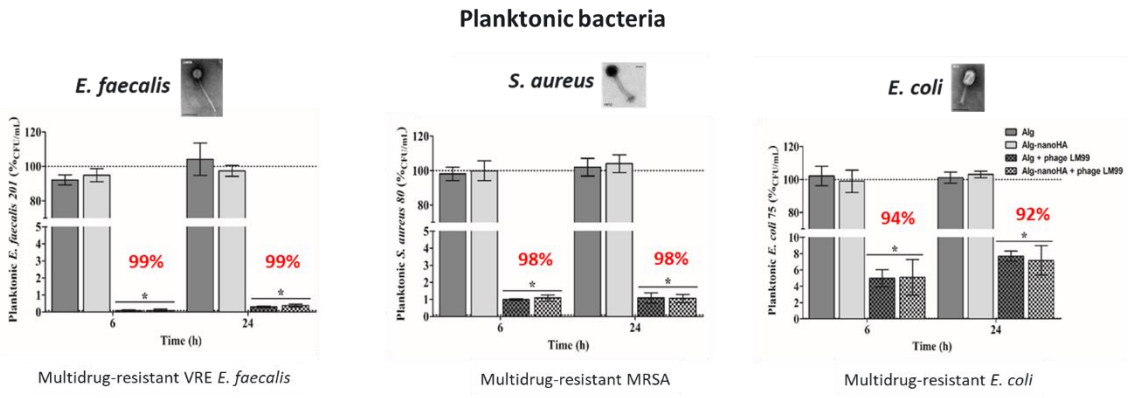

Supplementary support 2| Percentage of planktonic *E. faecalis*, *S. aureus* and *E. coli* growth in the presence of encapsulated phage 99, phage 12 and phage 75 on Alg-nanoHA30, respectively.